AD-A193 221 ADAPTIVE FINITE ELEMENT METHODS FOR SHELLS(U) 1/2
NORTHWESTERN UNIV EVANSTON IL DEPT OF CIVIL ENGINEERING
T BELYTSCHKO ET AL. 30 JAN 88 AFOSR-TR-88-0277
UNCLASSIFIED F49620-85-C-0128 F/G 13/2 NL

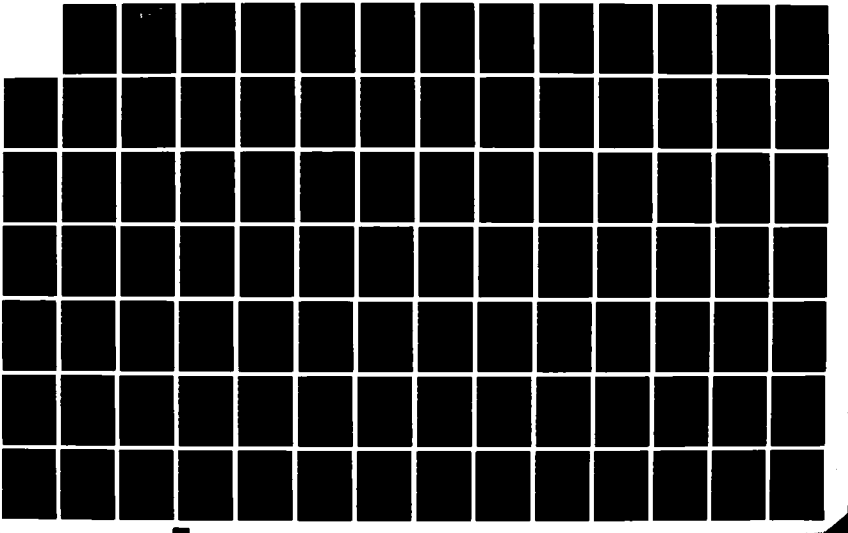

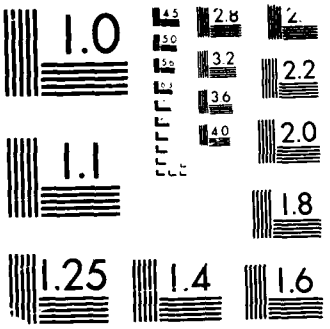

MICROCOPY RESOLUTION TEST CHART

AD-A193 221

UNCLASSIFIED

SECURITY CLASSIFICATION OF THIS PAGE

DTIC FILE COPY

REPORT DOCUMENTATION PAGE

1a. REPORT SECURITY CLASSIFICATION: UNCLASSIFIED	1b. RESTRICTIVE MARKINGS
2a. SECURITY CLASSIFICATION AUTHORITY	3. DISTRIBUTION/AVAILABILITY OF REPORT: Approved for public release, distribution unlimited
2b. DECLASSIFICATION/DOWNGRADING SCHEDULE	
4. PERFORMING ORGANIZATION REPORT NUMBER(S)	5. MONITORING ORGANIZATION REPORT NUMBER(S): AFOSR-TR- 88-0277
6a. NAME OF PERFORMING ORGANIZATION: Northwestern University	6b. OFFICE SYMBOL (If applicable):
6c. ADDRESS (City, State and ZIP Code): Department of Civil Engineering, Evanston, IL 60208	7b. ADDRESS (City, State and ZIP Code): Building 410, Bolling AFB, D.C. 20332-6448
7a. NAME OF MONITORING ORGANIZATION: USAF, AFSC, Air Force Office of Scientific Research	
8a. NAME OF FUNDING/SPONSORING ORGANIZATION: AFOSR	8b. OFFICE SYMBOL (If applicable): NA
8c. ADDRESS (City, State and ZIP Code): Bldg 410, Bolling AFB D.C. 20332-6448	9. PROCUREMENT INSTRUMENT IDENTIFICATION NUMBER: F49620-85-C-0128
	10. SOURCE OF FUNDING NOS. — PROGRAM ELEMENT NO.: 61102F; PROJECT NO.: 2302; TASK NO.: B1; WORK UNIT NO.:
11. TITLE (Include Security Classification): ADAPTIVE METHODS FOR FAILURE ANALYSIS OF SHELLS	
12. PERSONAL AUTHOR(S): T. Belytschko, Wing Kam Liu, Hsiu-Guo Chang	
13a. TYPE OF REPORT: Final Technical	13b. TIME COVERED: FROM Sept 01 85 TO Dec 31 87
14. DATE OF REPORT (Yr., Mo., Day): 1988 January 30	15. PAGE COUNT: 125
16. SUPPLEMENTARY NOTATION	
17. COSATI CODES — FIELD / GROUP / SUB. GR.	18. SUBJECT TERMS (Continue on reverse if necessary and identify by block number): finite elements, adaptive meshes, shells

19. ABSTRACT (Continue on reverse if necessary and identify by block number)

An adaptive finite element procedure is developed for the transient analysis of nonlinear shells. The scheme is an h-method which employs fission and fusion. Criteria based on incremental work and deviation of the bilinear finite element approximation to the shell from a Kirchhoff-Love surface are used as criteria for adaptivity. The example problems show that the adaptive schemes are capable of achieving substantial improvements in accuracy for a given computational effort. They include both material and geometric nonlinearities and local and global buckling.

In order to formulate an r-adaptive method, the conservation laws, the constitutive equations, and the equation of state for path-dependent materials are formulated for an arbitrary Lagrangian-Eulerian description. Both geometrical and material nonlinearities are included in this setting. A Petrov-Galerkin method is

(continued on reverse)

20. DISTRIBUTION/AVAILABILITY OF ABSTRACT: UNCLASSIFIED/UNLIMITED ☒ SAME AS RPT ☐ DTIC USERS ☐	21. ABSTRACT SECURITY CLASSIFICATION: UNCLASSIFIED
22a. NAME OF RESPONSIBLE INDIVIDUAL: Dr. Arje Nachman	22b. TELEPHONE NUMBER (Include Area Code): (202) 767-4937 — 22c. OFFICE SYMBOL: NM

DD FORM 1473, 83 APR — EDITION OF 1 JAN 73 IS OBSOLETE.

SECURITY CLASSIFICATION OF THIS PAGE

UNCLASSIFIED

19. ABSTRACT (continued)

developed for the stress update so that the history dependence and the resulting convective term on the stress tensor can be treated. A collocation-weighted residual scheme is also developed. In addition, the tangent stiffness matrix for the equilibrium equation is derived from the principle of virtual work. Various methods for solving the finite element equations are presented, and several numerical examples are analyzed to examine some features of the proposed methods. The first are some elastic-plastic wave propagation problems which serve to check the correctness of the numerical scheme. The second is a flexural problem, the response of which is dominated by the formation of hinge lines. The adaptive mesh technique enables this problem to be solved with a much coarser mesh.

ADAPTIVE FINITE ELEMENT METHODS FOR SHELLS

Principal Investigator: Ted Belytschko

Final Technical Report

September 1, 1985 - December 31, 1987

Department of Civil Engineering
Northwestern University
Evanston, Illinois 60208

Air Force Research Grant F49620-85-C-0128

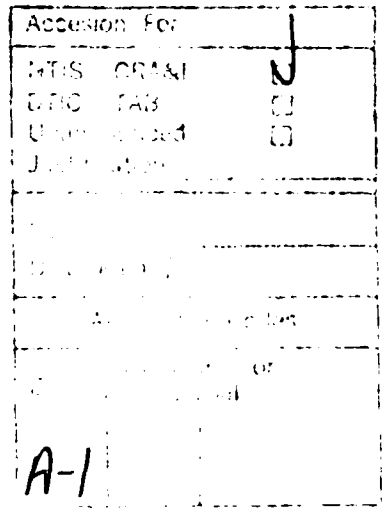

TABLE OF CONTENTS

PREFACE

This research was conducted under the direction of Professor T. Belytschko. The following research personnel participated in the research in the program: Professor W. K. Liu, Dr. H. Stolarski, Dr. J.S-J. Ong, Mr. H.G. Chang, Mr. D. Lasry, Mr. E.J. Plaskacz, and Mr. E. Law.

The following papers supported by AFOSR under this grant or the preceding years of support, grant F-49620-82-K-0013, were published in this time period.

T. Belytschko, W.K. Liu, J.S-J. Ong and D. Lam, "Implementation and Application of 9-Node Lagrange Shell Element with Spurious Mode Control," Computers and Structures, 20(1-3), 121-128, 1985.

N. Carpenter, H. Stolarski and T. Belytschko, "A Flat Triangular Shell Element with Improved Membrane Interpolations," Communications in Applied Numerical Methods, 1, 161-168, 1985.

H. Stolarski, N. Carpenter and T. Belytschko, "A Kirchhoff-Mode Method for C^0 Bilinear and Serendipity Plate Elements," Computer Methods in Applied Mechanics and Engineering, 50, 121-145, 1985.

T. Belytschko, H. Stolarski, W.K. Liu, N. Carpenter and J.S-J. Ong, "Stress Projection for Membrane and Shear Locking in Shell Finite Elements," Computer Methods in Applied Mechanics and Engineering, 51(1-3), 221-258, 1985.

T. Belytschko and W.K. Liu, "Improved Spurious Mode Control Through Mixed Variational Principles," Proc. Finite Element Methods for Nonlinear Problems - Europe - U.S. Symposium, Trondheim, Norway, 1985 (ed. Bergan, Bathe, Wunderlich), Springer - Berlin Heidelberg, 299-315, 1986.

N. Carpenter, H. Stolarski and T. Belytschko, "Improvements in 3-Node Triangular Shell Elements," International Journal for Numerical Methods in Engineering, 23(9), 1643-1667, 1986.

H. Stolarski and T. Belytschko, "On the Equivalence of Mode Decomposition and Mixed Finite Elements Based on the Hellinger-Reissner Principle: Part I: Theory," Computer Methods in Applied Mechanics and Engineering, 58(3), 249-265, 1986.

H. Stolarski and T. Belytschko, "On the Equivalence of Mode Decomposition and Mixed Finite Elements Based on the Hellinger-Reissner Principle: Part II: Applications," Computer Methods in Applied Mechanics and Engineering, 58(3), 265-285, 1986.

The following doctorates were supported by this research:

Nicholas John Carpenter, "Improved Low-Order Triangular Shell Finite Elements," August 1985.

James Shau-Jen Ong, "A Consistent Control of Spurious Modes for 9-Node Lagrange Element," June 1986.

1. INTRODUCTION

The nonlinear transient analysis of structures is a particularly promising field for adaptive procedures, because, among the various classes of structural finite element applications, it is computationally the most demanding. Furthermore, it is the class of applications in which a priori selection of an appropriately refined mesh is most difficult, since the areas of the mesh which need to be refined depend on the evolution of the response, which cannot be foreseen by the analyst. Thus, while expert systems may prove to be quite effective in guiding a user to design appropriate meshes for linear-elastic, static problems, it is doubtful that this could be done in a typical nonlinear transient problem, such as the simulation of a high-energy disposition on a missile nose or a front-end crash of an automobile. In this type of analysis, the computational power must be focused on those parts of the mesh which undergo the most severe deformation, such as hinging and wrinkling, and the sites of such deformations are not determinable a priori. Furthermore, it is desirable to start various types of simulations, such as a frontal and side crash, with the same mesh and let the response dictate any refinement.

While nonlinear transient analysis is one of the most promising areas for adaptive procedures, it is also the most challenging. Perusal of the reviews of the adaptive field recently written by Noor and Babuska (1987) and Oden and Demkowicz (1988) reveal that the bulk of the theoretical work has been devoted to determining local error estimates for linear static problems; these estimates are used to select the elements or subdomains to be refined. These error estimates have evolved into two main types:

1. residual error criteria based on the magnitude of the residual in the governing equations;

2. error indicators based on interpolation and extension methods.

A difficulty in applying these methods to shells is that in the most effective elements for shell analysis, namely bilinear quadrilateral elements such as described in Belytschko et al (1984) and in Hallquist and Benson (1986), even the shape of the shell is not adequately represented. In other words, while the residual for the bilinear description of the shell may indicate a small residual, the errors may be quite large due to discrepancies between the configuration of the Kirchhoff-Love shell surface and the bilinear finite element representation.

However, this drawback also provides an opportunity, for in fact it is in the regions of maximal deviation between the bilinear representation and the shell surface that the finite element mesh is most inadequate. Since an average normal to the shell surface can be estimated at all times, the deviation of the bilinear representation and a more accurate approximation to the shell surface can be computed and used to indicate where mesh refinement will prove useful.

Another aspect of the approach taken here is that we have not endeavored to obtain a certain level of accuracy by the refinement. This choice was based on two reasons: (1) it is impossible at this time, with the available mathematical tools for error estimation, to estimate the local error in a nonlinear transient solution; (2) in most computer systems, the fast memory allocated to a run must be set at the beginning of the run.

Therefore, the philosophy of the adaptive process described here is to obtain the most accuracy for a given set of computational resources. As will be seen in the examples, this philosophy is quite effective. By using an adaptive mesh, it is generally possible to obtain a solution of comparable accuracy with half the total number of elements, and hence, half the computational resources in an explicit program, as with a fixed mesh.

2. FINITE ELEMENT FORMULATION

The shape of the midsurface is described in this finite element model by

$$x_i = N_I(\xi)\, x_{iI} \tag{2.1}$$

where x_{iI} are the coordinates of node I and $N_I(\xi)$ are the bilinear isoparametric shape functions. Lowercase subscripts designate Cartesian components, and uppercase subscripts designate node numbers; repeated indices are summed over their range, 4 for uppercase, 3 for lowercase.

The shape functions $N_I(\xi)$ are functions of the reference variables ξ_i, $i = 1,2$, also written as $\xi_1 = \xi$, $\xi_2 = \eta$, and they are given by

$$N_I = \frac{1}{4}(1 + \xi_I\xi)(1 + \eta_I\eta) \tag{2.2}$$

where ξ_I and η_I are the coordinates of the nodes at the corners of the reference domain defined by $-1 \le \xi \le 1$, $-1 \le \eta \le 1$. Note that unless a mesh of these elements is quite refined, they provide a rather poor model for the curved surface of a shell. In a regular mesh on a cylindrical shell, these elements are in fact all flat, and any interaction between flexure and membrane response only occurs at the nodes. Furthermore, in a region of large curvature, this model can deteriorate even more severely with very large angles between adjacent elements. However, before discussing this further, the basic mechanics of this finite element formulation will be described.

In the formulation, two types of coordinates are used in addition to the global Cartesian coordinates:

1. for each element, an element coordinate system $(\hat{x},\hat{y},\hat{z})$ with base vectors $\underset{\sim}{e}_1$, $\underset{\sim}{e}_2$, and $\underset{\sim}{e}_3$ is defined so that $\underset{\sim}{e}_1$ and $\underset{\sim}{e}_2$ are tangent to the midsurface and rotate with the element;
2. for each node, a triad $\underset{\sim}{b}_i$ is defined so that it rotates with the node, with $\underset{\sim}{b}_3$ normal to the midsurface of the shell in the undeformed configuration.

Whereas in the original formulation of Belytschko et al (1984) the original orientation of $\underset{\sim}{b}_i$ was arbitrary, it is used here to locate new nodes created in the adaptive process and therefore must initially be approximately normal to the midsurface of the shell.

The deformation of the element is governed by the Mindlin-Reissner hypothesis, which allows transverse shear but requires the normal to remain straight, so the velocity of a generic point in the shell is given in terms of the velocity of the midsurface v_i^m and the angular velocity ω_i by

$$v_i = v_i^m - \hat{z}\,(\underset{\sim}{e}_3 \times \underset{\sim}{\omega})_i \tag{2.3}$$

where $\hat{z}$, by the definition of the element coordinates, is the distance of a point from the midsurface.

The velocity field is given by

$$v_i^m = N_I \, v_{iI}^m \tag{2.4}$$

$$\omega_i = N_I \, \omega_{iI} \tag{2.5}$$

The strain rates (velocity strains or stretching) are given in terms of the nodal velocities in the element coordinate system by

$$\hat{d}_{xx} = \frac{\partial \hat{v}_x^m}{\partial \hat{x}} + \hat{z} \frac{\partial \hat{\omega}_y}{\partial \hat{x}} \tag{2.6a}$$

$$\hat{d}_{yy} = \frac{\partial \hat{v}_y^m}{\partial \hat{y}} - \hat{z} \frac{\partial \hat{\omega}_x}{\partial \hat{y}} \tag{2.6b}$$

$$2\hat{d}_{xy} = \frac{\partial \hat{v}_x^m}{\partial \hat{y}} + \frac{\partial \hat{v}_y^m}{\partial \hat{x}} + \hat{z} \left(\frac{\partial \hat{\theta}_y}{\partial \hat{y}} - \frac{\partial \hat{\theta}_x}{\partial \hat{x}} \right) \tag{2.6c}$$

$$2\hat{d}_{xz} = \frac{\partial \hat{v}_z^m}{\partial \hat{x}} + \hat{\theta}_y \tag{2.6d}$$

$$2\hat{d}_{yz} = \frac{\partial \hat{v}_z^m}{\partial \hat{y}} - \hat{\theta}_x \tag{2.6e}$$

Since the element uses one-point quadrature, the strains are evaluated at a single point, the origin of the reference plane which is given by $\xi=\eta=0$.

The velocity strains at this point are given by

$$\hat{d}_{xx} = B_{xI}\,\hat{v}_{xI} + \hat{z}\,(B'_{xI}\,\hat{v}_{xI} + B_{xI}\,\hat{\omega}_{yI}) \tag{2.7a}$$

$$\hat{d}_{yy} = B_{yI}\,\hat{v}_{yI} + \hat{z}\,(B'_{yI}\,\hat{v}_{yI} - B_{yI}\,\hat{\omega}_{xI}) \tag{2.7b}$$

$$\hat{d}_{xy} = B_{yI}\,\hat{v}_{xI} + B_{xI}\,\hat{v}_{yI} + \hat{z}\,(B'_{yI}\,\hat{v}_{xI} + B'_{xI}\,\hat{v}_{yI} - B_{xI}\,\hat{\omega}_{xI} + B_{yI}\,\hat{\omega}_{yI}) \tag{2.7c}$$

$$2\hat{d}_{xz} = B_{xI}\,\hat{v}_{zI} + s_I\,\hat{\omega}_{yI} \tag{2.7d}$$

$$2\hat{d}_{yz} = B_{yI}\,\hat{v}_{zI} - s_I\,\hat{\omega}_{xI} \tag{2.7e}$$

where

$$s_I = N_I(\underline{0}) = \frac{1}{4}[1,1,1,1] \tag{2.8a}$$

$$B_{xI} = \frac{\partial N_I(\underline{0})}{\partial \hat{x}} = \frac{1}{2A}[\hat{y}_{24}, \hat{y}_{31}, \hat{y}_{42}, \hat{y}_{13}] \tag{2.8b}$$

$$B_{yI} = \frac{\partial N_I(\underline{0})}{\partial \hat{y}} = \frac{1}{2A}[\hat{x}_{42}, \hat{x}_{13}, \hat{x}_{24}, \hat{x}_{31}] \tag{2.8c}$$

$$B'_{iI} = \frac{1}{2A}\begin{bmatrix} \hat{n}_{y,\eta} - C\,\hat{y}_{,\eta} & -(\hat{n}_{y,\xi} - C\,\hat{y}_{,\xi}) \\ -(\hat{n}_{x,\eta} - C\,\hat{x}_{,\eta}) & \hat{n}_{x,\xi} - C\,\hat{x}_{,\xi} \end{bmatrix} \begin{Bmatrix} N_{I,\xi} \\ N_{I,\eta} \end{Bmatrix} \tag{2.8d}$$

$$C = \frac{1}{2A}(\hat{x}_{,\xi}\,\hat{n}_{y,\eta} + \hat{y}_{,\eta}\,\hat{n}_{x,\xi} - \hat{x}_{,\eta}\,\hat{n}_{y,\xi} - \hat{y}_{,\xi}\,\hat{n}_{x,\eta}) \tag{2.8e}$$

$$x_{IJ} = x_I - x_J \tag{2.8f}$$

$$y_{IJ} = y_I - y_J \tag{2.8g}$$

and $\underline{n}$ is the normal to the shell.

The nodal forces are computed from the stresses by one-point quadrature, which yields

$$\hat{f}_{xI} = A\,(B_{xI}\,\delta_{xx} + B'_{xI}\,m_{xx} + B_{yI}\,\delta_{xy} + B'_{yI}\,m_{xy}) \tag{2.9a}$$

$$\hat{f}_{yI} = A\,(B_{yI}\,\delta_{yy} + B'_{yI}\,m_{yy} + B_{xI}\,\delta_{xy} + B'_{xI}\,m_{xy}) \tag{2.9b}$$

$$\hat{f}_{zI} = A\,(B_{yI}\,\delta_{yz} + B_{xI}\,\delta_{xz}) \tag{2.9c}$$

$$\hat{m}_{xI} = -A\,(B_{yI}\,m_{yy} + B_{xI}\,m_{xy} + s_I\,\delta_{yz}) \tag{2.9d}$$

$$\hat{m}_{yI} = A\,(B_{xI}\,m_{xx} + B_{yI}\,m_{xy} + s_I\,\delta_{xz}) \tag{2.9e}$$

where

$$\delta_{ij} = \int_{-h/2}^{h/2} \hat{\sigma}_{ij}\,dz \tag{2.9f}$$

$$m_{ij} = \int_{-h/2}^{h/2} \hat{\sigma}_{ij} \hat{z} \, dz \tag{2.9g}$$

and h is the thickness.

The one-point quadrature element is rank deficient, so it is associated with spurious singular modes, as described in Belytschko et al (1984). Their control is also described therein.

The incremental work is computed in each element by

$$\Delta W_e^{int} = \int \Delta t \, (\underset{\sim}{d}^{n+\frac{1}{2}})^T \, (\underset{\sim}{\sigma}^n + \underset{\sim}{\sigma}^{n+1}) \, dV \tag{2.10a}$$

where

$$\underset{\sim}{d}^T = [d_{xx}, \, d_{yy}, \, d_{xy}, \, d_{xz}, \, d_{yz}] \tag{2.10b}$$

$$\underset{\sim}{\sigma}^T = [\sigma_{xx}, \, \sigma_{yy}, \, \sigma_{xy}, \, \sigma_{xz}, \, \sigma_{yz}] \tag{2.10c}$$

and Δt is the time increment; superscripts indicate the time step. This quantity is used to check stability and as a criterion for mesh adaptation in some of the studies.

3. FUSION AND FISSION ADAPTIVITY

The type of adaptivity which has been adopted here is an h-type, where the mesh is selectively refined in parts of the domain during the evolution of the solution. In addition, the refined elements are fused when they are no longer needed, so that computational power is not wasted on those parts of the domain which no longer undergo a changing deformation pattern. The motivation for including the fusion process is that in transient nonlinear problems, certain parts of the domain in effect "freeze", so that coarse meshes can capture their behavior effectively.

The adaptive process consists of fission, in which an element is split into four, and fusion, in which a group of four elements is combined into one. These processes are illustrated in Fig. 1. For purposes of organization, any group of four elements which is created by fission is called a molecule.

There are three aspects to the implementation of fission-fusion adaptivity:

1. criteria for fission and fusion; the evaluation of these criteria is called a judgment;
2. the initial conditions for element and nodal variables at the nodes and elements which are created by fission;
3. the initial conditions for element variables of elements created by fusion.

Fission-Fusion Criteria

Two criteria have been adopted for making judgments on fission-fusion

1. an incremental internal work criterion;

2. a discontinuity criterion based on the increase in the angle between two adjacent elements.

According to the incremental internal work criterion, the elements which are fissioned are those which sustain the most work. Because this variable usually has an oscillatory character in an explicit solution of a transient problem, the judgment is made on the basis of the total incremental work done over the last five time steps. For the purpose of comparing elements of different sizes, the total incremental energy in a molecule is used as the criterion. Thus, fusion is indicated whenever the incremental work in a group of four elements which has been created by a previous fission is smaller than the incremental energy in other molecules.

Even with the filtering that is brought about by taking the incremental work over five steps, the incremental work criterion can lead to an oscillatory pattern of fission followed by fusion in many molecules in a transient process. Therefore, a time delay has been included which prevents fission or fusion unless it is indicated by two consecutive judgments. This type of retardation of the adaptive process appears to be needed in explicit treatments of nonlinear structural dynamics with adaptive meshes if excessive "churning" between fission and fusion is to be avoided.

The second criterion we have studied is based on the change in angle between two elements. The basis for this criterion is that one of the largest sources of errors in this finite element procedure is the inability of the piecewise bilinear elements to capture the correct shape and moment-curvature interaction of the shell as the deformation localizes. Severe deformation in shells is usually associated with large curvatures; since the bilinear element cannot represent large curvatures directly, it is associated with severe "kinking" between elements, which can be detected by monitoring the angle between elements. For those elements which satisfy the

angle criterion for fission, both elements on each side of the line are subdivided into four elements.

An advantage of the angle criterion over the incremental work criterion is that it can be applied to more than one level of fission-fusion without need of additional parameters. The incremental work criterion, if it is to be used for two levels of fission-fusion, requires the specification of a ratio at which the second level of fission is initiated.

Since it is difficult to relate any of these criteria to the ultimate accuracy of a solution, one technique we have frequently used is to simply specify the maximum number of elements and use the criteria to select where those elements are placed. In this procedure, we start with a uniform mesh which contains a fraction of the maximum number of elements allowed. After five time steps, the elements are fissioned in decreasing order of the amplitudes of their error indicators until the maximum number of elements is obtained.

Fission Process

When a molecule is fissioned next to an unfissioned molecule, as shown in Fig. 2, nodes are created adjacent to unsplit sides, so they cannot be handled by the usual equations of motion. In order to correctly handle compatibility, these nodes must be treated as "slave" nodes which are driven by the adjacent "master" nodes. In addition, in order to introduce a good representation of the shell as quickly as possible, it is useful to use the nodal vectors $\underset{\sim}{b}_i$ for an approximation of the curved Kirchhoff-Love surface on which the new nodes are placed.

The procedure for setting the initial configuration of the nodes is as follows. The surface is approximated by

$$x_I = x_{iI} N_I + \sum_{J=1}^{4} S_{Ji} \tag{3.1}$$

where

$$S_{1i} = (\phi_{12} H_1(\xi) + \phi_{21} H_2(\xi)) n_i |\underline{r}_{ij}| (N_1 + N_2) \tag{3.2}$$

where $H_I(\xi)$ are the Hermite interpolants, so that $H_{I,\xi}(\xi_J) = \delta_{IJ}$ and ϕ_{IJ} is the slope of the Kirchhoff surface relative to the bilinear approximation, which is obtained by

$$\phi_{IJ} = -(\underline{b}_3 \cdot \underline{r}_{IJ})/|\underline{r}_{IJ}| \tag{3.3}$$

The initial velocities of the nodes are obtained from the bilinear interpolation (2.1). The initial element variables for the elements are taken from the parent element. The mass matrix is reassembled after fission. Nodes which are formed at sides which are continuous sides of the adjacent elements are considered slave nodes. All other new nodes are master nodes. Thus, an interior node is always a master node, but if only a single, isolated molecule undergoes fission, all other new nodes are slave nodes.

Fusion Process

In the fusion process, no new nodes are created; the velocities and displacements at the nodes which remain are assumed to be continuous during fusion. The number of elements is reduced from four to one; the historical state variables (stress components and yield) are taken to be the area-weighted average of the parent element stresses. State variables such as the yield stress are adjusted so they remain consistent. For example, if the majority of the elements is plastic, the yield stress is adjusted so that the fused element is also yielding.

4. NUMERICAL EXAMPLES

All numerical examples described in this section were performed on a Harris 800 computer in single precision. A single-precision word consists of 11 significant digits (base 10) on this computer.

Since closed-form solutions are not available for nonlinear transient problems, two types of comparisons are used for the adaptive solutions:

1. numerical results obtained by finer meshes;
2. experimental results.

The first example concerns a clamped beam which is impulsively loaded over the center portion as shown in Fig. 3. Using symmetry, half of the beam is modelled by m × n quadrilateral plate elements, with m elements across the 1.2 in. width and n elements over the 5 in. half-span. The x and z components of the translations and rotations about the x and z axes were constrained.

Figure 4 shows the midspan deflection obtained by two fixed meshes and an 8- to 10-element adaptive mesh. As can be seen, the adaptive mesh is quite close to the 20-element fixed mesh for the first 0.5 msec, and it matches the maximum displacement quite well. Subsequently, it diverges somewhat from the fine-mesh solution.

Figure 5 shows the pattern of mesh adaptivity. The first elements to be fissioned are those beneath the impulsive load; the location of the fissioned elements then moves back and forth between the center and the support, like the hinge in the rigid-plastic solution, and finally fixes itself at the clamped wall.

The profiles of the beam obtained by a fine fixed mesh and the adaptive mesh are compared in Fig. 6. As can be seen, the profiles compare quite

well, except at the final time, 0.49 msec, when the node at the adaptive mesh at x = 3.0 in. deviates markedly.

This beam was resolved with a 2 × 20 fixed mesh and a 16-element adaptive mesh. The midspan deflection is shown in Fig. 7. In this case, the adaptive mesh corresponds very closely with the fixed mesh, even though it required only 40% of the elements. The potential savings in computational resources is even greater because, in the adaptive mesh, half of the elements could employ a time step twice as large as that used in the fixed mesh.

A more complex example for the adaptive mesh is provided by the cylindrical panel problem shown in Fig. 8. An initial velocity of 5650 in/sec is applied to the 3.08 in. × 10.205 area indicated in Fig. 8. The panel is simply supported at its ends and clamped at the sides. An Ilyushin plasticity model, which is expressed in terms of the resultant moments and membrane forces, m_{ij} and δ_{ij}, is used in the computation.

Two adaptive meshes were used in the computation: a 96-element mesh based on a 4 × 8 mesh of molecules; a 218-element mesh based on an 8 × 16 mesh of molecules. The results are compared to uniform fixed meshes with 32, 96, 128, 218, and 512 elements.

The displacement time histories for the coarse adaptive mesh are compared to three of the fixed-mesh results in Figs. 9 and 10 at points A (z = -6.28 in.) and B (z = -9.42 in.) which are indicated in Fig. 8. Remarkably, the 53-element adaptive result almost coincides with the 128-element fixed-mesh result for the first 0.4 msec. Subsequently, the results of the two meshes deviate somewhat, and the adaptive results become slightly rough, which is caused by excessive churning of the fission-fusion process

Note that the fixed-mesh results with fewer elements deviate substantially from the finest fixed-mesh results.

The displacements for the fine adaptive mesh are compared to the fixed meshes in Figs. 11 and 12 at points A and B, respectively. Here the 218-element adaptive mesh corresponds quite closely with the 512 uniform fixed mesh and exhibits marked improvement over a 200-element fixed mesh.

Deformed mesh plots for the finer adaptive mesh are shown at various times in Fig. 13. Here the incremental energy was used for the fission-fusion criterion. It can be seen that after 0.0125 msec, the crown settles downward like a plateau and the fissioning process migrates laterally towards the line where the curvature is maximum. During this time, the crown moves down in a frozen plateau-like state. After that, the crown develops a convex curvature when viewed from above, and the elements in the crown are again fissioned. The end of the simulation again exhibits churning of fission-fusion, which is a tendency that needs to be fixed: it is probably due to the fact that incremental work is quite small in the later stages because most of the deformation has taken place, so the incremental work in molecules is quite uniformly distributed, allowing the fission-fusion process to be triggered by small oscillations in the solution.

Experimental results have been obtained for this shell by Morino et al (1971), who reported a maximum deflection of 1.24 in. at point A. The finest fixed and adaptive meshes yielded maximum deflections of 1.20 and 1.17 in., respectively.

The deformed profiles are shown in Figs. 14 and 15 for the 512-element fixed mesh and the 218-element adaptive mesh. The development of a hinge-like pattern at about x = 2.0 in. and the attendant fission process are quite clearly seen in Fig. 14. Figure 15 shows a cross section in the y-z

plane of symmetry. The fission process which takes place while the crown is moving like a flat plateau, followed by the fission which develops when the crown curves, is quite clearly seen.

The third example is a hollow, cylindrical column which is subjected to a compressive axial load. This problem is of interest because it exhibits both global and local buckling, the latter resulting in buckling of the cross section. Numerical results and experimental results have been reported for this problem by Kennedy et al (1986). The problem parameters are given in Table 1.

The cylinder is loaded by prescribing an upward velocity of 500 in/sec to the bottom nodes of the model, with the top fixed. To trigger the lateral buckling mode, an imperfection given by

$$\Delta x = 0.01 \sin \frac{2\pi z}{\ell}$$

where ℓ is the length of the column and z is the coordinate along the axis of the column, is added to the x-coordinate of all nodes. The pattern of adaptivity is shown in Fig. 16. Initially, the fission process moves up and down the column similar to a reflected wave. The fission process then coalesces at the nodes of the lateral buckling mode, where they remain, except for the fission which takes place at the compressive buckles at the top and bottom of the column. The displacements of two points in the adaptive mesh are compared to corresponding points in a finer fixed mesh in Fig. 17. The results show good agreement.

5. CONCLUSIONS

An adaptive procedure based on an h-scheme has been developed for the nonlinear transient analysis of shells. This includes the development of suitable criteria for fission and fusion and the formulation of the fission and fusion processes. Two criteria have been found useful for the bilinear quadrilateral elements commonly used in transient analysis by explicit time integration:

1. the incremental internal work criterion;
2. the relative angle criterion, which is a measure of the deviation of the bilinear surface from the Kirchhoff-Love surface associated with the nodal orientations.

Furthermore, to avoid excessive churning of the fission-fusion process, time delays had to be incorporated in the judgment process. Nevertheless, churning becomes a problem with the incremental work criterion in the later stages of impulsively loaded problems when the work on the system decreases.

The results we have obtained show that the adaptive schemes are capable of achieving substantial improvements in accuracy for a given computational effort. Generally, an adaptive mesh is capable of achieving the same level of accuracy as a fixed mesh with less than half of the computational resources. The fission process tends to take place in the subdomains where the maximum deformation occurs.

The h-adaptive procedure is limited in its ability to focus on the subdomains of maximum deformation by the fact that the molecules which are subdivided are fixed in the reference configuration. Therefore, hinge lines which occur at small angles relative to the mesh lines are not captured effectively. For this reason, an h-r adaptive procedure which permits motion of the nodes is now under development. An essential ingredient of

such a process is an arbitrary Eulerian-Lagrangian method, which is described in the appendix.

REFERENCES

T. Belytschko, J. I. Lin, and C.-S. Tsay (1984). "Explicit Algorithms for the Nonlinear Dynamics of Shells", Computer Methods in Applied Mechanics and Engineering, 42, 225-251.

J. O. Hallquist and D. J. Benson (1986). "DYNA3D User's Manual (Nonlinear Dynamic Analysis of Structures in Three Dimensions)", Report UCID-19592, Revision 2, University of California, Lawrence Livermore National Laboratory, Livermore, CA.

J. M. Kennedy, T. Belytschko, and J. I. Lin (1986). "Recent Developments in Explicit Finite Element Techniques and Their Application to Reactor Structures", Nuclear Engineering and Design, 97(1), 1-24.

L. Morino, J. W. Leech, and E. A. Witmer (1971). "An Improved Numerical Calculation Technique for Large Elastic-Plastic Transient Deformations of Thin Shells: Part 2 - Evaluation and Applications", Journal of Applied Mechanics, 38(2), 429-436.

A. K. Noor and I. Babuska (1987). "Quality Assessment and Control of Finite Element Solutions", Finite Elements in Analysis and Design, 3(1), 1-26.

J. T. Oden and L. Demkowicz (1988). "Advances in Adaptive Improvements: A Survey of Adaptive Finite Elements in Computational Mechanics", in State of the Art Surveys in Computational Mechanics, ed. A. K. Noor et al, ASME, New York, in press.

Table 1

Dimensions and Material Properties of Cylindrical Column

Wall thickness	1 in.
Column diameter	13 in.
Column length	160 in.
Young's modulus	$E = 2.8 \times 10^7$ psi
Density	$\rho = 8.31 \times 10^{-4}$ lb-sec^2/in^4
Poisson's ratio	$\nu = 0.25$
Yield stress	$v = 35000$ psi

10 piecewise linear stress-strain curves are used to approximate plastic behavior

	Plastic moduli (psi)	Plastic stresses (psi)
(1)	6.60×10^5	4.75×10^4
(2)	4.50×10^5	5.65×10^4
(3)	4.00×10^5	6.45×10^4
(4)	2.75×10^5	7.00×10^4
(5)	2.50×10^5	7.50×10^4
(6)	2.25×10^5	7.95×10^4
(7)	2.20×10^5	8.35×10^4
(8)	1.75×10^5	8.70×10^4
(9)	1.50×10^5	9.00×10^4
(10)	1.25×10^5	1.15×10^6

LIST OF FIGURES

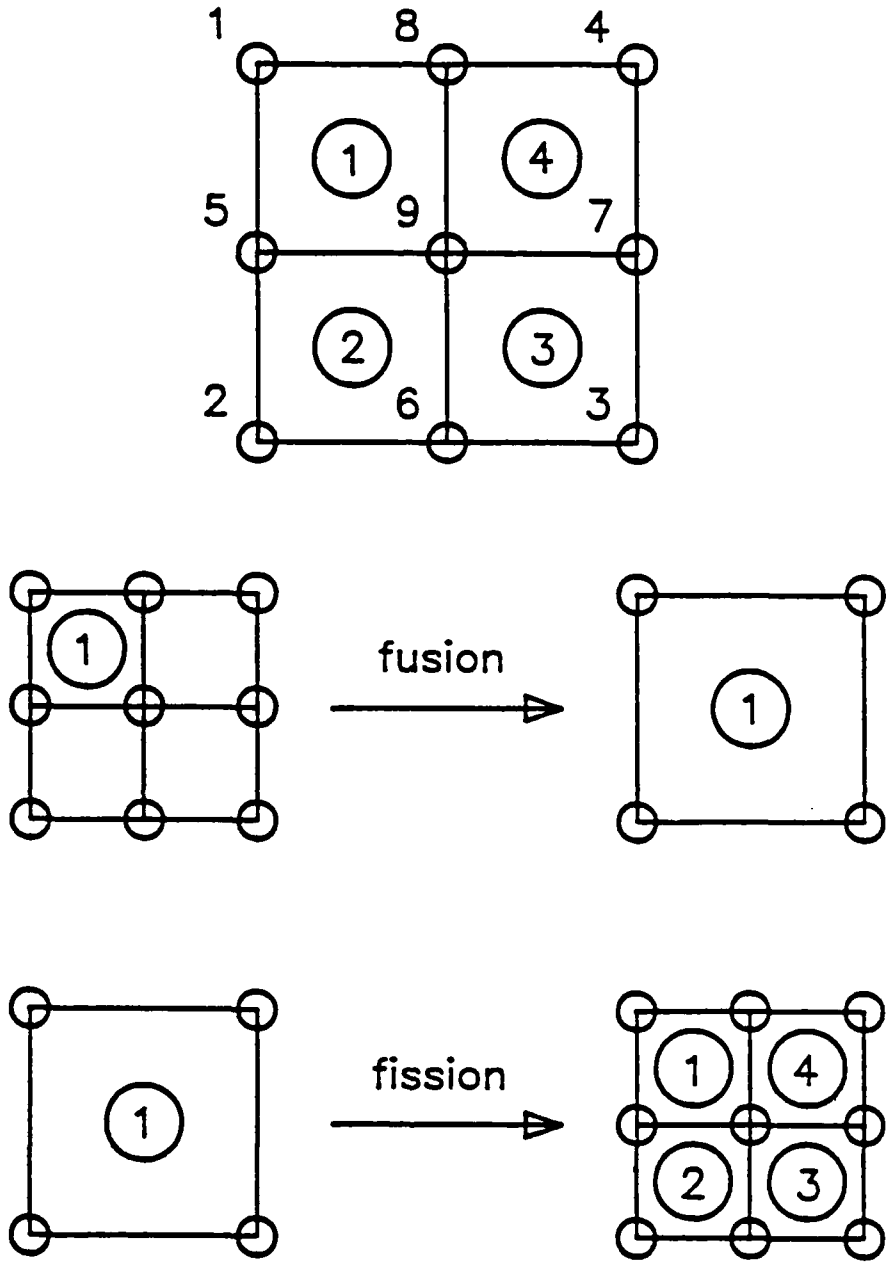

Figure 1

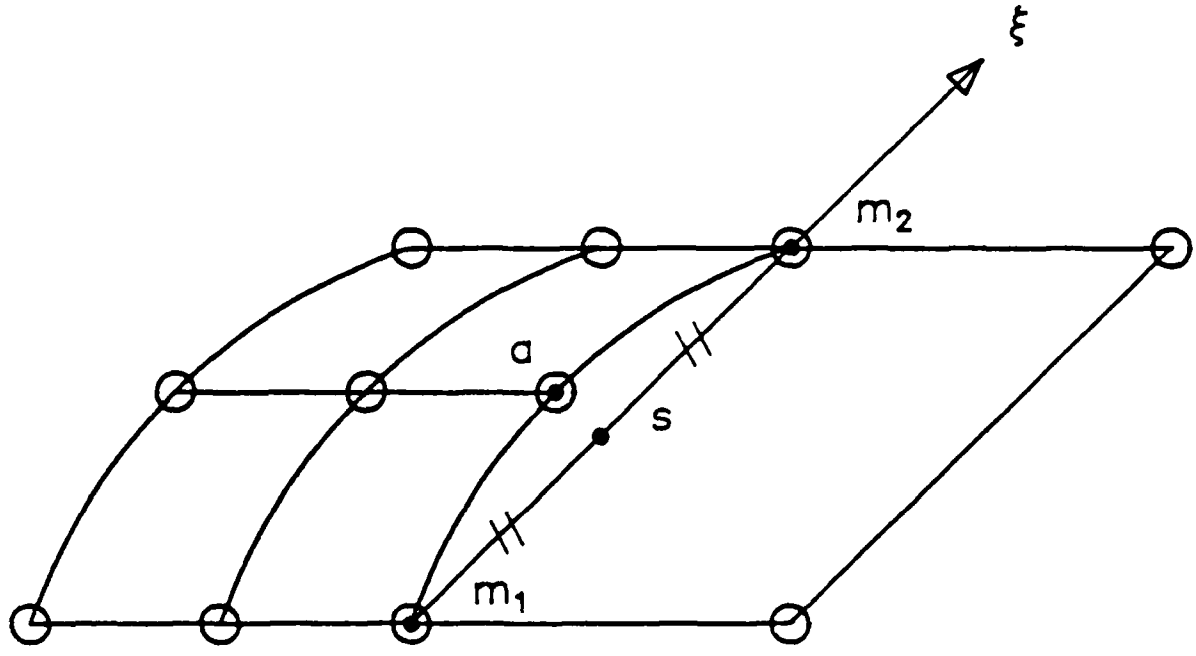

Figure 2

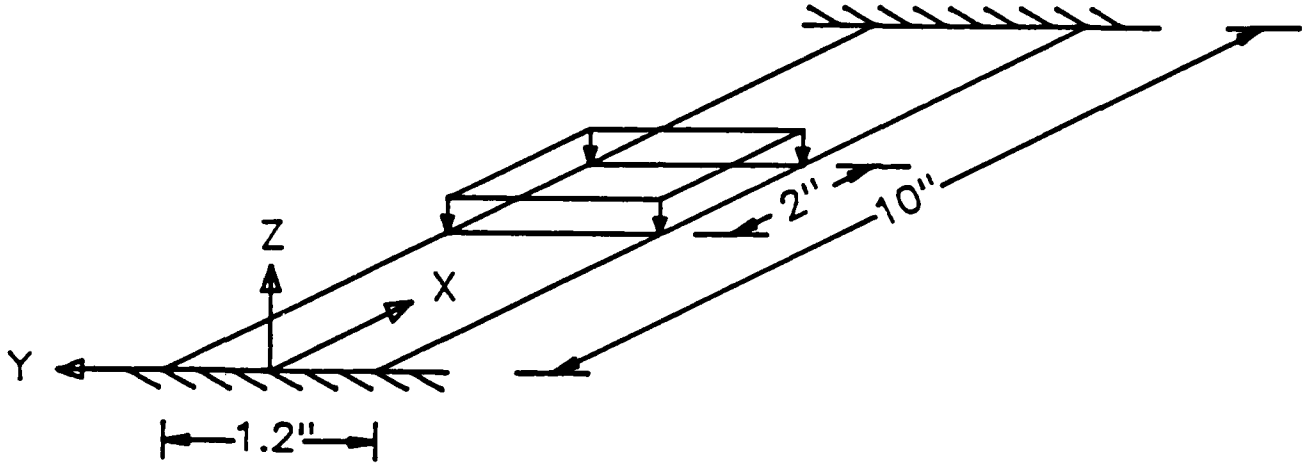

Figure 3

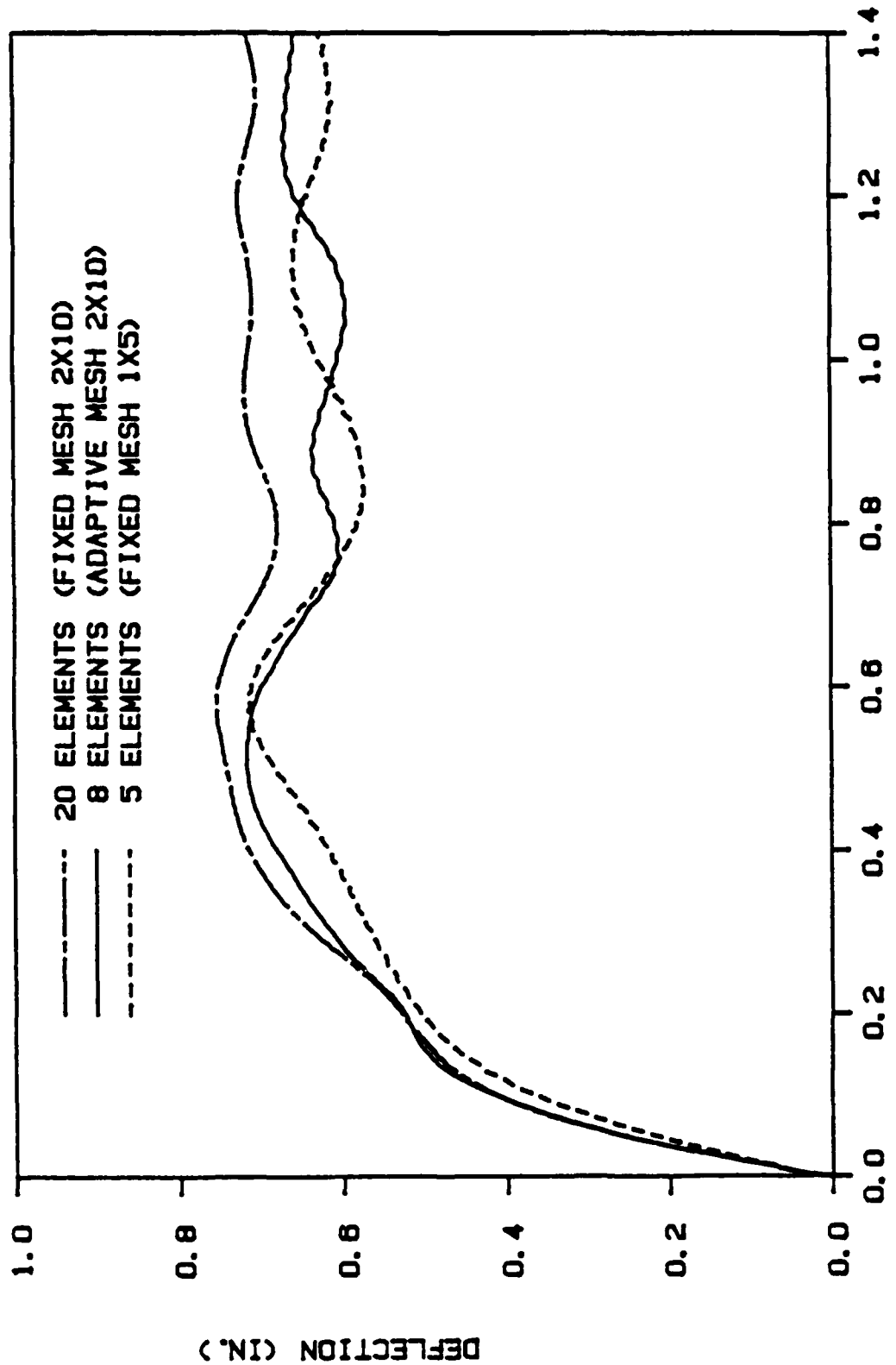
20 ELEMENTS (FIXED MESH 2X10)
8 ELEMENTS (ADAPTIVE MESH 2X10)
5 ELEMENTS (FIXED MESH 1X5)
DEFLECTION (IN.)
1.0
0.8
0.6
0.4
0.2
0.0
0.0
0.2
0.4
0.6
0.8
1.0
1.2
1.4
TIME (MSEC.)

Figure 4

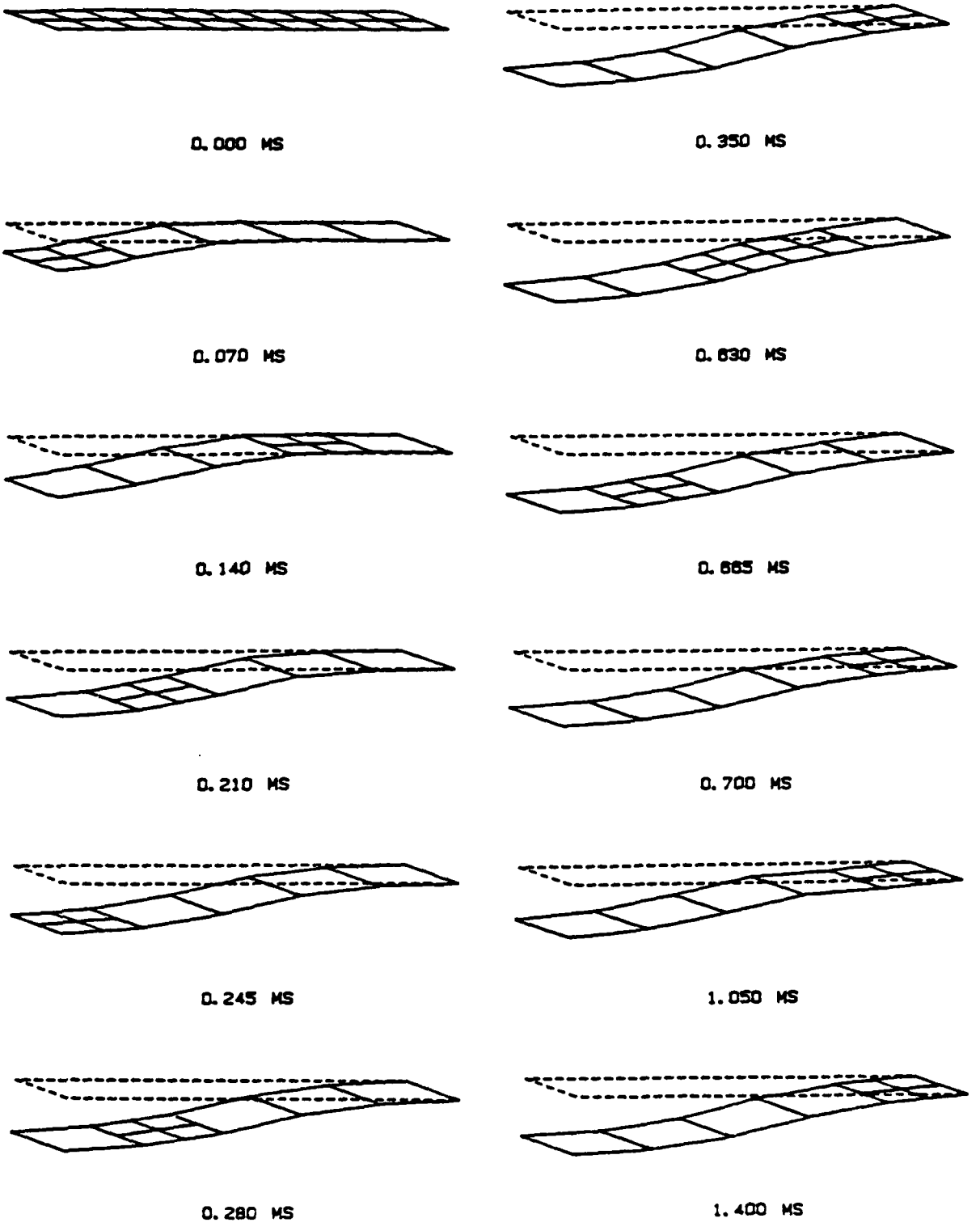
0.000 MS
0.350 MS
0.070 MS
0.630 MS
0.140 MS
0.865 MS
0.210 MS
0.700 MS
0.245 MS
1.050 MS
0.280 MS
1.400 MS

Figure 5

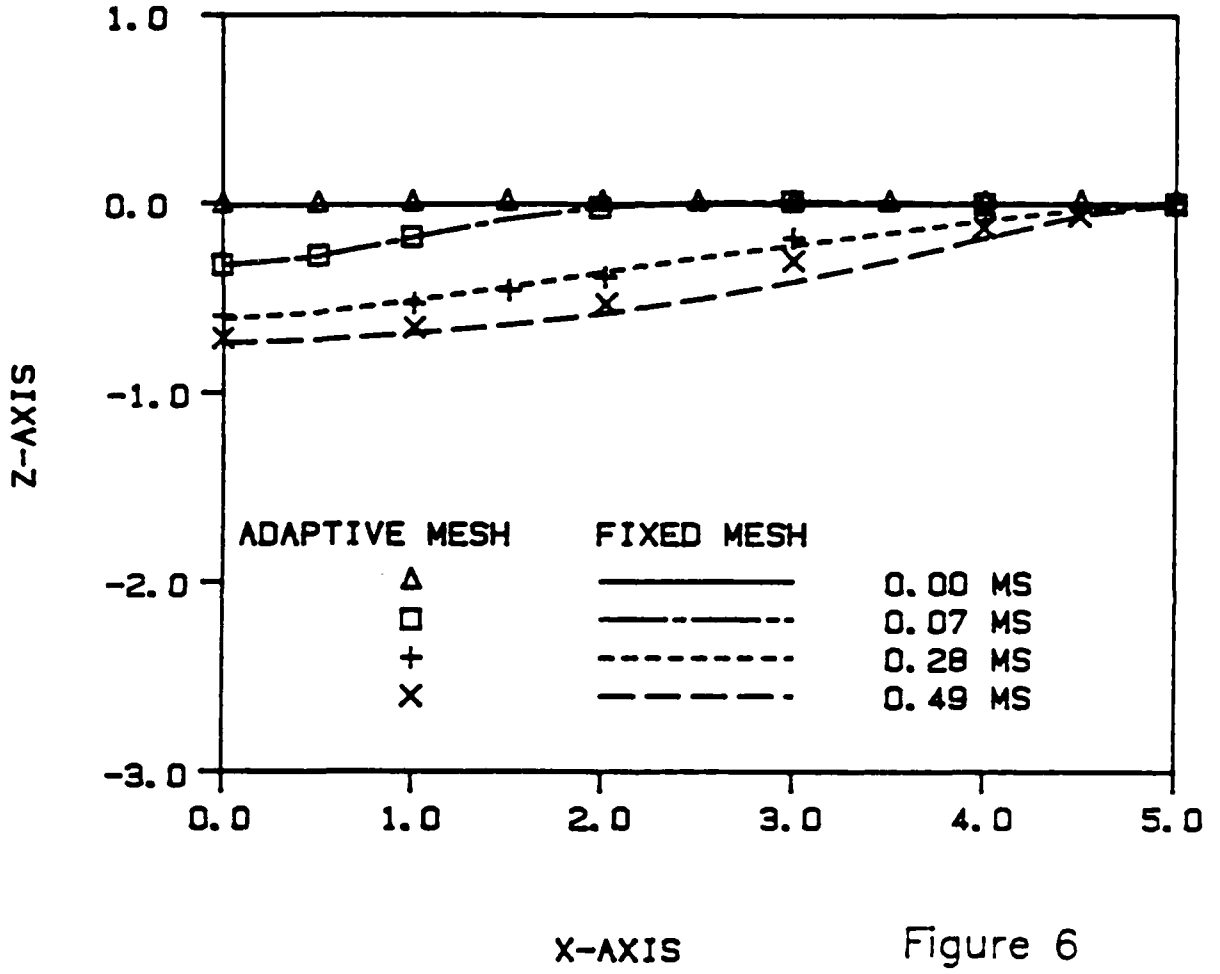
1.0
0.0
-1.0
-2.0
-3.0
Z-AXIS
0.0
1.0
2.0
3.0
4.0
5.0
X-AXIS
ADAPTIVE MESH
FIXED MESH
0.00 MS
0.07 MS
0.28 MS
0.49 MS

Figure 6

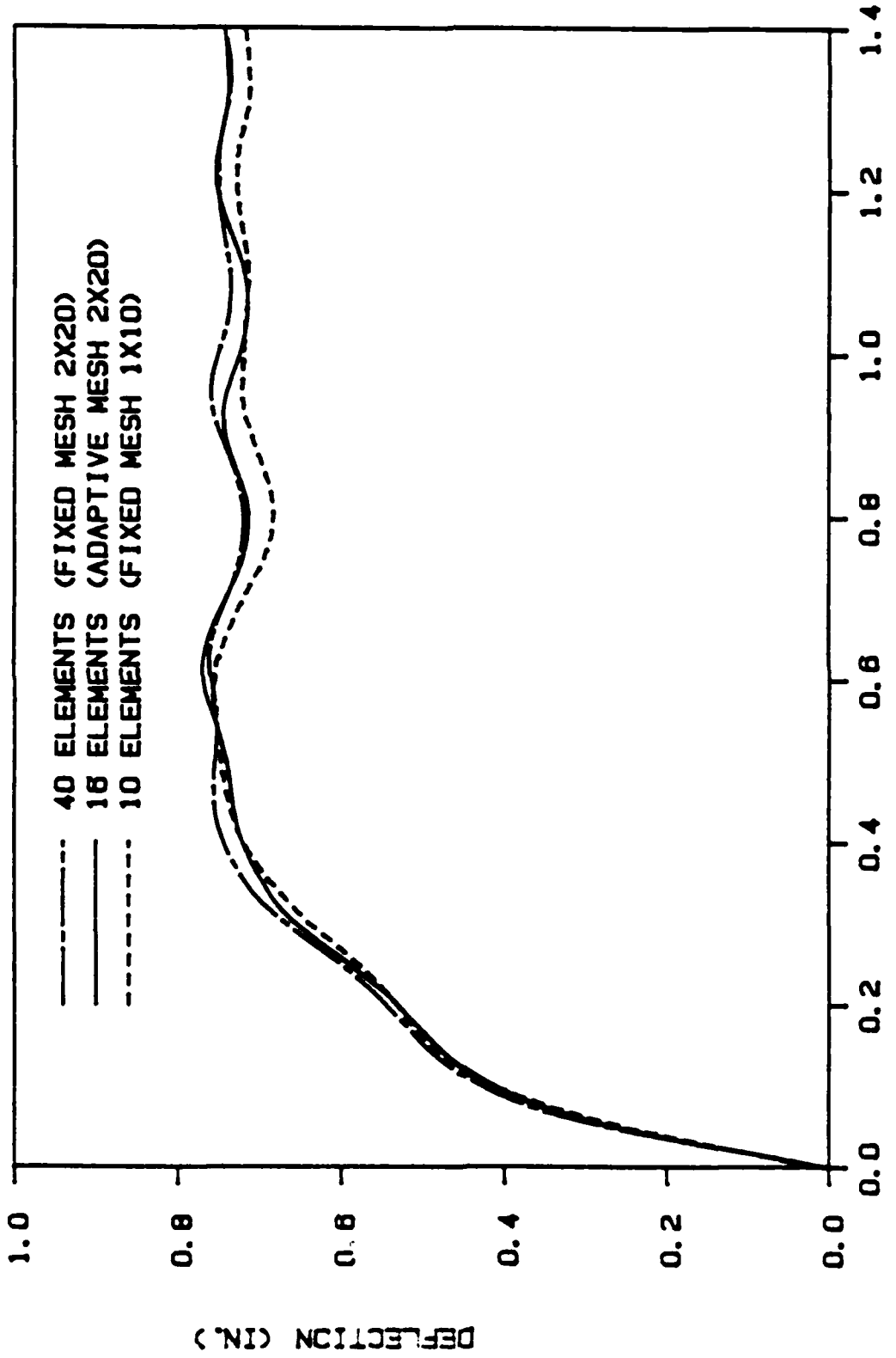
40 ELEMENTS (FIXED MESH 2X20)
16 ELEMENTS (ADAPTIVE MESH 2X20)
10 ELEMENTS (FIXED MESH 1X10)
DEFLECTION (IN.)
1.0
0.8
0.6
0.4
0.2
0.0
0.0
0.2
0.4
0.6
0.8
1.0
1.2
1.4
TIME (MSEC.)

Figure 7

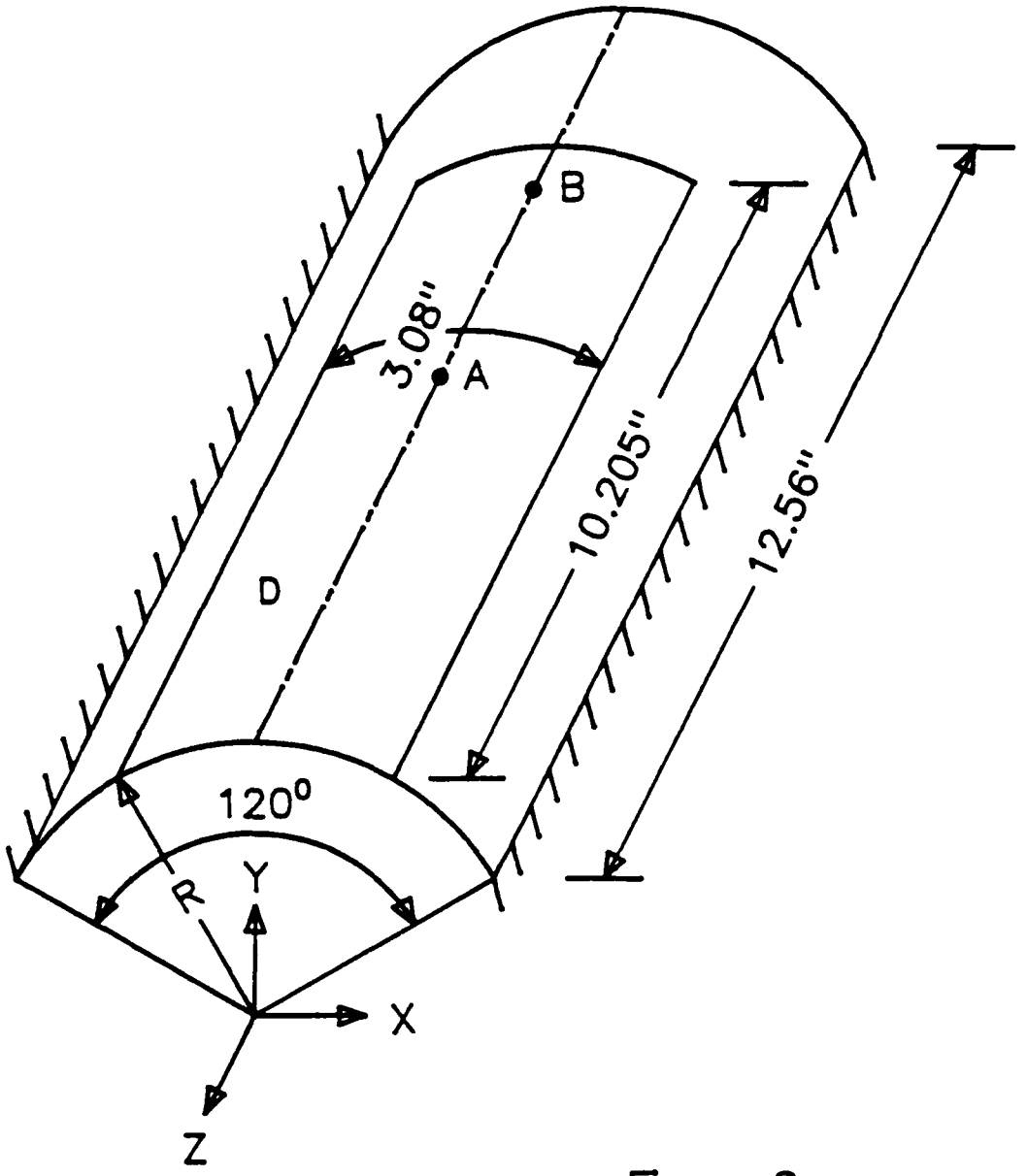

Figure 8

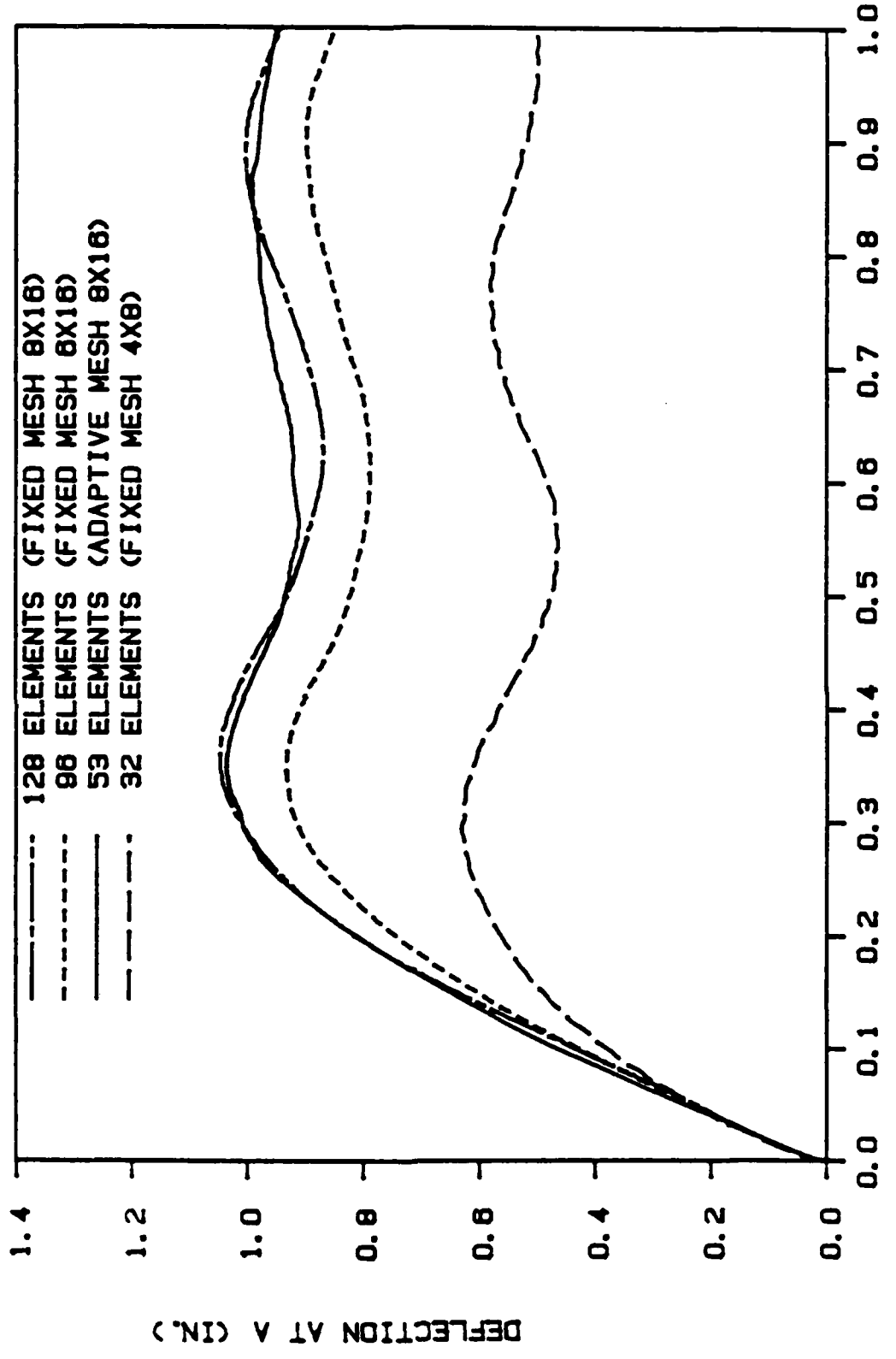
128 ELEMENTS (FIXED MESH 8X16)
98 ELEMENTS (FIXED MESH 8X16)
53 ELEMENTS (ADAPTIVE MESH 8X16)
32 ELEMENTS (FIXED MESH 4X8)
DEFLECTION AT A (IN.)
TIME (MSEC.)
0.0
0.2
0.4
0.6
0.8
1.0
1.2
1.4
0.1
0.3
0.5
0.7
0.9

Figure 9

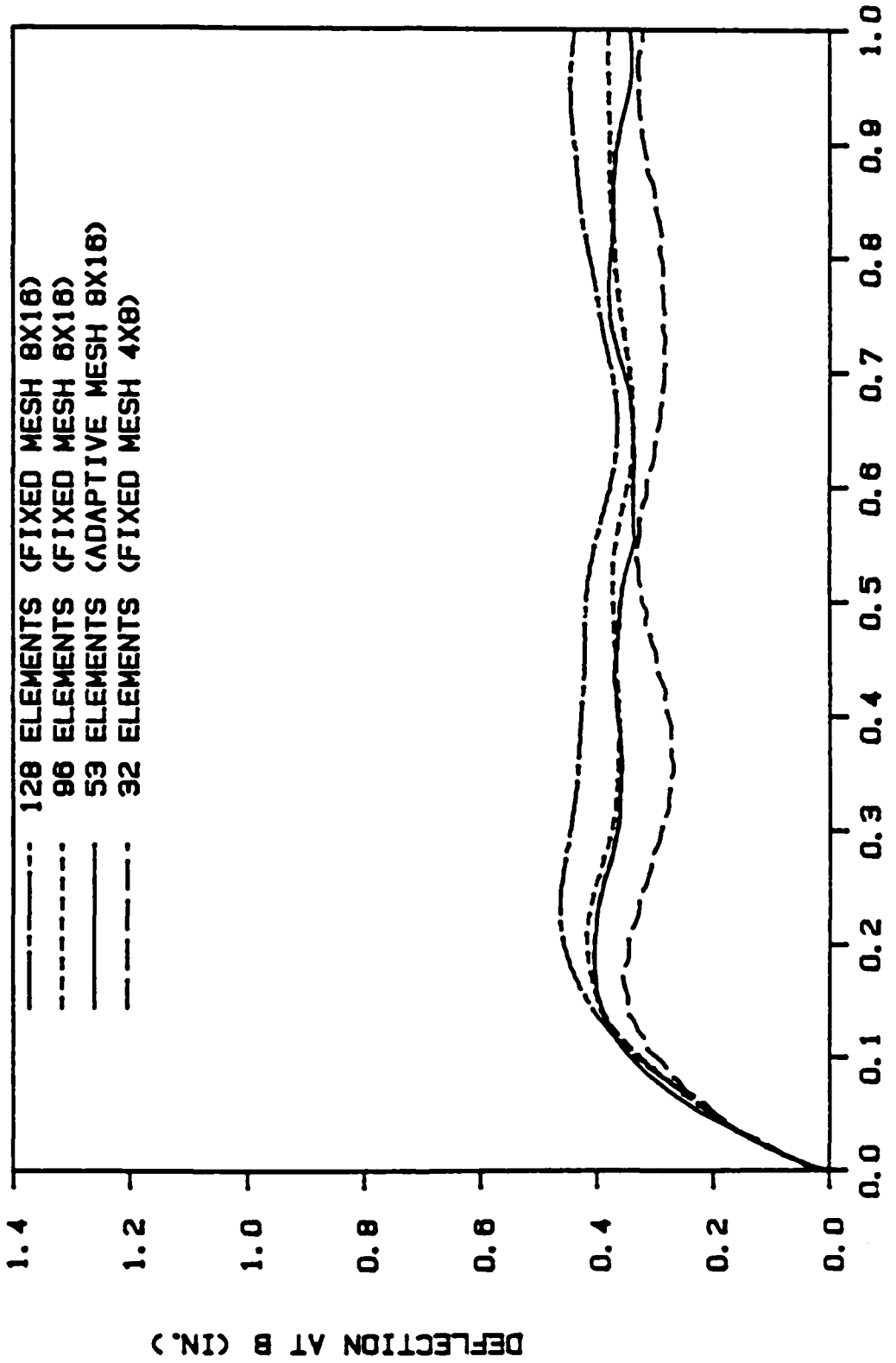
128 ELEMENTS (FIXED MESH 8X16)
96 ELEMENTS (FIXED MESH 6X16)
53 ELEMENTS (ADAPTIVE MESH 8X16)
32 ELEMENTS (FIXED MESH 4X8)
DEFLECTION AT B (IN.)
TIME (MSEC.)
0.0
0.2
0.4
0.6
0.8
1.0
1.2
1.4
0.0
0.1
0.2
0.3
0.4
0.5
0.6
0.7
0.8
0.9
1.0

Figure 10

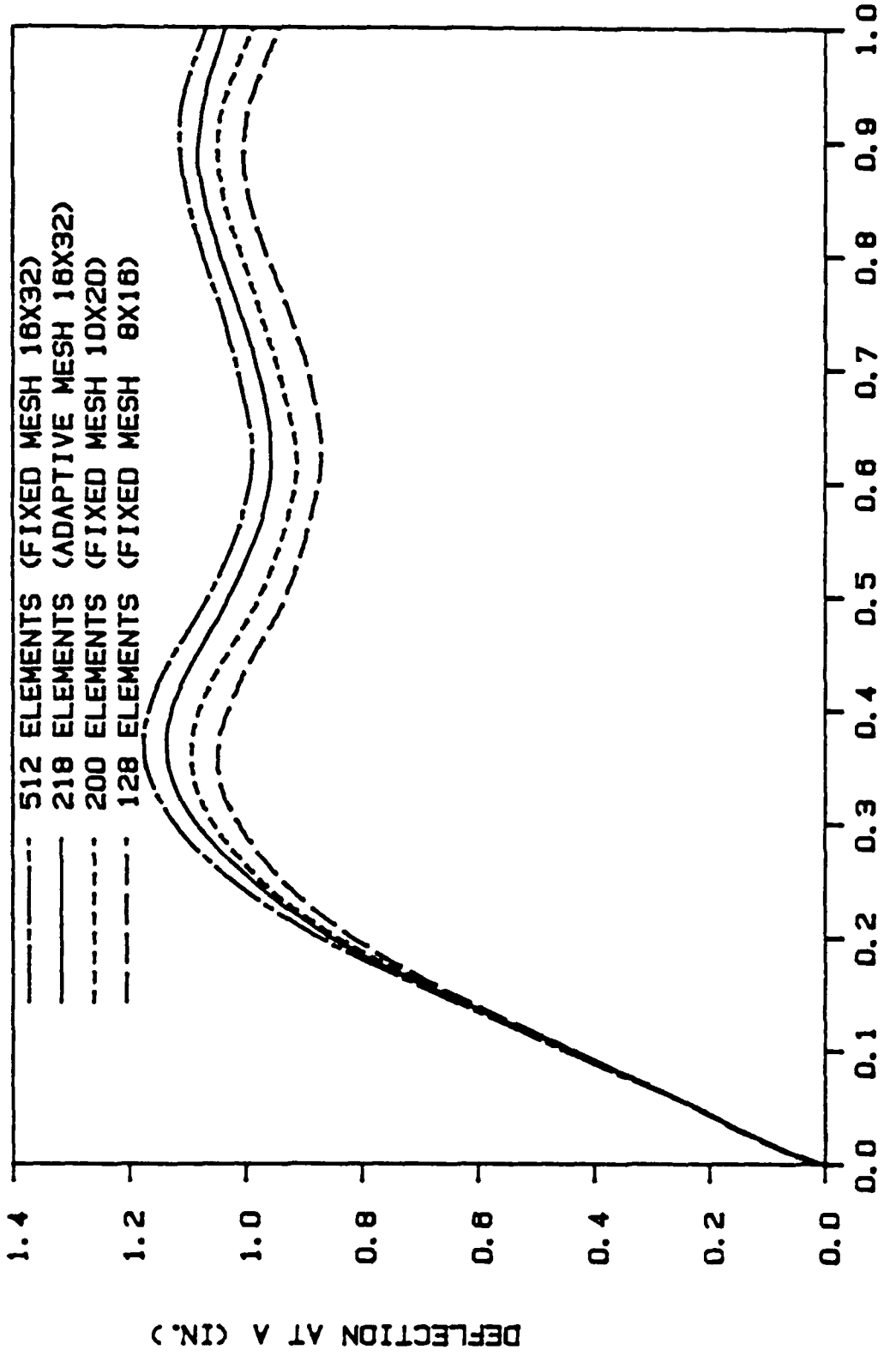
512 ELEMENTS (FIXED MESH 16X32)
218 ELEMENTS (ADAPTIVE MESH 16X32)
200 ELEMENTS (FIXED MESH 10X20)
128 ELEMENTS (FIXED MESH 8X16)
DEFLECTION AT A (IN.)
TIME (MSEC.)
0.0
0.2
0.4
0.6
0.8
1.0
1.2
1.4
0.0
0.1
0.2
0.3
0.4
0.5
0.6
0.7
0.8
0.9
1.0

Figure 11

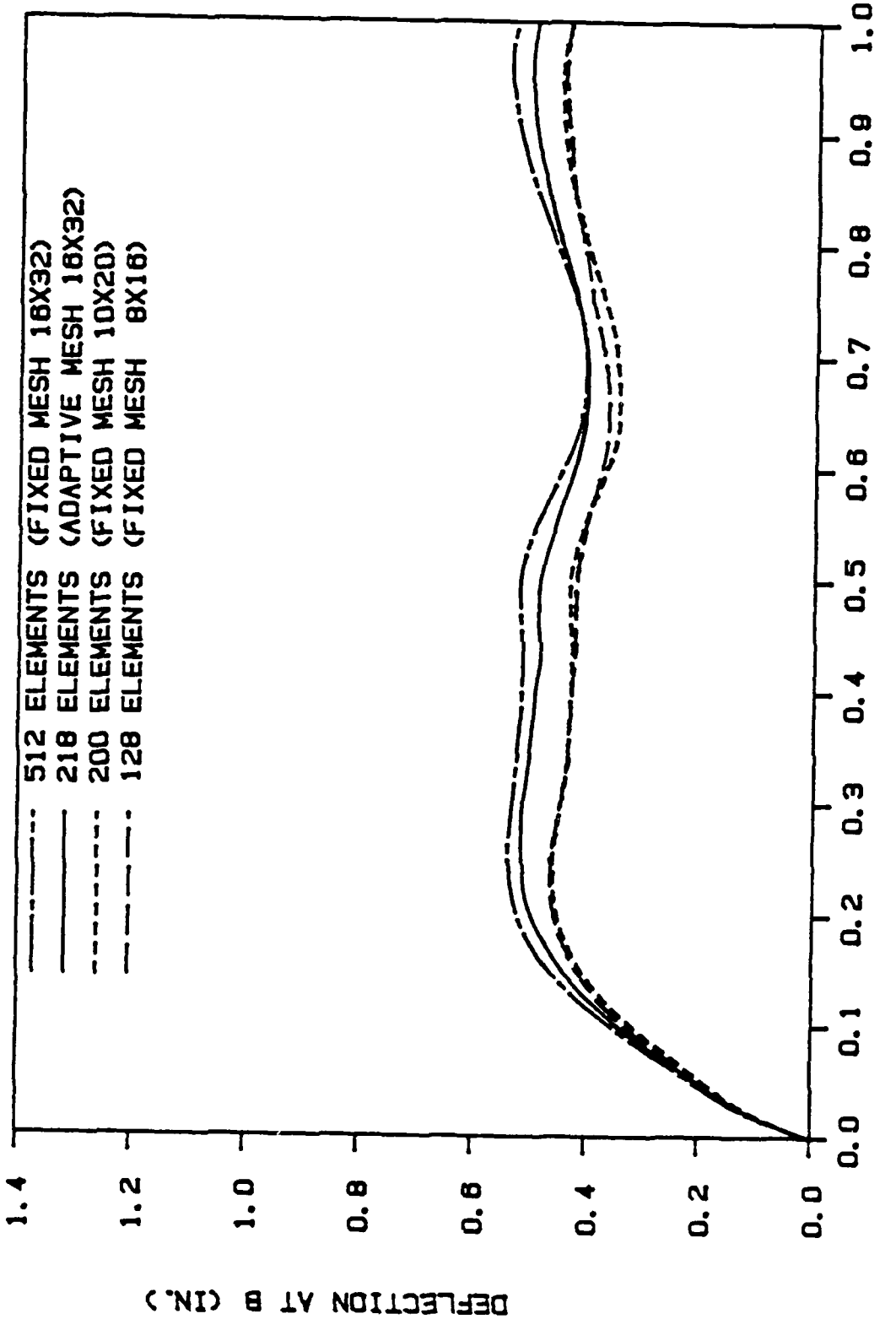
512 ELEMENTS (FIXED MESH 16X32)
218 ELEMENTS (ADAPTIVE MESH 16X32)
200 ELEMENTS (FIXED MESH 10X20)
128 ELEMENTS (FIXED MESH 8X16)
DEFLECTION AT B (IN.)
TIME (MSEC.)
0.0
0.2
0.4
0.6
0.8
1.0
1.2
1.4
0.1
0.3
0.5
0.7
0.9

Figure 12

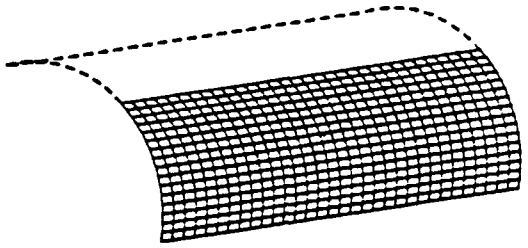

0.000 MS

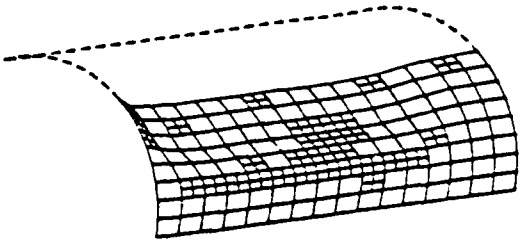

0.100 MS

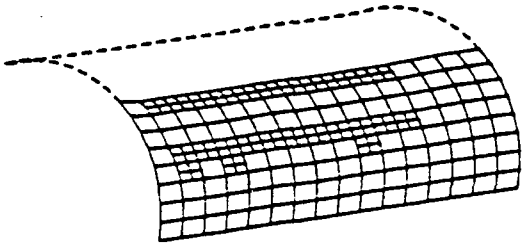

0.0125 MS

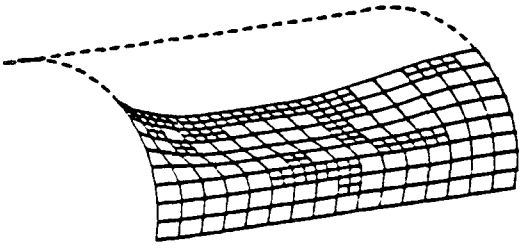

0.200 MS

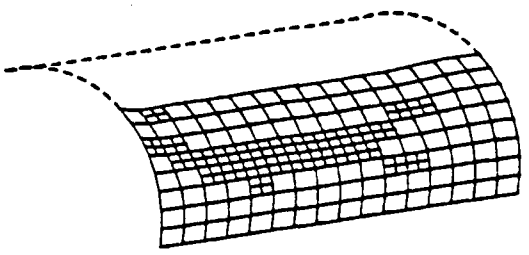

0.025 MS

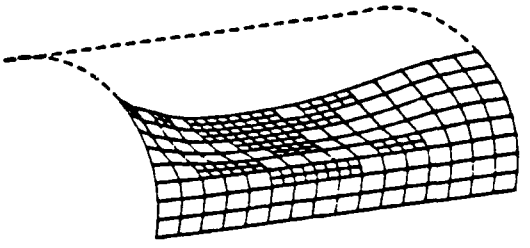

0.250 MS

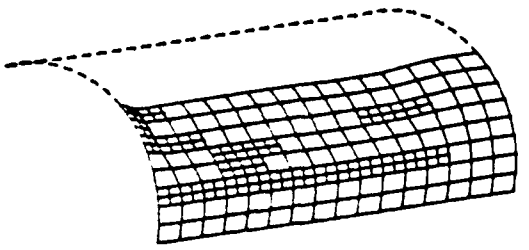

0.050 MS

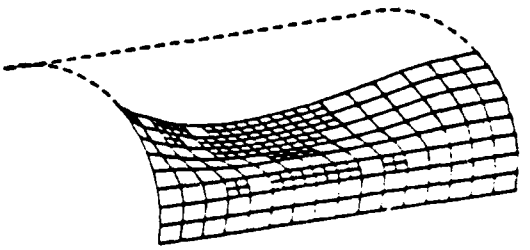

0.300 MS

Figure 13

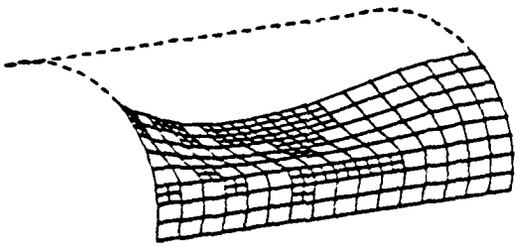

0.350 MS

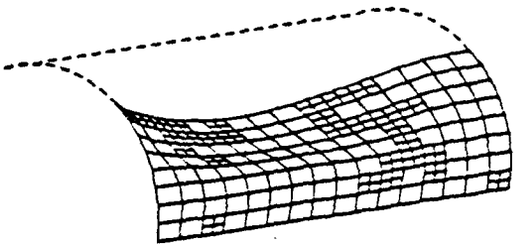

0.700 MS

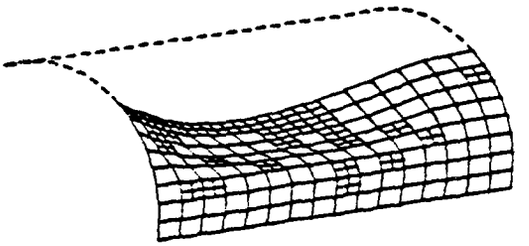

0.400 MS

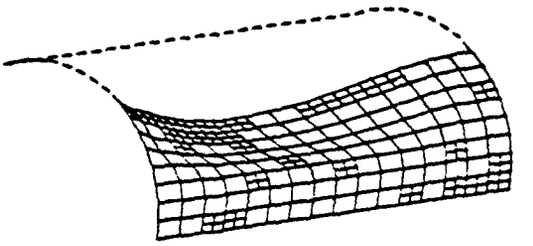

0.800 MS

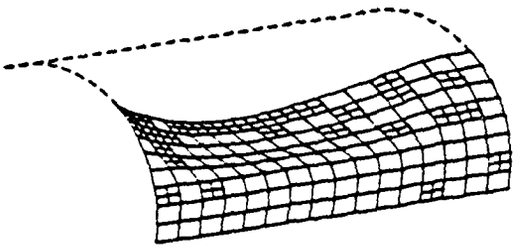

0.500 MS

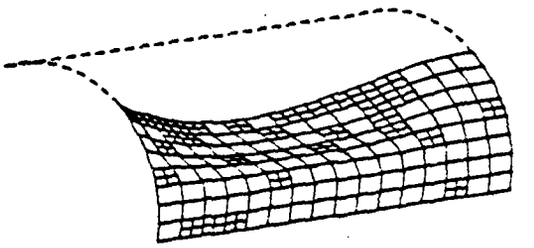

0.900 MS

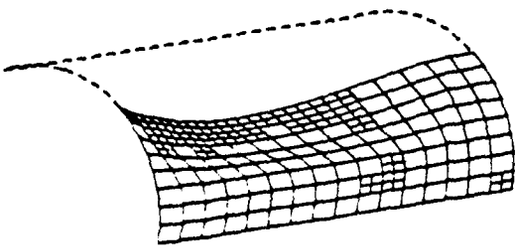

0.600 MS

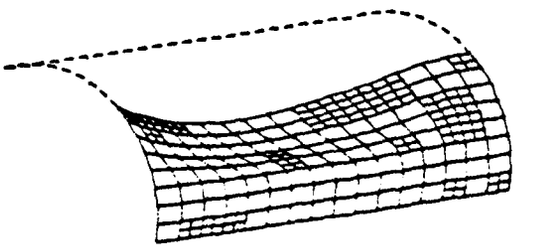

1.000 MS

Figure 13 (Continued)

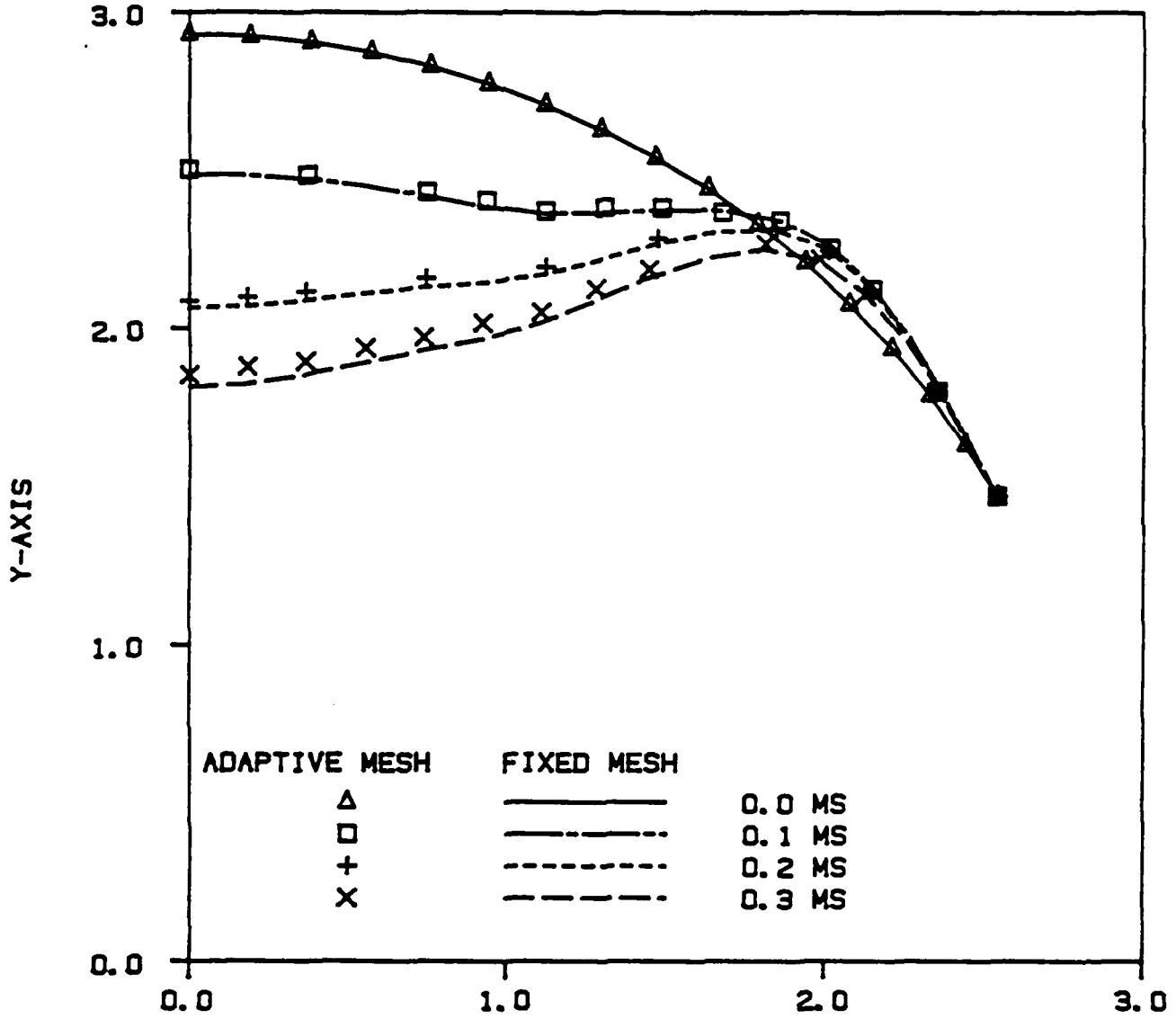
3.0
2.0
1.0
0.0
Y-AXIS
0.0
1.0
2.0
3.0
X-AXIS
ADAPTIVE MESH
FIXED MESH
0.0 MS
0.1 MS
0.2 MS
0.3 MS

Figure 14

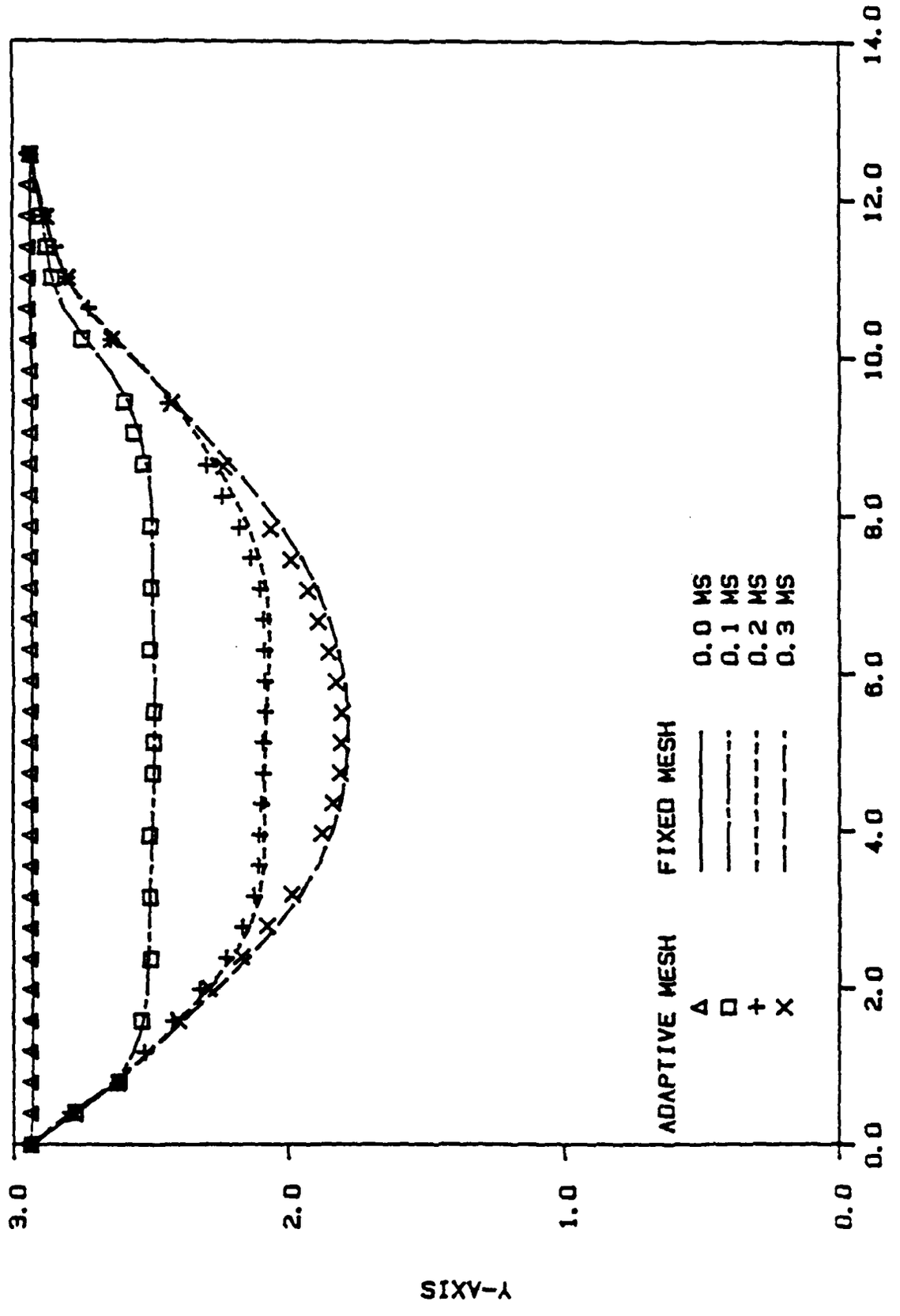
3.0
2.0
1.0
0.0
Y-AXIS
0.0
2.0
4.0
6.0
8.0
10.0
12.0
14.0
Z-AXIS
ADAPTIVE MESH
FIXED MESH
Δ
□
+
X
0.0 MS
0.1 MS
0.2 MS
0.3 MS

Figure 15

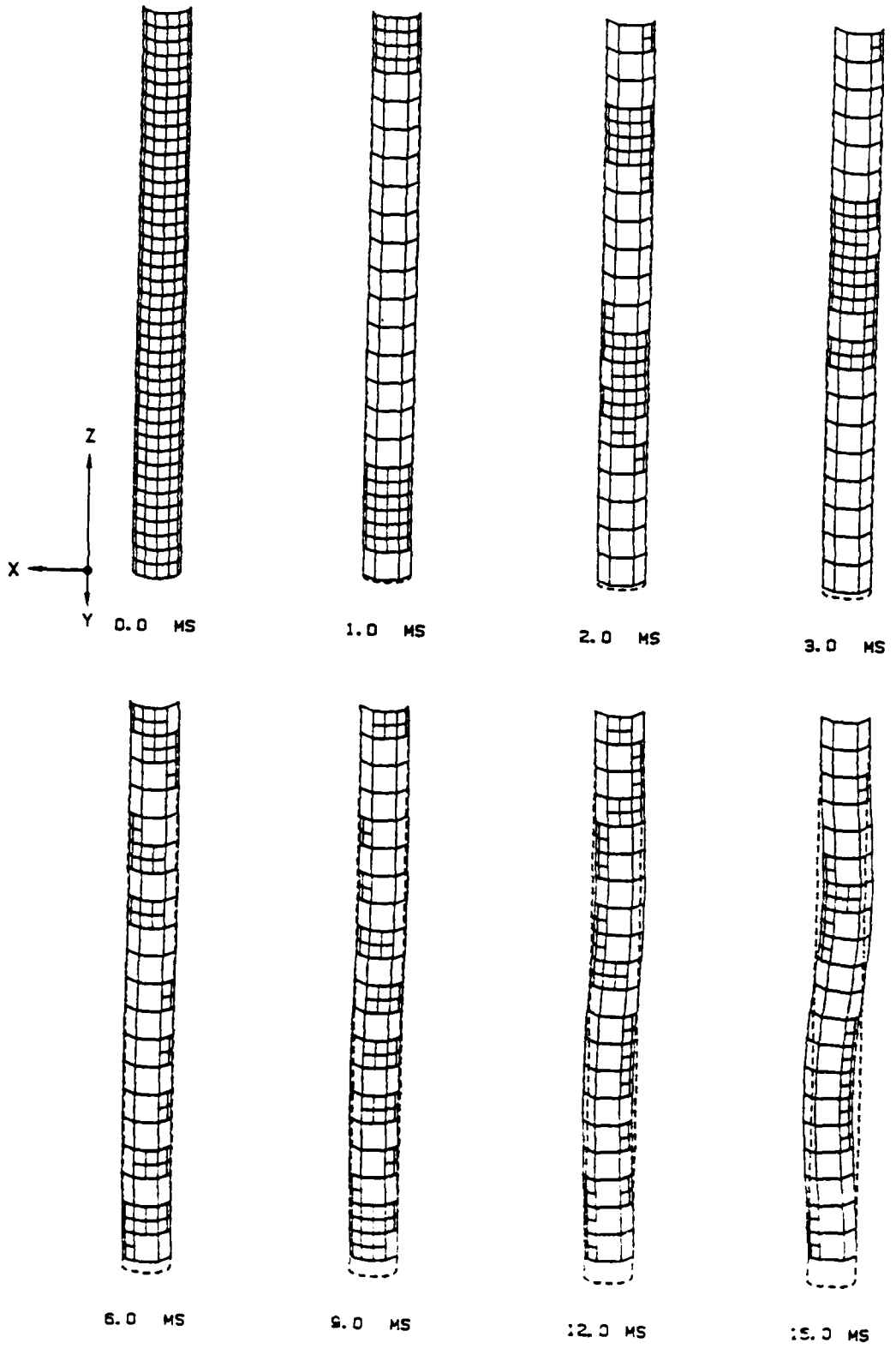

Figure 16

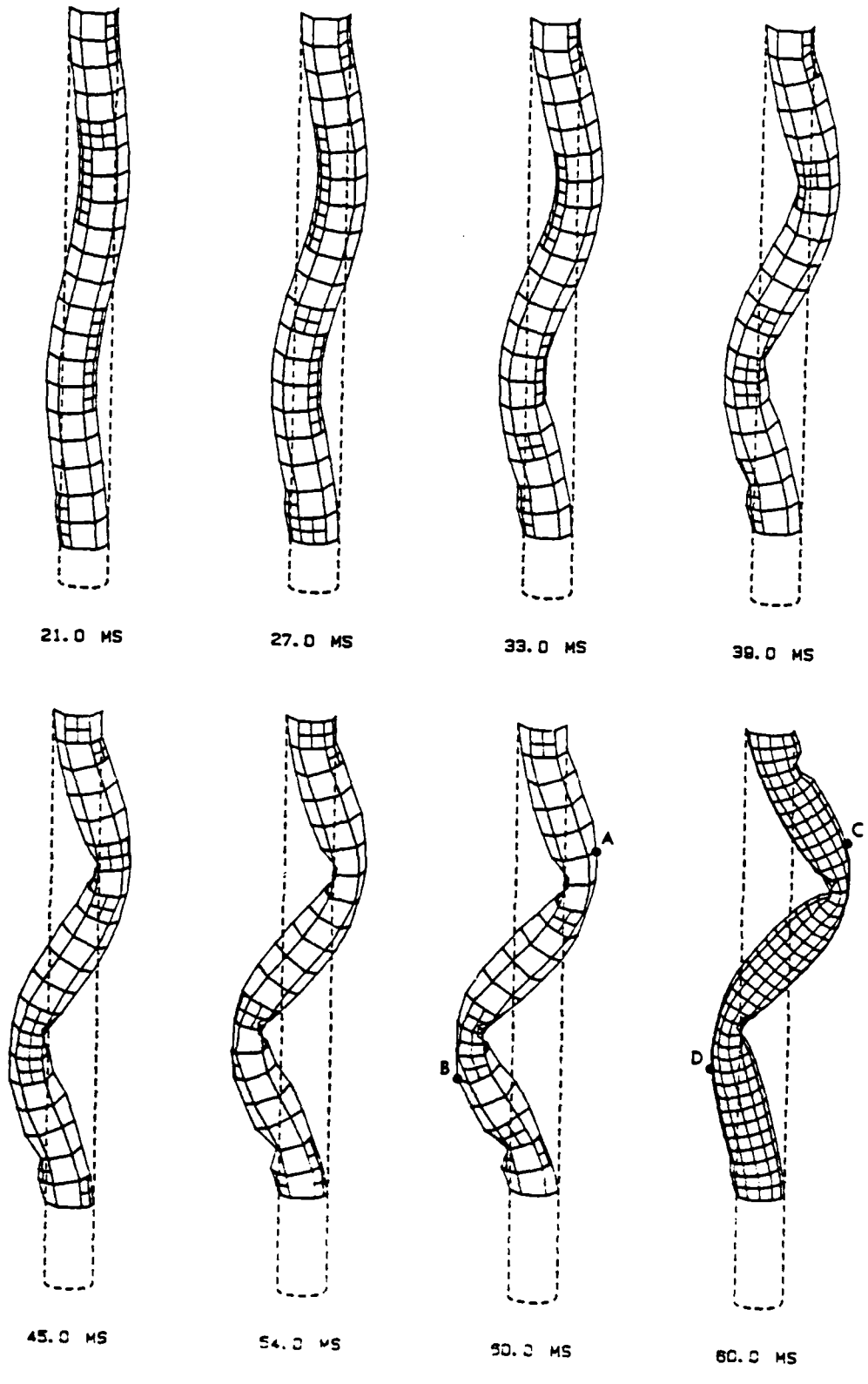

Figure 16 (Continued)

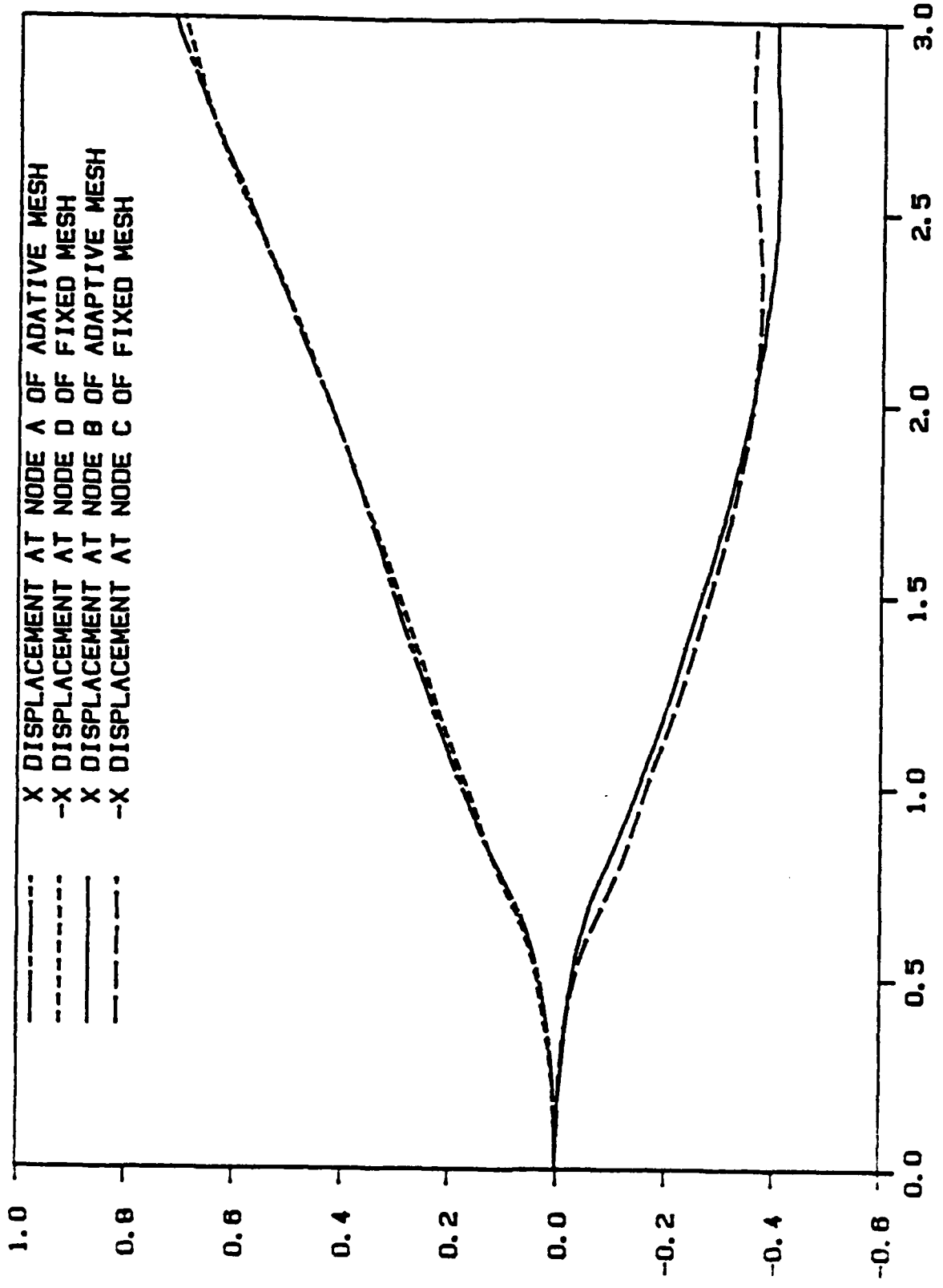
X DISPLACEMENT AT NODE A OF ADATIVE MESH
-X DISPLACEMENT AT NODE D OF FIXED MESH
X DISPLACEMENT AT NODE B OF ADAPTIVE MESH
-X DISPLACEMENT AT NODE C OF FIXED MESH
DISPLACEMENT (X 20 IN.)
1.0
0.8
0.6
0.4
0.2
0.0
-0.2
-0.4
-0.6
0.0
0.5
1.0
1.5
2.0
2.5
3.0
TIME (MSEC.)

Figure 17

APPENDIX

CHAPTER 1

INTRODUCTION

The analysis of shells into the failure domain or post-buckling domain is becoming of increasing importance in the design of certain classes of structures, particulary when the survivability or vulnerability of the structure is a key question. Areas of design in which failure analysis is important are the design of defense structures and in the analysis of re-entry vehicles. In both cases the loads to be sustained are extremely high or the cost of superfluous strength are severe, so it is necessary to be able to predict the behavior of the shell substantially beyond the classical buckling load, because buckling by itself does not constitute failure of the structure. Many structures are in fact designed to buckle and the key question in the survivability or viability of such structures is whether the final displacements and deformations are within design limits. The prediction of the displacements of a shell in such severe environments requires an analysis of the shell structure into the post-buckling regime.

The analysis of shell structures in the post-buckling regime still poses formidable difficulties. The major source of these difficulties is the fact that in the post-buckling regime, high strains and large deformations are often localized in small regions of the shell. Unless very refined meshes are used in the vicinity of these buckles, large errors occur in the predicted deformation of the shell, which detracts severely from the usefulness of the analysis.

This work seeks to remedy these difficulties by developing adaptive mesh techniques for analyzing the post-buckling behavior of shells. The proposed work consists of two major tasks:

1. the development of an effective technique for moving and refining the mesh so that the post-buckling response of shells can be effectively analyzed;
2. the development of methods for integrating the stress tensor in time in history-dependent materials in meshes which move relative to the material.

This report addresses the second question. In particular, some novel methods have been developed which can effectively treat moving meshes for path-dependent materials. The resolution of this difficulty represents a major step toward the ultimate goal.

These adaptive mesh techniques in transient problems are inherently by nature neither Lagrangian nor Eulerian but arbitrary-Eulerian-Lagrangian (ALE) and we will use this terminology here. This concept was first proposed in Noh [1964] under the name "Coupled Eulerian-Lagrangian." Similar applications to compressible flow problems are reported by Trulio [1966]. Later in Hirt et al. [1974], the ALE method is employed in conjunction with an implicit formulation for the solution of two-dimensional flows. In that paper, the calculations for each time step are separated into three phases. The first phase consists of an explicit Lagrangian calculation for the velocities and specific internal energies. Secondly, a Lagrangian implicit iteration procedure adjusts the state variables based on the predicted variables obtained in the first phase. This implicit procedure eliminates the usual Courant-type numerical stability condition. Finally, in the rezoning phase, the convective fluxes for the conservation equations are computed to account for the mesh motions. An extended version of this computational technique to three-dimensional flows contained within arbitrarily shaped or moving boundaries is reported in Pracht [1975] and Stein et al. [1977].

The ALE method was introduced into the finite element method in Donea et al. [1977] and Belytschko and Kennedy [1978] in response to the need for nonlinear simulation techniques in nuclear safety analyses. The advantages of the ALE method in fluid-structure interaction are apparent since the fluid domain can be teated by the ALE formulation and the structural domain can be handled by the usual Lagrangian description. In these articles, the effort is primarily directed toward inviscid compressible fluids, while in Hughes et al. [1978], a finite element procedure for viscous incompressible flows and free surface flows is presented in conjunction with a general kinematical theory for the ALE description. A similar formulation has later been reported in Liu and Ma [1982]. The capability of ALE method to handle an expanding gas bubble immersed in a fluid has been demonstrated in Belytschko et al. [1982]. The mesh motions for this problem are prescribed according to a simple control algorithm in which the boundary nodes are considered Lagrangian and the mesh velocities for the intermediate nodes are lineary interpolated between the boundary velocities.

Recently, the application of the ALE concept to contact problems between flexible structures is proposed in Haber and Abel [1983] in which the displacement vector is separated into the Lagrangian and Eulerian parts. The slip compatibility conditions are met by making the Lagrangian displacements common to elements on either side of the interface. Separate Eulerian displacements are associated with elements on one side of the interface to model the slip conditions. This concept is extended in Haber [1984] for quasi-static solid mechanics and Haber and Koh [1985].

The articles cited above are mainly directed toward linear path-independent materials like Hookean solids and Newtonian fluids. The stress states for these materials are solely determined by the displacement or

velocity fields. When the ALE method is applied to materials with memory, the state variables for an element are affected by the migration of material points which may carry different stress and strain histories. This difficulty arises because the adaptive or ALE mesh does not model the same set of material points throughout the simulation. A similar situation is encountered in Derbalian et al. [1978] when the Eulerian description is employed for plastic forming analysis. In this paper, the difficulty is side-stepped by interpolating the stress histories at each incremental step.

Obviously, a consistent treatment for the transport of the histories of all path-dependent quantities through the mesh is necessary for the analysis of these materials. It is therefore the purpose of the current effort to develop a general formulation and an explicit computational procedure for nonlinear adoptive finite element analyses. Furthermore, to provide a better understanding of the adaptive methods in nonlinear mechanics, the linearization procedure for the equilibrium equation is addressed in this work to examine some features of the method.

The scope of the present investigation is arranged as follows. In Chapter 2, the notations for material, spatial, and referential coordinates are introduced. The relationship between the material and referential time derivatives is reviewed with the definition of the relative velocity between the material and mesh velocities. The balance laws, which include the continuity equation, momentum equation and energy equation, constitutive equations, and equation of state in the adaptive description are reviewed. The stress-velocity product is defined to circumvent the difficulty associated with treating the gradient of the stresses in the constitutive equation. The weak formulation and matrix equations are derived. Based on the principle of virtual work, the linearization procedure in the adaptive description is

performed for the Cauchy stress and velocity gradient. The resulting rate form for the virtual internal energy has a strong resemblance to the Lagrangian description. The tangent stiffness matrices consist of two parts: the first one is identical to the Lagrangian description and the second part arises when the ALE description is employed. The explicit expressions for these two matrices are given, and the latter for the contributions from the ALE description.

Numerical methods for the ALE equations are detailed in Chapter 3. Techniques for nonlinear convective effects, which characterize the ALE description, are reviewed. These include the upwind method, Petrov-Galerkin, and Taylor-Galerkin formulations. The difficulty of treating the gradient of stresses in the ALE description is discussed. The remedy of this issue is separated into two parts. The first part includes the construction of the stress-velocity product in conjunction with an artificial viscosity technique to achieve the streamline upwind effect. The determination of the artificial viscosity parameter is accomplished by recourse to the analytic solutions for a one-dimensional constitutive eqution. A collocation weighted residual formulation for the constitutive equation is presented in the second part. This procedure is formulated such that it can handle any number of quadrature points for the family of displacement elements. An efficient two-quadrature point element suitable for nonlinear calculations is discussed. The usage of this element to account for both the geometric and material nonlinearities is described. An explicit time integration algorithm based on the predictor-corrector method is presented. Several numerical examples are analyzed to demonstrate the effectiveness of the present development.

CHAPTER 2

ARBITRARY LAGRANGIAN-EULERIAN FORMULATION OF FIELD EQUATIONS

2.1 Review of Governing Equations in Arbitrary Lagrangian-Eulerian Description

The material, spatial, and referential coordinates are denoted by $\underset{\sim}{X}$, $\underset{\sim}{x}$ and $\underset{\sim}{\chi}$, respectively. Throughout this dissertation, standard indicial notation is adopted; lower case subscripts denote the components of a tensor and repeated subscripts imply a summation over the number of space dimensions (NSD). A comma followed by a subscript designates the partial derivative with respect to the corresponding spatial variable.

The superposed dot and star denote the time derivative with the material and referential coordinates fixed, respectively. The relationship between these two derivatives are expressed here as [Hughes et al., 1978]

$$(\dot{}) = (^{*}) + c_i(\ )_{,i} \tag{2.1}$$

where c_i is the relative velocity between the material (v_i) and mesh velocity ($\hat{v}_i$),

$$c_i = v_i - \hat{v}_i \tag{2.2}$$

The term $c_i(\ )_{,i}$ in Eq. (2.1) represents the convective effect due to

the relative motion between the material and the mesh. In particular, when $\underset{\sim}{c}$ is chosen to be $\underset{\sim}{v}$, i.e., $\underset{\sim}{\chi} = \underset{\sim}{x}$, the familiar Eulerian time derivative is obtained.

The equations which govern the continuum in the ALE description are the three conservation laws [Donea, 1977]

<u>mass</u>: $$\overset{*}{\rho} + c_i \rho_{,i} = -\rho v_{i,i} \tag{2.3}$$

<u>momentum</u>: $$\rho \overset{*}{v_i} + \rho c_j v_{i,j} = \tau_{ij,j} + b_i \tag{2.4}$$

<u>energy</u>: $$\rho \overset{*}{e} + \rho c_i e_{,i} = \tau_{ij} v_{(i,j)} + \rho a - q_{i,i} \tag{2.5}$$

The Cauchy stress may be decomposed into the deviatoric stress tensor s_{ij} and the hydrostatic pressure p

$$\tau_{ij} = s_{ij} - p\delta_{ij} \tag{2.6}$$

which are given by the rate constitutive equation

$$\overset{*}{s}_{ij} + c_k s_{ij,k} = C_{ijkl} v_{(k,l)} + s_{kj} v_{[i,k]} + s_{ki} v_{[j,k]} \tag{2.7}$$

and the equation of state

$$\overset{*}{p} + c_i p_{,i} = P(\rho, e) \tag{2.8}$$

respectively. In the above, ρ is the density; b_i is the body force per unit volume; e is the internal energy; δ_{ij} is the Kronecker delta; $p(\rho,e)$ is the function for the equation of state; $v_{(i,j)}$ is the velocity strain tensor

$$v_{(i,j)} = \frac{1}{2}(v_{i,j} + v_{j,i}) \tag{2.9}$$

and $v_{[i,j]}$ is the spin tensor

$$v_{[i,j]} = \frac{1}{2}(v_{i,j} - v_{j,i}) \tag{2.10}$$

a is the internal heat generation; q_i is the heat flux; and C_{ijkl} is the material response tensor which relates any frame-invariant rate of the Cauchy stress [Prager, 1961] to the velocity strain. Both geometric and material nonlinearities are included in the setting of Eqs. (2.3-8).

REMARK 2.1.1: The right hand sides of Eqs. (2.3-5,2.7-8) remain the same for all descriptions [Liu, 1984].

REMARK 2.1.2: Eqs. (2.3-5,2.7-8) are referred as the "quasi-Eulerian" description in Belytschko et al. [1980] because these equations have a strong resemblance to the Eulerian equations. In particular, the Eulerian equations can be readily obtained by choosing $\underset{\sim}{\chi} = \underset{\sim}{v}$, i.e., $\underset{\sim}{\chi} = \underset{\sim}{x}$.

REMARK 2.1.3: Eq. (2.7) is equivalent to the following equations:

$$\overset{*}{s}_{ij} + y_{ijk,k} - c_{k,k}s_{ij} = C_{ijk\ell}v_{(k,\ell)} + s_{kj}v_{[i,k]} + s_{ki}v_{[j,k]} \tag{2.11}$$

and

$$y_{ijk} = s_{ij}c_k \tag{2.12}$$

where y_{ijk} is the stress-velocity product. In the following finite element computation, these two equations will replace Eq. (2.7) in the weak form; see Section 3.3 for a discussion.

2.2 Finite Element Equations

The variational equations corresponding to the conservation equations, Eqs. (2.3-5,2.7-8), are obtained by multiplying by the test functions, $\delta\rho$, δv_i, δe, δs_{ij}, δy_{ijk} and δp, over the spatial domain R_x, and employing the divergence theorem to imbibe the traction force vector $\underline{h}$ on the boundary Γ_x^h and the amount of heat ϑ transmitted through Γ_x^ϑ.

mass

$$\int_{R_x} \delta\rho \overset{*}{\rho} dR_x + \int_{R_x} \delta\rho c_i \rho_{,i} dR_x = -\int_{R_x} \delta\rho \rho v_{i,i} dR_x \tag{2.13}$$

momentum

$$\int_{R_x} \rho\delta v_i \overset{*}{v}_i dR_x + \int_{R_x} \rho\delta v_i c_j v_{i,j} dR_x = -\int_{R_x} \delta v_{i,j} \tau_{ij} dR_x$$

$$+ \int_{R_x} \delta v_i b_i dR_x + \int_{\Gamma_x^h} \delta v_i h_i d\Gamma_x \tag{2.14}$$

energy

$$\int_{R_x} \rho\delta e \overset{*}{e} dR_x + \int_{R_x} \rho\delta e c_i e_{,i} dR_x = \int_{R_x} \delta e_{,i} q_i dR_x + \int_{R_x} \delta e \tau_{ij} v_{(i,j)} dR_x$$

$$+ \int_{R_x} \delta e \rho a dR_x - \int_{\Gamma_x^\vartheta} \delta e \vartheta d\Gamma_x \tag{2.15}$$

constitutive

$$\int_{R_x} \delta s_{ij} \overset{*}{s}_{ij} dR_x + \int_{R_x} \delta s_{ij} y_{ijk,k} dR_x - \int_{R_x} \delta s_{ij} c_{k,k} s_{ij} dR_x$$

$$= \int_{R_x} \delta s_{ij} C_{ijk\ell} v_{(k,\ell)} dR_x + \int_{R_x} \delta s_{ij} \{ s_{kj} v_{[i,k]} + s_{ki} v_{[j,k]} \} dR_x \tag{2.16}$$

and

$$\int_{R_x} \delta y_{ijk} y_{ijk} dR_x = \int_{R_x} \delta y_{ijk} s_{ij} c_k dR_x \tag{2.17}$$

equation of state

$$\int_{R_x} \delta p \overset{*}{p} dR_x + \int_{R_x} \delta p c_i p_{,i} dR_x = \int_{R_x} \delta p p(\rho,e) dR_x \tag{2.18}$$

Eq. (2.13) and Eq. (2.15) represent the control volume forms of material and energy conservation, respectively. Eq. (2.14) is a generalization of the principle of virtual work to the control volume form with the first integral brought in as d'Alembert forces.

In finite element methods, the domain of interest R_x is subdivided into elements. Different sets of shape functions, $\underset{\sim}{\ell}$, $\underset{\sim}{\ell}^{\rho}$, $\underset{\sim}{\ell}^{e}$, $\underset{\sim}{\ell}^{s}$, $\underset{\sim}{\ell}^{y}$ and $\underset{\sim}{\ell}^{p}$, and corresponding sets of test functions, $\bar{\underset{\sim}{\ell}}$, $\bar{\underset{\sim}{\ell}}^{\rho}$, $\bar{\underset{\sim}{\ell}}^{e}$, $\bar{\underset{\sim}{\ell}}^{s}$, $\bar{\underset{\sim}{\ell}}^{y}$ and $\bar{\underset{\sim}{\ell}}^{p}$, are introduced to interpolate the velocity, density, internal energy, deviatoric stress, stress-velocity product $\underset{\sim}{y}$ and hydrostatic pressure, respectively. Note that the test functions and shape functions for deviatoric stresses are used only in the

constitutive equations. The matrix equations corresponding to Eqs. (2.13-18) are:

<u>mass</u> $$\underset{\sim}{M}^{\rho}\dot{\underset{\sim}{\rho}} + \underset{\sim}{N}^{\rho}\underset{\sim}{\rho} + \underset{\sim}{K}^{\rho}\underset{\sim}{\rho} = \underset{\sim}{0} \tag{2.19}$$

<u>momentum</u> $$\underset{\sim}{M}\dot{\underset{\sim}{v}} + \underset{\sim}{N}\,\underset{\sim}{v} + \underset{\sim}{f}^{int} = \underset{\sim}{f}^{ext} \tag{2.20}$$

<u>energy</u> $$\underset{\sim}{M}^{e}\dot{\underset{\sim}{e}} + \underset{\sim}{N}^{e}\underset{\sim}{e} + \underset{\sim}{g} = \underset{\sim}{r} \tag{2.21}$$

<u>constitutive</u> $$\underset{\sim}{M}^{s}\dot{\underset{\sim}{s}} + \underset{\sim}{G}^{T}\underset{\sim}{y} - \underset{\sim}{D}\,\underset{\sim}{s} = \underset{\sim}{z} \tag{2.22}$$

and

$$\underset{\sim}{M}^{y}\underset{\sim}{y} = \underset{\sim}{N}^{y}\underset{\sim}{s} \tag{2.23}$$

<u>equation of state</u> $$\underset{\sim}{M}^{p}\dot{\underset{\sim}{p}} + \underset{\sim}{N}^{p}\underset{\sim}{p} = \underset{\sim}{u} \tag{2.24}$$

The superscript "T" denotes matrix transpose; $\underset{\sim}{M}$, $\underset{\sim}{M}^{\rho}$, $\underset{\sim}{M}^{e}$, $\underset{\sim}{M}^{s}$, $\underset{\sim}{M}^{y}$ and $\underset{\sim}{M}^{p}$ are the generalized mass matrices for the corresponding variables in Eqs. (2.19-24), respectively; $\underset{\sim}{N}$, $\underset{\sim}{N}^{\rho}$, $\underset{\sim}{N}^{e}$, $\underset{\sim}{N}^{y}$ and $\underset{\sim}{N}^{p}$ are the generalized convective matrices; $\underset{\sim}{K}^{\rho}$ is the stiffness matrix for density; $\underset{\sim}{f}^{int}$ is is the internal force vector; $\underset{\sim}{f}^{ext}$ is the external load vector; $\underset{\sim}{g}$ is the conductance vector; $\underset{\sim}{r}$ is the generalized energy source vector; $\underset{\sim}{G}$ is the divergence operator matrix; $\underset{\sim}{D}$ is the generalized diffusion matrix for the deviatoric stress; $\underset{\sim}{z}$ and $\underset{\sim}{u}$ are the generalized deviatoric stress and pressure vectors, respectively. The definitions for these matrices and vectors are given in Appendix A.

REMARK 2.2.1: The nonlinear convective terms, which characterize the ALE method, inevitably pose difficulties. Recently, finite element methods for non-self-adjoint systems (see Section 3.2 for a discussion) have been developed which do not suffer from crosswind diffusion when applied to the multi-dimensional convection-diffusion problems. These methods may be applied to handle the convective terms in Eqs. (2.19-21,2.23-24).

REMARK 2.2.2: All the matrices and vectors defined in Appendix A are integrated over the spatial domain R_x which changes continuously throughout the computation.

REMARK 2.2.3: The stress-velocity product $\underset{\sim}{y}$ is stored at each node as a vector with a dimension of (number of space dimensions)x(number of stress components). The diagonal form for $\underset{\sim}{M}^y$ is obtained by locating the numerical integration points at the nodes.

REMARK 2.2.4: A procedure for the stress update equations (2.22-23) is presented in the next chapter to clarify the temporal integration for path-dependent materials. All the path-dependent quantities are updated analogous to Eqs. (2.22-23). To the author's knowledge, it is a new approach to calculate the stress states for path-dependent materials in the ALE description.

2.3 Finite Element Formulation by the Principle of Virtual Work

The finite element procedure presented in the preceding section is formulated in the spatial domain and the Cauchy stress and the velocity strain are employed to measure the stress and strain states. In this section, the ALE finite element for the equilibrium equation is formulated with a recourse to the principle of virtual work in the referential system. It should be noted that the linearization procedures in this section are performed by keeping the referential coordinates constant which is in contrast to the usual rate formulations with the material coordinates held constant.

Denoting a virtual variation of displacement by δu_i, the principle of virtual work requires [Malvern, 1965]

$$\int_{R_x} \delta u_{i,j} \tau_{ij} dR_x = \int_{\Gamma_x^h} \delta u_k h_k d\Gamma_x + \int_{R_x} \delta u_k b_k dR_x \tag{2.25}$$

where the integration extends over the spatial domain. This expression may be transformed to the referential coordinate system as follows:

$$\int_{R_\chi} \frac{\partial \delta u_i}{\partial \chi_m} \frac{\partial \chi_m}{\partial x_j} \tau_{ij} J dR_\chi = \int_{\Gamma_\chi^h} \delta u_k h_k J^s d\Gamma_\chi + \int_{R_\chi} \delta u_k b_k J dR_\chi \tag{2.26}$$

In the above, J^s is the scalar ratio of differential areas $d\Gamma_x/d\Gamma_\chi$ and J is the determinant of the mapping tensor between spatial and referential coordinates given by

$$J = \det\left(\frac{\partial \underset{\sim}{x}}{\partial \underset{\sim}{\chi}}\right) \tag{2.27}$$

Eq. (2.26) can be recognized as the balance of virtual internal and external energy integrated over the referential coordinates.

$$W_{int} = W_{ext} \tag{2.28}$$

The tangent stiffness matrix corresponding to Eq. (2.26) can be obtained by considering the rate form for the virtual internal energy with the referential configuration held constant:

$$\overset{*}{W}_{int} = \int_{R_\chi} \frac{\partial \delta u_i}{\partial \chi_m} \left[\left(\frac{\partial \overset{*}{\chi}_m}{\partial x_j}\right) \tau_{ij} J + \frac{\partial \chi_m}{\partial x_j} \overset{*}{\tau}_{ij} J + \frac{\partial \chi_m}{\partial x_j} \tau_{ij} \overset{*}{J}\right] dR_\chi \tag{2.29}$$

As can be seen, three rate quantities reside in Eq. (2.29). The first rate term can be manipulated by considering the rate form for the identity

$$\frac{\partial \chi_m}{\partial x_j} \frac{\partial x_k}{\partial \chi_m} = \delta_{jk} \tag{2.30}$$

and it can be shown that

$$\left(\frac{\partial \overset{*}{\chi}_m}{\partial x_j}\right) \frac{\partial x_k}{\partial \chi_m} = - \frac{\partial \chi_n}{\partial x_j} \frac{\partial \overset{*}{x}_k}{\partial \chi_n} \tag{2.31}$$

With the substitution of mesh velocity [Hughes et al., 1978]

$$\hat{v}_k = \overset{*}{x}_k \tag{2.32}$$

Eq. (2.31) takes the form

$$\left(\frac{\partial \overset{*}{\chi}_m}{\partial x_j}\right) = -\frac{\partial \chi_m}{\partial x_k}\frac{\partial \chi_n}{\partial x_j}\frac{\partial \hat{v}_k}{\partial \chi_n}$$

$$= -\frac{\partial \chi_m}{\partial x_k}\frac{\partial \hat{v}_k}{\partial x_j} \tag{2.33}$$

The second rate term in Eq. (2.29) involves the rate of change of the Cauchy stress tensor which has been shown in Eq. (2.7)

$$\overset{*}{\tau}_{ij} = -c_k \tau_{ij,k} + C_{ijk\ell}{}^{v}(k,\ell) + S_{ijk\ell}{}^{v}[k,\ell] \tag{2.34}$$

In this equation, $-c_k \tau_{ij,k}$ is the transport of the stress histories. The term $C_{ijk\ell}{}^{v}(k,\ell)$ can be interpreted as the pure deformation part for the rate of change of the Cauchy stress. The fourth order generalized material response tensor $C_{ijk\ell}$ is

$$C_{ijk\ell} = C^{c}_{ijk\ell} \tag{2.35}$$

if the Jaumann stress rate [Prager, 1961] is used, whereas

$$C_{ijk\ell} = C^{c}_{ijk\ell} + C^{*}_{ijk\ell} \tag{2.36}$$

if the Truesdell stress rate is employed. The fourth order tensor $C^{*}_{ijk\ell}$ is given by

$$C^{*}_{ijk\ell} = -\tau_{ij}\delta_{k\ell} + \frac{1}{2}(\tau_{i\ell}\delta_{jk} + \tau_{j\ell}\delta_{ik} + \tau_{ik}\delta_{j\ell} + \tau_{jk}\delta_{i\ell}) \tag{2.37}$$

For most of the currently used material models, the material response tensor $C^{c}_{ijk\ell}$ possesses both major and minor symmetries. Several examples for the generalized material response tensor have been discussed in Liu [1984] which will not be repeated in the present study. The term $S_{ijk\ell}v_{[k,\ell]}$ in Eq. (2.34) is the rotational part for the rate of change of Cauchy stress and the fourth order tensor $S_{ijk\ell}$ is given by

$$S_{ijk\ell} = \frac{1}{2}(\tau_{i\ell}\delta_{jk} + \tau_{j\ell}\delta_{ik} - \tau_{ik}\delta_{j\ell} - \tau_{jk}\delta_{i\ell}) \tag{2.38}$$

The last rate quantity in Eq. (2.29) is given by Liu [1984]

$$\overset{*}{J} = J\hat{v}_{k,k} \tag{2.39}$$

Eq. (2.33) and Eq. (2.39) can be substituted into Eq. (2.29) to yield

$$\overset{*}{W}_{int} = \int_{R_\chi} \frac{\partial \delta u_i}{\partial \chi_m} \left[- \frac{\partial \chi_m}{\partial x_k} \frac{\partial \hat{v}_k}{\partial x_j} \tau_{ij} + \frac{\partial \chi_m}{\partial x_j} \overset{*}{\tau}_{ij} + \frac{\partial \chi_m}{\partial x_j} \tau_{ij} \hat{v}_{k,k} \right] J dR_\chi \quad (2.40)$$

which can be transformed back to the spatial domain as

$$\overset{*}{W}_{int} = \int_{R_x} \delta u_{i,j} [\overset{*}{\tau}_{ij} + \tau_{ij} \hat{v}_{k,k} - \tau_{ik} \hat{v}_{j,k}] dR_x \quad (2.41)$$

In case of $\hat{\underset{\sim}{v}} = \underset{\sim}{v}$, i.e., $(^*) = (\dot{})$, Eq. (2.41) degenerates to

$$\dot{W}_{int} = \int_{R_x} \delta u_{i,j} [\dot{\tau}_{ij} + \tau_{ij} v_{k,k} - \tau_{ik} v_{j,k}] dR_x \quad (2.42)$$

which is identical to the incremental expression for the virtual internal work in the Lagrangian description [Liu, 1984]. The rate constitutive equation, Eq. (2.34), may be substituted into Eq. (2.41) to yield

$$\begin{aligned} \overset{*}{W}_{int} = \int_{R_x} \delta u_{i,j} [& -c_k \tau_{ij,k} + C_{ijk\ell} v_{(k,\ell)} + S_{ijk\ell} v_{[k,\ell]} \\ & + \tau_{ij} \hat{v}_{k,k} - \tau_{ik} \hat{v}_{j,k}] dR_x \end{aligned} \quad (2.43)$$

When $\hat{v}_i = v_i - c_i$ is substituted into the last two terms, Eq. (2.43) can on,be written as

$$\overset{*}{W}_{int} = \int_{R_x} \delta u_{i,j}[(C_{ijk\ell} + T_{ijk\ell})v_{k,\ell} + (\tau_{ik}c_{j,k} - \tau_{ij}c_{k,k} - c_k\tau_{ij,k})]dR_x \tag{2.44}$$

where the components for the initial stress tensor can be shown as

$$T_{ijk\ell} = T^{C}_{ijk\ell} = \tau_{ij}\delta_{k\ell} - \frac{1}{2}\tau_{i\ell}\delta_{jk} + \frac{1}{2}\tau_{j\ell}\delta_{ik} - \frac{1}{2}\tau_{ik}\delta_{j\ell} - \frac{1}{2}\tau_{jk}\delta_{i\ell} \tag{2.45}$$

if the Jaumann stress rate is used, and

$$T_{ijk\ell} = T^{\Sigma}_{ijk\ell} = \tau_{j\ell}\delta_{ik} \tag{2.46}$$

if the Truesdell stress rate of the Cauchy stress is employed. As can be seen from Eqs. (2.45-46), only the components of $T^{\Sigma}_{ijk\ell}$ possess major symmetry. Hence, the Truesdell rate for the Cauchy stress will be employed in the subsequent finite element formulation in order to obtain a symmetric geometric stiffness matrix.

Similar to the generalized constitutive equation, the general formulation for the rate of change of the virtual internal work can be arranged in three parts: (1) the material response part, $D_{ijk\ell}v_{k,\ell}$; the initial stress part, $T_{ijk\ell}v_{k,\ell}$; and (3) the transport part, $\tau_{ik}c_{j,k} - \tau_{ij}c_{k,k} - c_k\tau_{ij,k}$. With these definitions,

$$\overset{*}{W}_{int} = \int_{R_x} \delta u_{i,j} D_{ijk\ell} v_{k,\ell} dR_x + \int_{R_x} \delta u_{i,j} T_{ijk\ell} v_{k,\ell} dR_x$$

$$+ \int_{R_x} \delta u_{i,j} (\tau_{ik} c_{j,k} - \tau_{ij} c_{k,k} - c_k \tau_{ij,k}) dR_x \tag{2.47}$$

in which

$$D_{ijk\ell} = \begin{cases} C^{\tau}_{ijk\ell} & \text{for Truesdell rate} \\ C^{c}_{ijk\ell} - C^{*}_{ijk\ell} & \text{for Jaumann rate} \end{cases} \tag{2.48}$$

and

$$T_{ijk\ell} = T^{\tau}_{ijk\ell} = \tau_{j\ell} \delta_{ik} \tag{2.49}$$

since the Truesdell stress rate has been chosen for the Cauchy stress tensor. Note that the first two terms in Eq. (2.47) are identical with the linearized expression for the virtual internal work in the Lagrangian description. The transport term arises when $c_i \neq 0$ (i.e., when the ALE description is used) and it is <u>independent</u> of the stress rate chosen for the Cauchy stress tensor.

<u>Discussions on the Virtual Internal Work in ALE Description</u>

The domain of integration for Eq. (2.47) can be transformed to the material system [Liu, 1984] as

$$\overset{*}{W}_{int} = \int_{R_X} \frac{\partial \delta u_i}{\partial X_j} \left(\delta_{ik} S_{j\ell} + \frac{\partial x_i}{\partial X_p} \frac{\partial x_k}{\partial X_q} C^s_{pjq\ell}\right) \frac{\partial v_k}{\partial X_\ell} dR_X$$

$$+ \int_{R_X} \delta u_{i,j} \frac{\partial x_i}{\partial X_p} \frac{\partial x_k}{\partial X_q} S_{pq} c_{j,k} dR_X$$

$$- \int_{R_X} \delta u_{i,j} \frac{\partial x_i}{\partial X_p} \frac{\partial x_i}{\partial X_q} S_{pq} c_{k,k} dR_X$$

$$- \int_{R_X} \delta u_{i,j} c_k \tau_{ij,k} \det\left(\frac{\partial x}{\partial \underset{\sim}{X}}\right) dR_X \qquad (2.50)$$

In this expression, the second Piola-Kirchhoff stress S_{pq} is related to the Cauchy stress by

$$\tau_{ij} = \frac{1}{\det\left(\frac{\partial x}{\partial X}\right)} \frac{\partial x_i}{\partial X_p} \frac{\partial x_j}{\partial X_q} S_{pq} \qquad (2.51)$$

The fourth order tensor $C^s_{ijk\ell}$ is the counterpart of the material response tensor for the Truesdell stress rate in the material domain

$$C^s_{ijk\ell} = \det\left(\frac{\partial x}{\partial \underset{\sim}{X}}\right) \frac{\partial X_i}{\partial x_p} \frac{\partial X_j}{\partial x_q} \frac{\partial X_k}{\partial x_r} \frac{\partial X_\ell}{\partial x_s} C^t_{pqrs} \qquad (2.52)$$

The material velocity defined by

$$v_k = \dot{x}_k \qquad (2.53)$$

can be expressed by using the chain rule

$$(^{*}) = (^{\cdot}) + \frac{\partial(\ )^{*}}{\partial X_i}\overset{*}{X}_i \tag{2.54}$$

as

$$\begin{aligned} v_k &= \dot{x}_k \\ &= \overset{*}{x}_k - \frac{\partial x_k}{\partial X_i}\overset{*}{X}_i \end{aligned} \tag{2.55}$$

The derivative of material velocity with respect to the material coordinates can be written as

$$\frac{\partial v_k}{\partial X_\ell} = \frac{\partial \overset{*}{x}_k}{\partial X_\ell} - \frac{\partial x_k}{\partial X_i}\frac{\partial \overset{*}{X}_i}{\partial X_\ell} \tag{2.56}$$

It is noted that the second derivative of spatial coordinates with respect to the material coordinates, $-\frac{\partial^2 x_k}{\partial X_\ell \partial X_i}\overset{*}{X}_i$ is neglected at this point because only the first derivative terms are required in the derivation of the tangent stiffness matrix.

The convective velocity, $c_k = v_k - \hat{v}_k$, can be similarly expressed in terms of the rate of material and spatial coordinates as

$$\begin{aligned} c_k &= (\overset{*}{x}_k - \frac{\partial x_k}{\partial X_i}\overset{*}{X}_i) - \overset{*}{x}_k \\ &= -\frac{\partial x_k}{\partial X_i}\overset{*}{X}_i \end{aligned} \tag{2.57}$$

in which the expressions for the material and mesh velocities given by Eq. (2.55) and Eq. (2.32), respectively, have been used. The spatial derivative of the convective velocity can be shown as

$$c_{k,j} = - \frac{\partial x_k}{\partial X_i} \overset{*}{X}_{i,j} \tag{2.58}$$

Eqs. (2.56-58) can be substituted into the rate of change of virtual internal work, Eq. (2.50), to yield

$$\begin{aligned}
\overset{*}{W}_{int} = & \int_{R_X} \frac{\partial \delta u_k}{\partial X_j} S_{ij} \left(\frac{\partial \overset{*}{x}_k}{\partial X_i} - \frac{\partial x_k}{\partial X_n} \frac{\partial \overset{*}{X}_n}{\partial X_i} \right) dR_X \\
& + \int_{R_X} \frac{\partial \delta u_k}{\partial X_j} \frac{\partial x_k}{\partial X_i} \frac{\partial x_r}{\partial X_q} C^s_{ijpq} \left(\frac{\partial \overset{*}{x}_r}{\partial X_p} - \frac{\partial x_r}{\partial X_n} \frac{\partial \overset{*}{X}_n}{\partial X_p} \right) dR_X \\
& - \int_{R_X} \frac{\partial \delta u_k}{\partial X_n} \frac{\partial x_k}{\partial X_i} S_{ij} \frac{\partial \overset{*}{X}_n}{\partial X_j} dR_X \\
& + \int_{R_X} \frac{\partial \delta u_k}{\partial X_j} \frac{\partial x_k}{\partial X_i} S_{ij} \frac{\partial \overset{*}{X}_n}{\partial X_n} dR_X \\
& - \int_{R_X} \delta u_{i,j} c_k \tau_{ij,k} \det \left(\frac{\partial x}{\partial \underset{\sim}{X}} \right) dR_X
\end{aligned} \tag{2.59}$$

It is noted that the first integral in Eq. (2.59) represents the initial stress effect; the second integral is the material response part; the third and fourth integrals arise because of the use of ALE

description ($c_i \neq 0$); and the last integral represents the transport of the stress histories in the ALE description.

An alternate derivation of Eq. (2.59) is presented in Haber and Abel [1983]. This formulation is subsequently improved by Haber [1984] in which the so-called "Mixed Eulerian-Lagrangian" description is inspired by the work of Hughes et al. [1978]. In this paper, the second Piola-Kirchhoff stress, the Green strain, and the virtual work expression are linearized to obtain the tangent stiffness matrix. Because of the choice of this conjugate pair of stress and strain, and the linearizaton procedure, tedious algebra is involved and the expression for the tangent stiffness matrix is only valid for linear elastic isotropic material. For comparison purposes, the rate counterpart of the Haber's formulaton is re-derived in Appendix B. The differences between the present and the Haber's formulations are summarized in Table 2.1. As can be seen, the transport of stress histories is not included in Haber's formulation. This deficiency results from the choice of the second Piola-Kirchhoff stress and the Green strain, and the linearization procedure for the constitutive equation. The transport of stress histories is very important for highly convective calculations such as the wave propagation problems presented in the next chapter.

Table 2.1. Comparisons between the Present and the Haber's Formulations

	Present Formulation	Haber [1984]
stress	τ_{ij} (Cauchy stress)	S_{ij} (second Piola-Kirchhoff stress)
strain	$v_{i,j}$ (velocity strain)	E_{ij} (Green strain)
constitutive equation	$\overset{*}{\tau}_{ij} = -c_k \tau_{ij,k} + C_{ijk\ell} v_{(k,\ell)} + S_{ijk\ell} v_{[k,\ell]}$	$\overset{*}{S}_{ij} = \tilde{C}_{ijk\ell} \overset{*}{E}_{k\ell}$ where $\tilde{C}_{ijk\ell}$ = constant
expressions for $\overset{*}{W}_{int}$	$\int_{R_X} \frac{\partial \delta u_k}{\partial X_j} S_{ij} \left(\frac{\partial \overset{*}{x}_k}{\partial X_i} - \frac{\partial x_k}{\partial X_n} \frac{\partial \overset{*}{X}_n}{\partial X_i} \right) dR_X$	same
	$+ \int_{R_X} \frac{\partial \delta u_k}{\partial X_j} \frac{\partial x_k}{\partial X_i} \frac{\partial x_r}{\partial X_q} C^s_{ijpq} \left(\frac{\partial \overset{*}{x}_r}{\partial X_p} - \frac{\partial x_r}{\partial X_n} \frac{\partial \overset{*}{X}_n}{\partial X_p} \right) dR_X$	same, except C^s_{ijpq} is replaced by $\tilde{C}_{ijpq}$
	$- \int_{R_X} \frac{\partial \delta u_k}{\partial X_n} \frac{\partial x_k}{\partial X_i} S_{ij} \frac{\partial \overset{*}{X}_n}{\partial X_j} dR_X$	same

Table 2.1 Continued.

$+ \int_{R_X} \frac{\partial \delta u_k}{\partial X_j} \frac{\partial x_k}{\partial X_l} S_{ij} \frac{\partial \overset{*}{X}_n}{\partial X_n} dR_X$	same
$- \int_{R_X} \delta u_{i,j} c_k \tau_{ij,k} \det\left(\frac{\partial \underset{\sim}{x}}{\partial \underset{\sim}{X}}\right) dR_X$	This term is omitted.

Computer Implementation of the ALE Tangent Stiffness Matrices

Introducing the interpolating functions

$$\delta u_i = \phi_a \delta u_{ia} \quad , \quad a = 1, \text{ number of nodes per element (NEN)} \tag{2.60}$$

$$\underset{\sim}{\bar{v}} = \begin{matrix} v_i \\ c_i \end{matrix} = \phi_b \begin{matrix} v_{ib} \\ c_{ib} \end{matrix} \quad , \; b = 1, \text{ NEN} \tag{2.61}$$

the matrix equation associated with the principle of virtual work reads

$$\underset{\sim}{K}^{tan} \underset{\sim}{\bar{v}} = \underset{\sim}{f}^{ext} - \underset{\sim}{f}^{int} \tag{2.62}$$

The element tangent stiffness matrix corresponding to the rate form of virtual internal work, Eq. (2.47), is composed of three matrices

$$\underset{\sim}{K}^{tan} = \underset{\sim}{K}^{D} + \underset{\sim}{K}^{G} + \underset{\sim}{K}^{ALE} \tag{2.63}$$

In computer implementation, it is inconvenient to deal with the indices of a fourth order tensor such as D_{ijkl}. Hence, the procedure given in Liu and Ma [1982] will be followed to develop the element tangent stiffness matrices. Interested readers are suggested to refer to this work for the expressions of $\underset{\sim}{K}^{D}$ and $\underset{\sim}{K}^{G}$ which will not be repeated here. The matrix $\underset{\sim}{K}^{ALE}$ can be shown as:

$$\underset{\sim}{K}_{ab}^{ALE} = \int_{R_x} \underset{\sim}{B}_a^T \bar{\underset{\sim}{T}}_1 \underset{\sim}{B}_b dR_x - \int_{R_x} \underset{\sim}{B}_a^T \bar{\underset{\sim}{T}}_2 \underset{\sim}{\Phi}_b dR_x \tag{2.64}$$

where the 9x3 matrix $\underset{\sim}{B}_b$ is given by

$$\underset{\sim}{B}_b = \begin{matrix} \phi_{b,1} & 0 & 0 \\ \phi_{b,2} & \phi_{b,1} & 0 \\ 0 & \phi_{b,2} & 0 \\ 0 & 0 & \phi_{b,3} \\ 0 & \phi_{b,3} & \phi_{b,2} \\ \phi_{b,3} & 0 & \phi_{b,1} \\ \phi_{b,2} & -\phi_{b,1} & 0 \\ 0 & \phi_{b,3} & -\phi_{b,2} \\ -\phi_{b,3} & 0 & \phi_{b,1} \end{matrix} = \begin{matrix} \underset{\sim}{B}_b^{\gamma} \\ \hline \\ \underset{\sim}{B}_b^{\vartheta} \end{matrix} \tag{2.65}$$

The 3x3 matrix $\underset{\sim}{\Phi}_b$ is

$$\underset{\sim}{\Phi}_b = \begin{matrix} \phi_b & 0 & 0 \\ 0 & \phi_b & 0 \\ 0 & 0 & \phi_b \end{matrix} \tag{2.66}$$

The 9x9 unsymmetric matrix $\bar{\underset{\sim}{T}}_1$ is

$$\underset{\sim}{\bar{T}}_1 =$$

$$\begin{array}{cccccccc}
0 & \frac{1}{2}\tau_2 & -\tau_1 & -\tau_1 & 0 & \frac{1}{2}\tau_6 & \frac{1}{2}\tau_2 & 0 & -\frac{1}{2}\tau_6 \\
-\frac{1}{2}\tau_2 & \frac{1}{4}(\tau_1+\tau_3) & -\frac{1}{2}\tau_2 & -\tau_2 & \frac{1}{4}\tau_6 & \frac{1}{4}\tau_5 & \frac{1}{4}(\tau_3-\tau_1) & \frac{1}{4}\tau_6 & -\frac{1}{4}\tau_5 \\
-\tau_3 & \frac{1}{2}\tau_2 & 0 & -\tau_3 & \frac{1}{2}\tau_5 & 0 & -\frac{1}{2}\tau_2 & \frac{1}{2}\tau_5 & 0 \\
-\tau_4 & 0 & -\tau_4 & 0 & \frac{1}{2}\tau_5 & \frac{1}{2}\tau_6 & 0 & -\frac{1}{2}\tau_5 & \frac{1}{2}\tau_6 \\
-\tau_5 & \frac{1}{4}\tau_6 & -\frac{1}{2}\tau_5 & -\frac{1}{2}\tau_5 & \frac{1}{4}(\tau_3+\tau_4) & \frac{1}{4}\tau_2 & -\frac{1}{4}\tau_6 & \frac{1}{4}(\tau_4+\tau_3) & \frac{1}{4}\tau_2 \\
-\frac{1}{2}\tau_6 & \frac{1}{4}\tau_5 & -\tau_6 & -\frac{1}{2}\tau_6 & \frac{1}{4}\tau_2 & \frac{1}{4}(\tau_1+\tau_4) & \frac{1}{4}\tau_5 & -\frac{1}{4}\tau_2 & \frac{1}{4}(\tau_1-\tau_4) \\
-\frac{1}{2}\tau_2 & \frac{1}{4}(\tau_1-\tau_3) & \frac{1}{2}\tau_2 & 0 & \frac{1}{4}\tau_6 & -\frac{1}{4}\tau_5 & -\frac{1}{4}(\tau_1+\tau_3) & \frac{1}{4}\tau_6 & \frac{1}{4}\tau_5 \\
0 & -\frac{1}{4}\tau_6 & -\frac{1}{2}\tau_5 & \frac{1}{2}\tau_5 & \frac{1}{4}(\tau_3-\tau_4) & \frac{1}{4}\tau_2 & \frac{1}{4}\tau_6 & -\frac{1}{4}(\tau_3+\tau_4) & \frac{1}{4}\tau_2 \\
\frac{1}{2}\tau_6 & \frac{1}{4}\tau_5 & 0 & -\frac{1}{2}\tau_6 & -\frac{1}{4}\tau_2 & \frac{1}{4}(\tau_4+\tau_1) & \frac{1}{4}\tau_5 & \frac{1}{4}\tau_2 & -\frac{1}{4}(\tau_1+\tau_4)
\end{array}$$

(2.67)

The 9x3 $\bar{\bar{I}}_2$ matrix involves the spatial derivatives of the Cauchy stress

$$\bar{\bar{I}}_2 = \begin{matrix} \tau_{1,1} & \tau_{1,2} & \tau_{1,3} \\ \tau_{2,1} & \tau_{2,2} & \tau_{2,3} \\ \tau_{3,1} & \tau_{3,2} & \tau_{3,3} \\ \tau_{4,1} & \tau_{4,2} & \tau_{4,3} \\ \tau_{5,1} & \tau_{5,2} & \tau_{5,3} \\ \tau_{6,1} & \tau_{6,2} & \tau_{6,3} \\ 0 & 0 & 0 \\ 0 & 0 & 0 \\ 0 & 0 & 0 \end{matrix} \qquad (2.68)$$

These ALE tangent stiffness matrices may be incorporated into any existing Lagrangian finite element code without changing the main body of the program, nevertheless, the amount of computations is still substantial. For this reason, the ALE tangent stiffness matrices are further rearranged as the product of several 3x3 matrices as follows.

The ALE tangent stiffness matrix corresponding to Eq. (2.47) can be arranged in three parts as

$$\underset{\sim}{K}^{ALE} = \underset{\sim}{K}^{(1)} - \underset{\sim}{K}^{(2)} - \underset{\sim}{K}^{(3)} \tag{2.69}$$

The first matrix can be shown as

$$\underset{\sim}{K}^{(1)}_{ab} = \int_{R_x} \underset{\sim}{\tau}\underset{\sim}{\bar{\phi}}_b \underset{\sim}{\phi}_a' dR_x \tag{2.70}$$

where the components of the 3x3 $\underset{\sim}{\tau}$ matrix are

$$\underset{\sim}{\tau} = \{\tau_{ij}\} = \begin{matrix} \tau_1 & \tau_2 & \tau_6 \\ \tau_2 & \tau_3 & \tau_5 \\ \tau_6 & \tau_5 & \tau_4 \end{matrix} \tag{2.71}$$

the components of the 3x3 $\underset{\sim}{\bar{\phi}}_b$ matrix are given by

$$\underset{\sim}{\bar{\phi}}_b = \begin{matrix} \phi_{b,1} & \phi_{b,1} & \phi_{b,1} \\ \phi_{b,2} & \phi_{b,2} & \phi_{b,2} \\ \phi_{b,3} & \phi_{b,3} & \phi_{b,3} \end{matrix} \tag{2.72}$$

and the components of the 3x3 $\underset{\sim}{\phi}_a'$ matrix are

$$\underset{\sim}{\phi}_a' = \begin{matrix} \phi_{a,1} & 0 & 0 \\ 0 & \phi_{a,2} & 0 \\ 0 & 0 & \phi_{a,3} \end{matrix} \tag{2.73}$$

The second matrix is given by

$$K_{ab}^{(2)} = \int_{R_x} \underset{\sim}{\tau}\bar{\underset{\sim}{\phi}}_a \underset{\sim}{\phi}_b' dR_x \tag{2.74}$$

and the last matrix $\underset{\sim}{K}^{(3)}$ is

$$\underset{\sim}{K}_{ab}^{(3)} = \int_{R_x} \underset{\sim}{\tau}_a' \underset{\sim}{\phi}_b dR_x \tag{2.75}$$

where the components of the 3x3 $\underset{\sim}{\tau}_a'$ matrix are

$$\underset{\sim}{\tau}_a' = \phi_{a,j} \begin{matrix} \tau_{1j,1} & \tau_{1j,2} & \tau_{1j,3} \\ \tau_{2j,1} & \tau_{2j,2} & \tau_{2j,3} \\ \tau_{3j,1} & \tau_{3j,2} & \tau_{3j,3} \end{matrix}$$

The components of the matrix $\underset{\sim}{\phi}_b$ have already been given by Eq. (2.66).

CHAPTER 3

NUMERICAL PROCEDURES FOR ALE EQUATIONS

3.1 Overview

The ALE formulation for conservation laws, constitutive equations, and equation of state have been considered and derivations from strong forms to matrix equations have also been given in the previous chapter. However, the overall effectiveness of the present effort depends to a large degree on the numerical procedures used for the system equations. It is the purpose of this chapter to present some numerical methods for the computations of the ALE equations which, in general, are impossible to integrate analytically.

Among the vast amount of numerical methods, subjects relevant to ALE computations include the evaluations of generalized mass matrices, internal and external force vectors, nonlinear convection effects, and new stress and strain states in addition to the construction of time-stepping algorithms. Since discussions of the mass matrix and force vectors have been well-documented in the literature [Zienkiewicz, 1977], these treatments will not be included in this investigation. For the on-growing area of nonlinear convective computations, a review of various approaches such as upwind methods, Petrov-Galerkin, and Taylor-Galerkin formulations is provided in the next section. The computations of stress and strain states for path-dependent materials are then presented in Section 3.3, which includes the discussion of the stress-velocity product and a collocation weighted residual formulation

for the constitutive equations. In Section 3.4, the nonlinear computational procedures for a two quadrature point element is presented. An explicit algorithm for the integration of the ALE equations is shown in Section 3.5 and the application of the present formulation to a number of problems is provided in Section 3.6.

3.2 Finite Element Methods for Non-Self-Adjoint Equations

The convective effect, which arises when the (Quasi-)Eulerian description is employed, has been one of the difficult topics in the development of numerical methods. The usual (Bubnov-)Galerkin method leads to a non-symmetric convective operator, and spurious spatial oscillations are exhibited at moderate to high Peclet numbers. Though highly refined meshes can remove these oscillations, the advantages of the finite element method may be diminished.

Several remedies have been devised to overcome this difficulty. In the finite difference category, the use of upwind differencing on the convective term is proposed in Richtmyer and Morton [1967] and later detailed in Spalding [1972]. A similar idea is introduced into the finite element method in Christie et al. [1976] in which the weight functions are skewed to achieve the upwind effect. Relevant early articles in these upwind-type finite elements include Heinrich et al. [1977], Hughes [1978] and Belytschko and Kennedy [1978], among others. Of particular interest in the present ALE calculations is the work presented in Brooks and Hughes [1982]. In this paper, the artificial diffusion operator is constructed in a tensorial form so as to act only in the flow direction (streamline upwind). The free parameter in this method is the amount of diffusion selected to maximize the solution accuracy. Detailed discussion of this streamline upwind method is beyond the scope of the present investigation; nevertheless, derivations of this method for the Navier-Stokes equation in the ALE

description can be found in Liu [1980], and this method will be employed to handle the convective effect at the present stage.

In addition to the above school of upwind techniques, the Petrov-Galerkin method proposed in Dendy [1974] consists of choosing different classes of functions for the weight and trial functions. Because of the potential of Petrov-Galerkin methods for flow problems, a large amount of literature has been accumulated. Among various techniques, the work presented in Hughes and Tezduyar [1984] and Morton et al. [1980] appear adapted to deal with the present ALE formulation. It is also worthwhile to point out that the Taylor-Galerkin formulations given in Donea [1984] and Lohner et al. [1984] appear to be potential candidates to handle the convective effect encountered in the ALE computations.

3.3 Stress Update Procedures

The stress state of a path-dependent material depends on the stress history of the material point. A stress-history can be readily treated in a Lagrangian description because elements contain the same material points regardless of the deformation of the continuum; similarly, quadrature points at which stresses are computed in Lagrangian elements coincide with material points throughout the deformation. On the other hand, in an ALE description, a mesh point does not necessarily coincide with a material point so that the stress history needs to be convected by the relative velocity $\underset{\sim}{c}$, as indicated in Eq. (2.7). Note that the spatial derivatives of the deviatoric stress are involved in the convection term.

When C^{-1} functions are used to interpolate the element stresses, the ambiguity of the stress derivatives at the element interface renders the calculation of the spatial derivatives of stress a difficult task. As mentioned in REMARK 2.1.3, this is remedied by replacing Eq. (2.7) by a set of coupled equations, Eqs. (2.11-12), and the corresponding matrix equations have been given in Eqs. (2.22-23). It should be noted that all the path-dependent material properties, such as yield strains, effective plastic strains, yield stresses and back stresses, should be convected via this procedure with $\underset{\sim}{s}$ replaced by each of these properties in turn, and with $\underset{\sim}{z}$ appropriately modified.

In this section, numerical methods for the definition of the stress-velocity product and computation of the incremental stresses

are presented. Although the following development is discussed in a two-dimensional setting, the extension to the three-dimensional case is straightforward.

Construction of the Stress-Velocity Product

In a nonlinear displacement finite element formulation, the velocities are stored at nodes while the stress histories, back stresses and yield radii are available only at quadrature points. In order to establish the nodal values for the stress-velocity product, a weak formulation is a logical necessity. In addition, based on the one-dimensional study presented later in this chapter, in which the upwind procedure is used to define this intermediate variable, the artificial viscosity technique (streamline upwind) [Brooks and Hughes, 1982] is considered here as a generalization of this upwind procedure to multi-dimensional cases. For the sake of clarity, the free indices i and j denoting the component of stress tensor will be dropped hereafter.

The relation for the stress-velocity product given in Eq. (2.12) is modified to accommodate the artifical viscosity tensor A_{km}

$$y_k = sc_k - A_{km,m} \tag{3.1}$$

The ingredients of the artificial viscosity tensor consist of a tensorial coefficient multiplied by the stress:

$$A_{km} = \mu_{km} s \tag{3.2}$$

where the tensorial coefficient is constructed to act only in the flow direction (streamline upwind effect) [Brooks and Hughes, 1982]

$$\mu_{km} = \bar{\mu} c_k c_m / c_n c_n \tag{3.3}$$

and the scalar $\bar{\mu}$ is given by

$$\bar{\mu} = \sum_{i=1}^{NSD} \alpha_i c_i h_i / NSD \tag{3.4}$$

Here h_i is the element length in the i-direction, NSD designates the number of space dimensions, and α_i is the artificial viscosity parameter discussed in Appendix B given by

$$\alpha_i = \pm \frac{1}{2} \text{ , for } c_i \gtrless 0 \tag{3.5}$$

The weak form corresponding to Eq. (3.1) can be obtained by multiplying by the test functions for the stress-velocity product and integrating over the spatial domain R_x.

$$\int_{R_x} \delta y_k y_k dR_x = \int_{R_x} \delta y_k s c_k dR_x - \int_{R_x} \delta y_k A_{km,m} dR_x \tag{3.6}$$

This equation may be written as

$$\int_{R_x} \delta y_k y_k dR_x = \int_{R_x} \delta y_k sc_k dR_x + \int_{R_x} \delta y_{k,m} A_{km} dR_x \tag{3.7}$$

by applying the divergence theorem and by assuming no traction associated with the artificial viscosity on the boundary. The expression for A_{km}, Eqs. (3.2-3), can be substituted into this equation to yield

$$\int_{R_x} \delta y_k y_k dR_x = \int_{R_x} (\delta y_k + \delta \bar{y}_k) sc_k dR_x \tag{3.8}$$

where

$$\delta \bar{y}_k = \delta y_{k,m} \bar{\mu} c_m / c_n c_n \tag{3.9}$$

can be viewed as a modification of the Galerkin finite element method because of the transport nature of stress-velocity product.

The shape functions for the stress-velocity product can be chosen to be the standard C^o functions. The number and position of numerical integration points for Eqs. (3.8-9) should be selected to be the quadrature points, since the stress histories in Eq. (3.8) are only available at these points.

Remark 3.3.1: The determination of the artificial viscosity parameter is accomplished with a recourse to the analytic solutions for a one-dimensional constitutive equation. The analytic solutions are obtained by employing the Laplace Transform technique which is detailed in Appendix C.

Multiple Stress Collocation Point Formulation

Following the procedures given in the previous sub-section, the stress-velocity product can be defined at each nodal point and it can be substituted into the constitutive equation as follows to calculate the rate of change of stresses.

$$\underset{\sim}{M}^{s}\overset{*}{\underset{\sim}{s}} = \underset{\sim}{z} - \underset{\sim}{G}^{T}\underset{\sim}{y} + \underset{\sim}{D}\,\underset{\sim}{s} \tag{3.10}$$

Definitions for the above matrices and vectors are given in Appendix A. Note that the interpolation functions for stresses need to be integrated over the spatial element domain in these definitions. However, the present displacement formulation carries stresses only at quadrature points in contrast to the Hellinger-Reissner and Hu-Washizu [Washizu, 1975] finite elements in which the stress interpolants are assumed.

Furthermore, the task to select the number of quadrature points for the displacement finite element poses another important issue. For example, the locking phenomenon for fully integrated elements arises when the material becomes incompressible. While selective reduced integration can overcome this difficulty, it is just as costly as full quadrature. To alleviate this computational hurdle, the use of one point quadrature combined with hourglass control is developed in Belytschko et al. [1984]. In addition, a nonlinear two-quadrature point element presented in the next section appears to be another candidate for large scale computations because it exhibits nearly the

same accuracy as the selective reduced integration element while with only one-third of the cost. The elements mentioned here, as well as others in the family of displacement elements, can be readily adopted in the ALE computations. It is obvious that a stress transport procedure suitable for any number of quadrature points is needed.

Inspired by the equivalence proof for the mixed and displacement elements in Belytschko et al. [1985], the displacement element is divided into M subdomains where M denotes the number of quadrature points. Each subdomain is designated by R_I (I = 1, M), which contains the quadrature point $\underset{\sim}{x}_I$, and no two subdomains overlap. Associated with R_I, a stress interpolating function ϕ_I^s is assigned and its value is prescribed only at quadrature point $\underset{\sim}{x} = \underset{\sim}{x}_I$ to be unity, or

$$\phi_I^s(\underset{\sim}{x}=\underset{\sim}{x}_I) = 1 \tag{3.11}$$

The test function in R_I is chosen to be the Dirac delta function

$$\bar{\phi}_I^s = \delta(\underset{\sim}{x}-\underset{\sim}{x}_I) \tag{3.12}$$

Substitutions of these functions into the constitutive equation given by Eq. (2.16) represents a mathematical requirement that the residual of the weak form vanishes at each collocative quadrature point. Because the collocation point is located right at the quadrature point, the algebraic equations resulting from Eq. (3.10) are dependent only on the information (stress history) associated with its host points.

Since the Dirac delta function has the important property that

$$\int_{R_x} F(\underset{\sim}{x})\delta(\underset{\sim}{x}-\underset{\sim}{x}_I)dR_x = F(\underset{\sim}{x}_I) \tag{3.13}$$

All of the matrices and vectors in Eq. (3.10) can be easily worked out without numerical integration and they are given in Appendix D.

Remark 3.3.2: In Appendix E, the stress update procedure is given for a uniform one-dimensional mesh; the resulting stress convective terms bear a strong similarity to the donor-cell differencing [Roache, 1972]. On the other hand, a simple averaging (or the central differencing) is obtained if the upwind effect is not applied to the convective terms.

3.4 An Efficient Nonlinear Element

In Liu et al. [1985], a "unified" stabilization procedure for the Laplace equation, the equation for continuum and the equation for plates and shells in two and three dimensions is presented. The major achievements are (1) control of the spurious singular modes for underintegrated finite elements; (2) enhancement of the computational efficiency without sacrificing the accuracy; and (3) alleviation of the locking phenomenon for continuum elements when the material becomes incompressible. Accurate solutions are achieved for linear isotropic (incompressible) materials. However, when the above IPS element is applied to plastic materials, the solution accuracy deteriorates and the proposed element tends to be too stiff when compared to the selective reduced integration (SRI) element.

A possible reason for this shortcoming in nonlinear calculations is due to too few (only one) stress sampling points in each element. The entire element must be in either a purely elastic or a purely plastic state determined by evaluating the constitutive equations at the element center. Consequently, the onset of plastic fronts and the plastic yielding effects cannot be accurately accounted for. On the other hand, the SRI element permits different stress states in elements because the constitutive equations are calculated at four (for a two-dimensional bilinear interpolation of displacement) quadrature points. Nevertheless, in view of the large additional cost in computing the spatial derivatives of shape functions and in evaluating

the constitutive equations, there seems to be little benefit in using the SRI element.

Based on these considerations, research effort has been directed toward the development of an accurate two stress-sampling point element (IPS2), which retains the efficiency of the IPS element. The basic idea of the present approach is to adopt the approximation of the gradient operator matrix in Liu et al. [1984] and to evaluate the constitutive equation at two presumed quadrature points. For illustrative purposes, details of the two-dimensional plane-strain case are presented here.

The gradient operator matrix given in Liu et al. [1984] is

$$\underset{\sim}{B}_a = \underset{\sim}{B}_a(\underset{\sim}{0}) + \underset{\sim}{B}^{dev}_{a,\xi}(\underset{\sim}{0})\xi + \underset{\sim}{B}^{dev}_{a,\eta}(\underset{\sim}{0})\eta \tag{3.14}$$

where the subscript "a" ranges from 1 to the number of nodes per element. Definitions of $\underset{\sim}{B}_a(\underset{\sim}{0})$, $\underset{\sim}{B}^{dev}_{a,\xi}(\underset{\sim}{0})$ and $\underset{\sim}{B}^{dev}_{a,\eta}(\underset{\sim}{0})$ can be found in Appendix F. The incremental strain is

$$\Delta\underset{\sim}{\varepsilon}(\xi,\eta) = [\underset{\sim}{B}_a(\underset{\sim}{0}) + \underset{\sim}{B}^{dev}_{a,\xi}(\underset{\sim}{0})\xi + \underset{\sim}{B}^{dev}_{a,\eta}(\underset{\sim}{0})\eta]\Delta\underset{\sim}{d}_a \tag{3.15}$$

where $\Delta\underset{\sim}{d}_a$ is the incremental displacement vector. The incremental spin tensor can similarily be approximated by

$$\Delta\underset{\sim}{W}(\xi,\eta) = [\underset{\sim}{W}_a(\underset{\sim}{0}) + \underset{\sim}{W}_{a,\xi}(\underset{\sim}{0})\xi + \underset{\sim}{W}_{a,\eta}(\underset{\sim}{0})\eta]\Delta\underset{\sim}{d}_a \tag{3.16}$$

where $\underset{\sim}{W}_a(\underset{\sim}{0})$, $\underset{\sim}{W}_{a,\xi}(\underset{\sim}{0})$ and $\underset{\sim}{W}_{a,\eta}(\underset{\sim}{0})$ are given in Appendix G. The incremental strain and spin tensors are calculated at two quadrature points,

$$\underset{\sim}{\xi} = \left(\pm \frac{1}{\sqrt{3}} , \pm \frac{1}{\sqrt{3}} \right) \tag{3.17a}$$

$$\text{or} \quad \left(\pm \frac{1}{\sqrt{3}} , \mp \frac{1}{\sqrt{3}} \right) \tag{3.17b}$$

and the stress history, $\underset{\sim}{\tau}_n(\underset{\sim}{\xi}_\ell)$, and the back stresses, $\underset{\sim}{\sigma}_n(\underset{\sim}{\xi}_\ell)$, at time step n are rotated by $\underset{\sim}{Q}(\underset{\sim}{\xi}_\ell)$ to account for the rotational effect [Hughes and Winget, 1980].

$$\bar{\underset{\sim}{\tau}}_{n+1}(\underset{\sim}{\xi}_\ell) = [\underset{\sim}{Q}\ \underset{\sim}{\tau}_n\ \underset{\sim}{Q}^T]_{\underset{\sim}{\xi}_\ell} \tag{3.18a}$$

$$\bar{\underset{\sim}{\sigma}}_{n+1}(\underset{\sim}{\xi}_\ell) = [\underset{\sim}{Q}\ \underset{\sim}{\sigma}_n\ \underset{\sim}{Q}^T]_{\underset{\sim}{\xi}_\ell} \tag{3.18b}$$

where $\bar{\underset{\sim}{\tau}}_{n+1}(\underset{\sim}{\xi}_\ell)$ and $\bar{\underset{\sim}{\sigma}}_{n+1}(\underset{\sim}{\xi}_\ell)$ are the intermediate Cauchy stresses and back stresses, respectively. The expression for the orthogonal matrix $\underset{\sim}{Q}$ is

$$\underset{\sim}{Q} = \underset{\sim}{I} + (\underset{\sim}{I} - \frac{1}{2}\,\Delta\underset{\sim}{W})^{-1}\Delta\underset{\sim}{W} \tag{3.19}$$

where $\underset{\sim}{I}$ is the identity matrix. The incremental change of the stress state due to material deformation at the quadrature point $\underset{\sim}{\xi}_\ell$ can be

handled by the plasticity integration procedure. An example is the radial return method given in Krieg and Key [1976].

$$\Delta \underset{\sim}{\tau}(\xi_\ell) = \underset{\sim}{f}_\tau(\Delta \underset{\sim}{\varepsilon},\ \bar{\underset{\sim}{\tau}}_{n+1},\ \bar{\underset{\sim}{\sigma}}_{n+1},\ k_n, \ldots) \tag{3.20}$$

$$\Delta \underset{\sim}{\sigma}(\xi_\ell) = \underset{\sim}{f}_\sigma(\Delta \underset{\sim}{\varepsilon},\ \bar{\underset{\sim}{\tau}}_{n+1},\ \bar{\underset{\sim}{\sigma}}_{n+1},\ k_n, \ldots) \tag{3.21}$$

$$\Delta k(\xi_\ell) = f_k(\Delta \underset{\sim}{\varepsilon},\ \bar{\underset{\sim}{\tau}}_{n+1},\ \bar{\underset{\sim}{\sigma}}_{n+1},\ k_n, \ldots) \tag{3.22}$$

where Δk is the incremental change of the yield radius; $\underset{\sim}{f}_\tau$, $\underset{\sim}{f}_\sigma$, and f_k designate the plasticity integration procedure for $\Delta \underset{\sim}{\tau}$, $\Delta \underset{\sim}{\sigma}$, and Δk, respectively. The state of stresses at step n+1 is then updated by

$$\underset{\sim}{\tau}_{n+1}(\xi_\ell) = \bar{\underset{\sim}{\tau}}_{n+1}(\xi_\ell) + \Delta \underset{\sim}{\tau}(\xi_\ell) \tag{3.23}$$

$$\underset{\sim}{\sigma}_{n+1}(\xi_\ell) = \bar{\underset{\sim}{\sigma}}_{n+1}(\xi_\ell) + \Delta \underset{\sim}{\sigma}(\xi_\ell) \tag{3.24}$$

$$k_{n+1}(\xi_\ell) = k_n(\xi_\ell) + \Delta k(\xi_\ell) \tag{3.25}$$

The element internal force vector is

$$\underset{\sim}{f} = \int_{R_x} \underset{\sim}{B}^T \underset{\sim}{\tau}_{n+1}\ dR_x \tag{3.26}$$

The approach used in Eq. (3.14) can be applied again to approximate the gradient operator matrix $\underset{\sim}{B}$ in Eq. (3.26). Numerical integration, with weights equal to 2 and with the Jacobian assumed to be a constant,

(element area)/4, is employed to integrate the element internal force vector

$$\underset{\sim}{f} = \sum_{\ell=1}^{2} \frac{A}{2} [\underset{\sim}{B}_a(\underset{\sim}{0}) + \underset{\sim}{B}^{dev}_{a,\xi}(\underset{\sim}{0})\xi_\ell + \underset{\sim}{B}^{dev}_{a,\eta}(\underset{\sim}{0})\eta_\ell]^T \underset{\sim}{\tau}^{n+1}(\underset{\sim}{\xi}_\ell) \tag{3.27}$$

and A represents the area of the element.

The element internal force vector can be further arranged as

$$\underset{\sim}{f} = \underset{\sim}{f}_1 + \underset{\sim}{f}_{stab} \tag{3.28}$$

where the internal force resulting from the one point quadrature is

$$\underset{\sim}{f}_1 = \frac{A}{2} \begin{matrix} \langle\tau_{11}\rangle \underset{\sim}{b}_1 + \langle\tau_{12}\rangle \underset{\sim}{b}_2 \\ \langle\tau_{22}\rangle \underset{\sim}{b}_2 + \langle\tau_{12}\rangle \underset{\sim}{b}_1 \end{matrix} \tag{3.29}$$

and the contribution from the stabilization procedure is

$$\underset{\sim}{f}_{stab} = \frac{A}{6} \begin{matrix} ((\xi_1\alpha_{1\xi} + \eta_1\alpha_{1\eta})(2[\tau_{11}]-[\tau_{22}]-[\tau_{33}]) + \\ \qquad 3(\xi_1\alpha_{2\xi} + \eta_1\alpha_{2\eta})[\tau_{12}])\underset{\sim}{\gamma} \\ ((\xi_1\alpha_{2\xi} + \eta_1\alpha_{2\eta})[-[\tau_{11}]+2[\tau_{22}]-[\tau_{33}]) + \\ \qquad 3(\xi_1\alpha_{1\xi} + \eta_1\alpha_{1\eta})[\tau_{12}])\underset{\sim}{\gamma} \end{matrix} \tag{3.30}$$

In these expressions, the following definitions have been ...

$$\langle\tau_{ij}\rangle = \tau_{ij}(\underset{\sim}{\xi}_1) + \tau_{ij}(\underset{\sim}{\xi}_2) \quad ; \quad [\tau_{ij}] = \tau_{ij}(\underset{\sim}{\xi}_1) - \tau_{ij}(\underset{\sim}{\xi}_2)$$

AD-A193 221 ADAPTIVE FINITE ELEMENT METHODS FOR SHELLS(U) 2/2
NORTHWESTERN UNIV EVANSTON IL DEPT OF CIVIL ENGINEERING
T BELYTSCHKO ET AL. 30 JAN 88 AFOSR-TR-88-0277
UNCLASSIFIED F49620-85-C-0120 F/G 13/2 NL

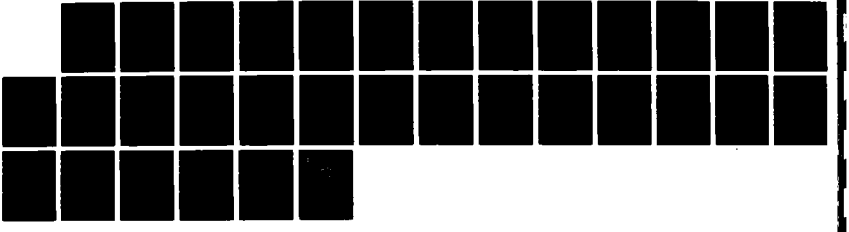

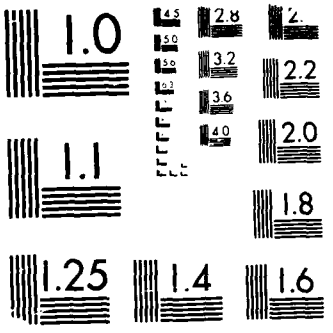

MICROCOPY RESOLUTION TEST CHART

$$\xi_1 = -\xi_2 \quad ; \quad \eta_1 = -\eta_2 \tag{3.31c,d}$$

$$\alpha_{1\xi} = -\frac{(\underset{\sim}{\xi}^T \underset{\sim}{y})}{4A} \quad ; \quad \alpha_{2\xi} = \frac{(\underset{\sim}{\xi}^T \underset{\sim}{x})}{4A} \tag{3.32a,b}$$

$$\alpha_{1\eta} = \frac{(\underset{\sim}{\eta}^T \underset{\sim}{y})}{4A} \quad ; \quad \alpha_{2\eta} = -\frac{(\underset{\sim}{\eta}^T \underset{\sim}{x})}{4A} \tag{3.33a,b}$$

Derivations for these expressions have been arranged in Appendix H.

Remark 3.4.1: The number of calculations for the spatial derivatives of shape functions, the number of evaluations for the constitutive equations, and the computer storage for rate-independent plastic calculations for SRI, IPS and IPS2 elements are reported in Table 3.1.

Remark 3.4.2: Based on the numerical examples given later, the displacement fields obtained by using either pair of quadrature points are identical, and the stress fields exhibit several percent differences in elements along the clamped boundary.

Table 3.1

Comparison of Computations and Storage for

SRI, IPS and IPS2 Elements

2-D Example	Spatial Derivatives of Shape Functions	Evaluation of Constitutive Equation	Storage Requirements
SRI	4 times	4 times	(3C.S.+3B.S.+1Y.R.) *4 = 28 words
IPS	1 time	1 time	9C.S.+3B.S.+1Y.R. = 13 words
IPS2	1 time	2 times	(3C.S.+3B.S.+1Y.R.) *2 = 14 words

C.S.: Cauchy Stress; B.S.: Back Stress; Y.R.: Yield Radius

3.5 Explicit Time Integration Algorithm

For simplicity, the coupled equations will be integrated by an explicit scheme. Lumped mass matrices are used to enhance the computational efficiency. If $(\ )_n$ and $(\ )_{n+1}$ denote the matrices at times $t_n = n\Delta t$ and $t_{n+1} = (n+1)\Delta t$, respectively, where Δt is the time increment, the explicit predictor-corrector method [Hughes and Liu, 1978] gives

The mass equation:

$$\overset{*}{\underset{\sim}{\rho}}_{n+1} = -(\underset{\sim}{M}^{\rho}_n)^{-1}(\underset{\sim}{N}^{\rho\tilde{}}_n\underset{\sim}{\rho}_{n+1} + \underset{\sim}{K}^{\rho\tilde{}}_n\underset{\sim}{\rho}_{n+1}) \tag{3.34}$$

$$\underset{\sim}{\tilde{\rho}}_{n+1} = \underset{\sim}{\rho}_n + (1-\alpha)\Delta t\overset{*}{\underset{\sim}{\rho}}_n \tag{3.35}$$

$$\underset{\sim}{\rho}_{n+1} = \underset{\sim}{\tilde{\rho}}_{n+1} + \alpha\Delta t\overset{*}{\underset{\sim}{\rho}}_{n+1} \tag{3.36}$$

The momentum equations:

$$\overset{*}{\underset{\sim}{v}}_{n+1} = (\underset{\sim}{M}_n)^{-1}(\underset{\sim}{f}^{ext}_{n+1} - \underset{\sim}{f}^{int}_n - \underset{\sim}{N}_n\underset{\sim}{\tilde{v}}_{n+1}) \tag{3.37}$$

$$\underset{\sim}{\tilde{v}}_{n+1} = \underset{\sim}{v}_n + (1-\gamma)\Delta t\overset{*}{\underset{\sim}{v}}_n \tag{3.38}$$

$$\underset{\sim}{v}_{n+1} = \underset{\sim}{\tilde{v}}_{n+1} + \gamma\Delta t\ \overset{*}{\underset{\sim}{v}}_{n+1} \tag{3.39}$$

Eq. (3.37) needs to be used in conjunction with

$$\tilde{d}_{n+1} = d_n + \Delta t v_n + (\frac{1}{2} - \beta)\Delta t^2 \overset{*}{v}_n$$

$$d_{n+1} = \tilde{d}_{n+1} + \beta\Delta t^2 \overset{*}{v}_{n+1} \tag{3.41}$$

to calculate the f_n^{int}.

The energy equation:

$$\overset{*}{e}_{n+1} = (M_n^e)^{-1}(r_{n+1} - g_n - N_n^e \tilde{e}_{n+1}) \tag{3.42}$$

$$\tilde{e}_{n+1} = e_n + (1 - \zeta)\Delta t \overset{*}{e}_n \tag{3.43}$$

$$e_{n+1} = \tilde{e}_{n+1} + \zeta\Delta t \overset{*}{e}_{n+1} \tag{3.44}$$

The constitutive equation:

$$\tilde{y}_{n+1} = (M_n^y)^{-1} N_n^y \tilde{s}_{n+1} \tag{3.45}$$

$$\overset{*}{s}_{n+1} = (M_n^s)^{-1}(z_{n+1} - G_n^T \tilde{y}_{n+1} + D_n \tilde{s}_{n+1}) \tag{3.46}$$

$$\tilde{s}_{n+1} = s_n + (1-\kappa)\Delta t \overset{*}{s}_n \tag{3.47}$$

$$s_{n+1} = \tilde{s}_{n+1} + \kappa\Delta t \overset{*}{s}_{n+1} \tag{3.48}$$

where α, β, γ, ζ and κ are the computational parameters. For explicit calculations, the following constraints on the parameters are used:

$$\alpha = 0 \; ; \; \beta = 0 \; , \; \gamma > \frac{1}{2} \; ; \; \zeta = 0 \; ; \; \kappa = 0 \tag{3.49}$$

The flowchart of the computational procedure for the class of pressure-insensitive materials is as follows:

(1) Initialization. Set $n = 0$, input initial conditions.

(2) Time stepping loop. $t \in [0, t_{max}]$.

(3) Integrate the mesh velocity to obtain the mesh displacement and spatial coordinates.

(4) Calculate incremental hydrostatic pressure by integrating Eqs. (3.45-46) with $\underset{\sim}{s}$ and $\underset{\sim}{z}$ replaced by $\underset{\sim}{p}$ and $\underset{\sim}{u}$, respectively.

   a. The rate of pressure due to convection.

   b. The rate of pressure due to deformation.

(5) Calculate incremental deviatoric stresses, yield stresses and back stresses by integrating Eqs. (3.45-46).

   a. The rate of stresses due to convection.

   b. The rate of stresses due to rotation.

   c. The rate of stresses due to deformation.

(6) Compute the internal force vector.

(7) Compute the acceleration by the equations of motion, Eq. (3.37).

(8) Compute the density by equation of mass conservation, Eq. (3.34).

(9) Compute the internal energy by the equation of energy conservation, Eq. (3.42).

(10) Integrate acceleration to obtain velocity.

(11) If $(n+1)\Delta t > t_{max}$, stop; otherwise replace n by $n+1$ and go to (2).

3.6 Numerical Examples

3.6.1 One-Dimensional Wave Propagation Problem

An elastic-plastic wave propagation problem is used to assess this ALE approach in conjunction with the simple averaging and the proposed stress update method. The problem statement, given in Fig. 3.1, represents a one-dimensional, infinitely long, elastic-plastic hardening rod. Constant density and isothermal conditions are assumed to simplify the problem. It should be noted that this elastic-plastic wave propagation problem does not require an ALE mesh and the problem was selected because it provides a severe test of the stress update procedure and because of the availability of an analytic solution. The problem is solved using 400 elements which are uniformly spaced with a mesh size of 0.1. The mesh is arranged so that no reflected wave will occur during the time interval under consideration. Material properties and computational parameters are also depicted in Fig. 3.1. Four stages are involved in this problem:

(1) $t \in [0, t_1]$, the mesh is fixed. A square wave is generated at the origin.

(2) $t \in [t_1, t_2]$, the mesh is fixed and the wave travels along the bar.

(3) $t \in [t_2, t_3]$, two cases are studied.

CASE A: The mesh is moved uniformly to the left hand side with a constant speed $-\hat{v}^*$.

CASE B: Same as CASE A except the mesh is moved to the right.

1 D ELASTIC(-PLASTIC) WAVE PROPAGATION

$\rho=1$ $E=10^4$ $E/E_T=3$ $\tau_y=75$ $\tau^*=-100$

$\Delta x=\Delta\chi=0.1$ $\hat{v}=0.25\sqrt{E/\rho}$ $\beta=0.0$ $\gamma=0.6$

1. $t\in[0, t_1]$ mesh fixed, wave generated

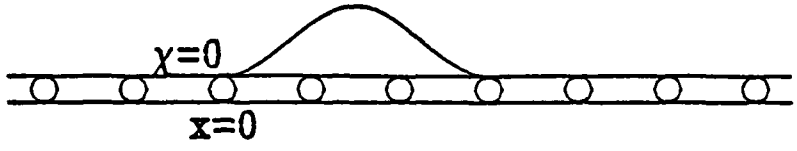

2. $t\in[t_1, t_2]$ mesh fixed, wave travelling

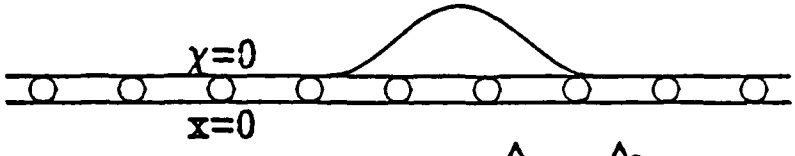

3A. $t\in[t_2, t_3]$ CASE A : move mesh with $\hat{v} = -\hat{v}$

$t_1=45$ $t_2=80$ $t_3=160$ (10^{-3})

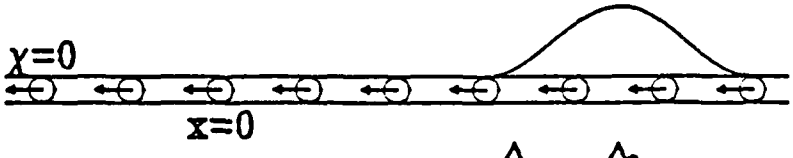

3B. $t\in[t_2, t_3]$ CASE B : move mesh with $\hat{v} = +\hat{v}$

$t_1=45$ $t_2=240$ $t_3=320$ (10^{-3})

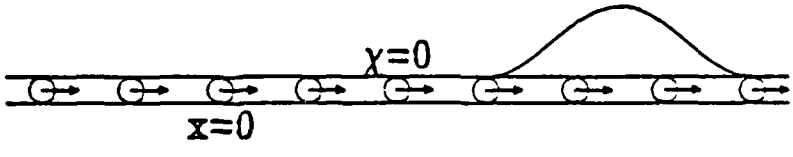

4. $t = t_3$ report stress vs. spatial coordinate

Fig. 1

(4) $t = t_3$, the stress is reported as a function of spatial coordinates in Fig. 3.2 and Fig. 3.3 for CASE A and CASE B, respectively.

For both cases, the momentum and stress transport are taken into account by employing the full upwind method for elastic and elastic-plastic materials. The results are compared to

(1) the simple averaging runs, in which the momentum transport is handled by the full upwind method and the stress transport is computed by the simple averaging method, and

(2) fixed mesh runs, in which the finite element mesh is fixed in space and the results are pretty close to the analytic solutions.

The relative velocity, $\underset{\sim}{c} = \underset{\sim}{v} - \hat{\underset{\sim}{v}}$, in CASE A ($\hat{\underset{\sim}{v}} < \underset{\sim}{0}$) is greater than CASE B ($\hat{\underset{\sim}{v}} > \underset{\sim}{0}$); therefore, the transport effect of the former is more significant. These phenomena have been studied in Figs. 3.2-3 by varying the time step reported in Table 3.2. The wave arrival time for both the proposed method and the simple averaging method agree well with the fixed mesh runs. However, the averaging method causes severe unrealistic spatial oscillations in CASE A because of the significant transport effect. The method proposed here eliminates these oscillations completely. Based on these studies, it is found that the transport of stresses as well as yield stresses (and back stresses for kinematic hardening) plays an important role in the ALE computations for path-dependent materials, and the proposed update procedure is quite accurate and effective.

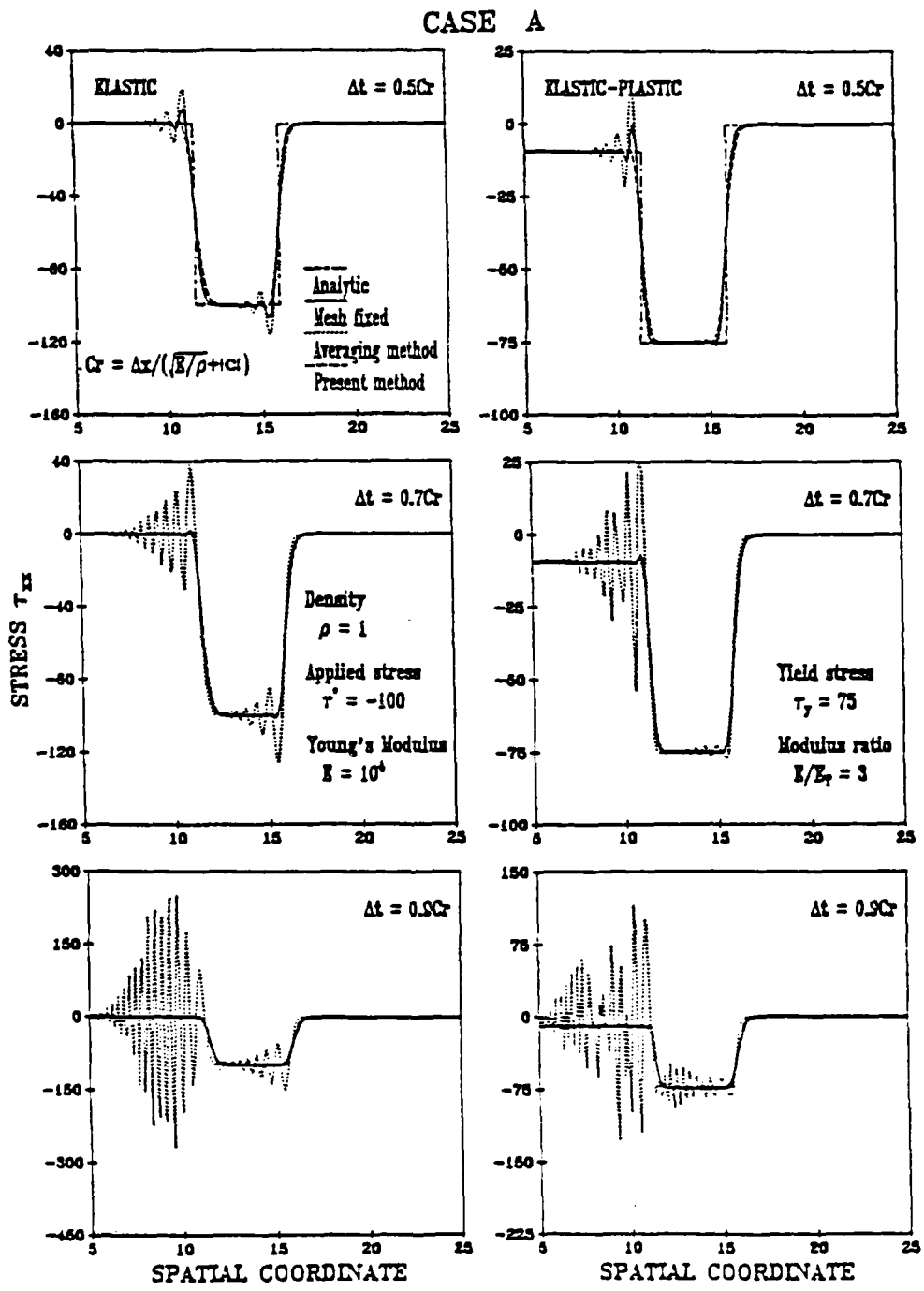
CASE A
ELASTIC
Δt = 0.5Cr
ELASTIC-PLASTIC
Δt = 0.5Cr
Analytic
Mesh fixed
Averaging method
Present method
Cr = Δx/(√(E/ρ)+|c|)
Δt = 0.7Cr
Δt = 0.7Cr
Density
ρ = 1
Applied stress
τ° = -100
Young's Modulus
E = 10⁶
Yield stress
τy = 75
Modulus ratio
E/Et = 3
Δt = 0.9Cr
Δt = 0.9Cr
STRESS τxx
SPATIAL COORDINATE
SPATIAL COORDINATE

Fig. 2

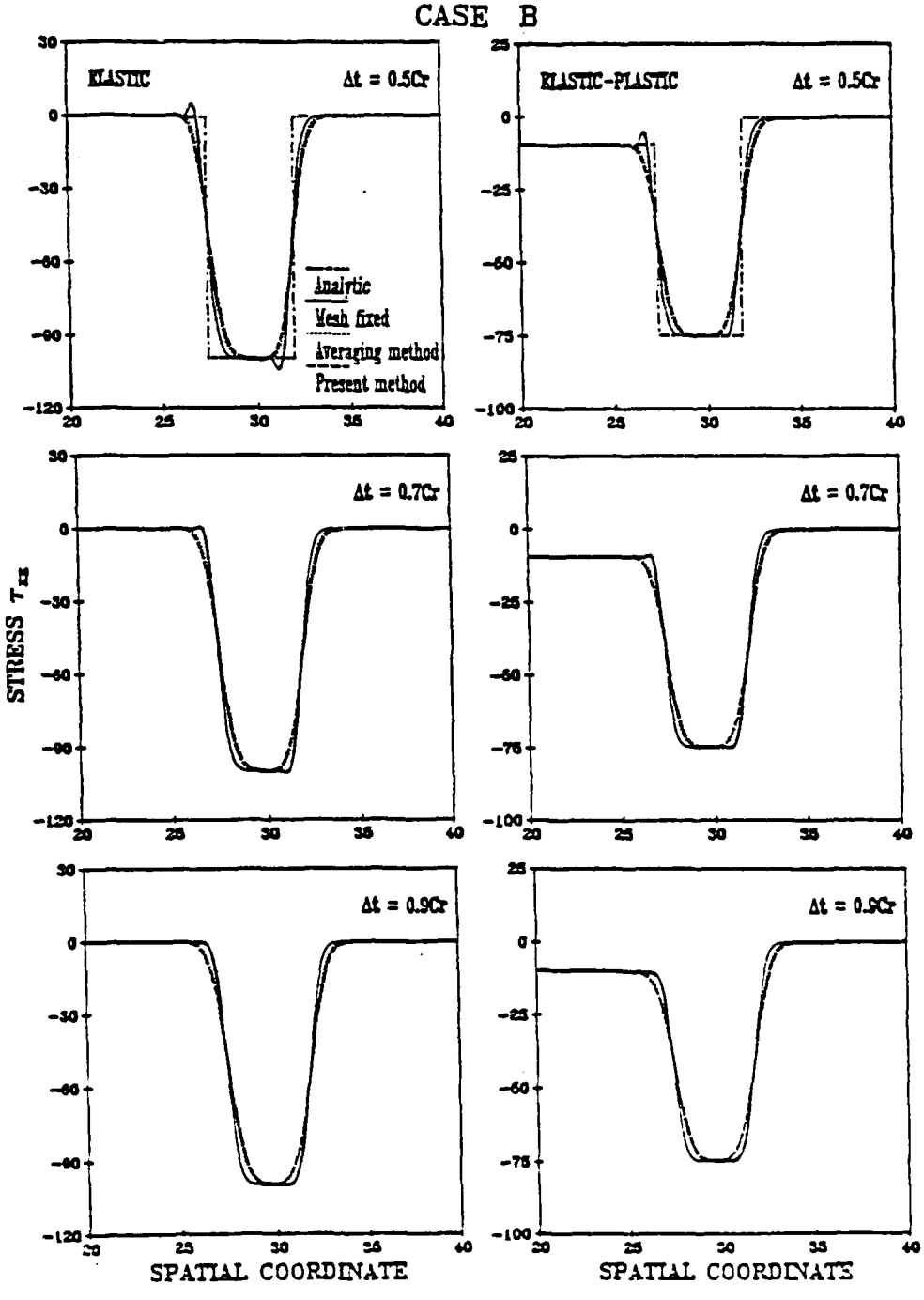
CASE B
ELASTIC
Δt = 0.5Cr
ELASTIC-PLASTIC
Δt = 0.5Cr
Analytic
Mesh fixed
Averaging method
Present method
Δt = 0.7Cr
Δt = 0.7Cr
Δt = 0.9Cr
Δt = 0.9Cr
STRESS T_{xx}
SPATIAL COORDINATE
SPATIAL COORDINATE

Fig. 3

Table 3.2. The step sizes and numbers of time steps for elastic-plastic wave propagation example

Time Step Δt	$\frac{\Delta t}{C_r}$	Number of Time Steps	
		CASE A	CASE B
0.040	0.5	400	800
0.056	0.7	286	571
0.072	0.9	222	444

$C_r = \Delta x/(\sqrt{E/\rho} + |c|)$

3.6.2 Two-Dimensional Elastic-Plastic Wave Propagation

In addition to the preceding problem, a two-dimensional plane-strain elastic-plastic wave propagation problem is considered here as an another test for both the IPS2 element and the proposed multi-stress-point transport procedure. A 100x50 mesh is used to model a spatial domain of size 10x5. The radial return procedure given in Krieg and Key [1976] is used and isotropic hardening is assumed. The geometric configuration, material properties and computational parameters are given in Fig. 3.4.

The evolutions of this stress wave propagation problem using IPS2 element are illustrated in Fig. 3.4. One component of the stress tensor τ_{22} is reported at various times. The traction force $h_y = 1000$ is applied on the boundary as a Heaviside function and this loading is terminated at time $t = 0.02$. The Rayleigh waves [Graff, 1975] can be observed in Fig. 3.4. Their effect decreases rapidly with depth and their speed of propagation is smaller than that of body waves. Immediately after $t = 0.02$, the finite element meshes are prescribed to move with the velocity $v_1 = -0.4\sqrt{E/\rho}$. At time $t = 0.03$, the computations are stopped and the stress distributions along lines $y = 1.5$, 2.0, and 3.0 are reported in Fig. 3.5 for both the elastic and elastic-plastic cases. Also included in this figure are the stresses obtained by IPS2 and SRI elements without mesh motions.

The numerical results for the IPS2 and SRI elements without mesh motion agree well for both the elastic and elastic-plastic cases. When the mesh is moving with 40% of the elastic wave speed, the wave arrival

TWO-DIMENSIONAL ELASTIC-PLASTIC WAVE

ρ=1 E=10^4 ν=0.25 E/E_T=100 τ_y=300 isotropic hardening

β=.0 γ=.6 Δt=.0005 $R_x=\{x|-5<x<5,\ 0<y<5\}$ $\Delta x=\Delta y$=.1

$h_y(x=0, -.5<y<.5,\ t<.02)$ =1000

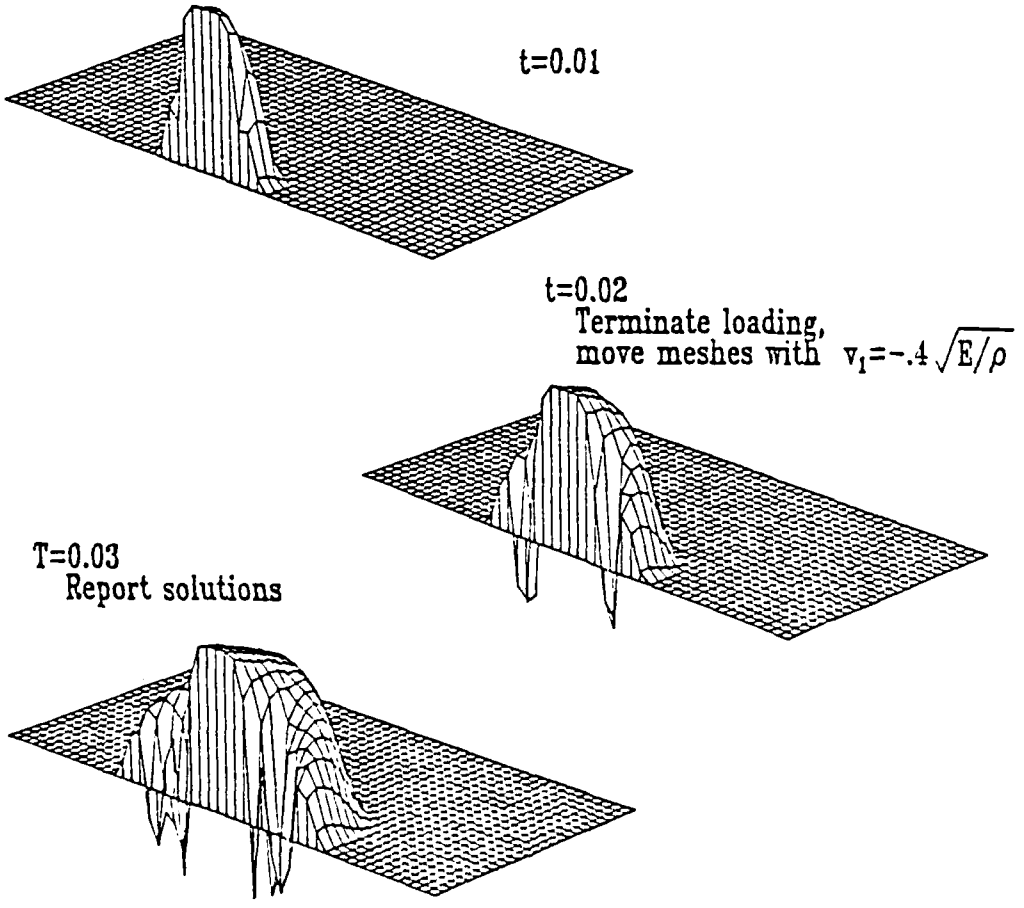

Fig. 4

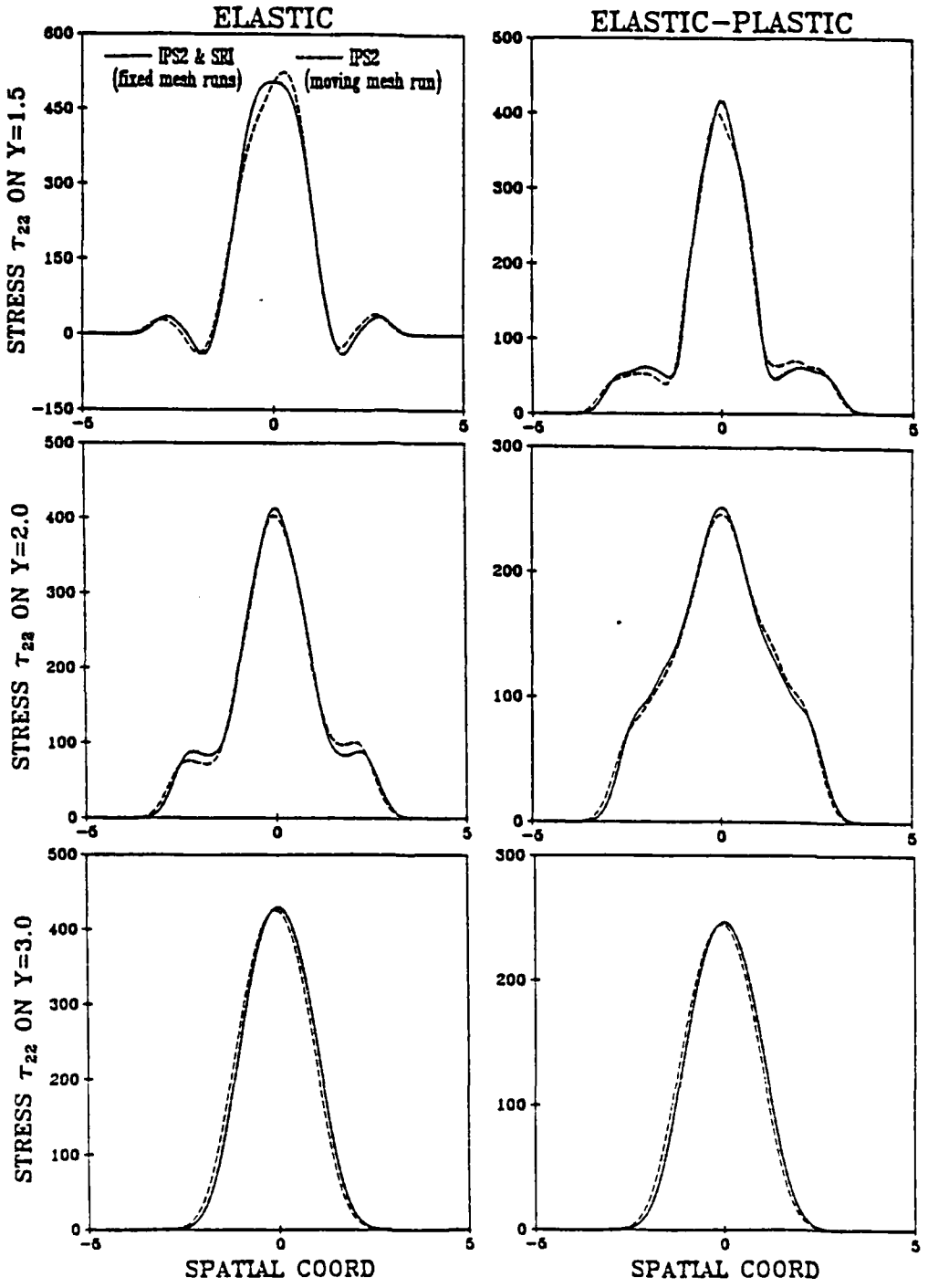
ELASTIC
ELASTIC-PLASTIC
IPS2 & SRI (fixed mesh runs)
IPS2 (moving mesh run)
STRESS τ_{22} ON Y=1.5
STRESS τ_{22} ON Y=2.0
STRESS τ_{22} ON Y=3.0
SPATIAL COORD
SPATIAL COORD

Fig. 5

time agrees well while several percent difference in wave amplitudes can be observed as compared to the fixed mesh runs. This discrepancy is due to the convective effects in the momentum and constitutive equations, since these convective effects are the only difference between the fixed and moving mesh runs.

3.6.3 Plane-Strain Elastic-Plastic Beam

A two-dimensional plane-strain dynamic elastic-plastic deformation problem is used to assess the proposed IPS2 element. The problem statement and essential and natural boundary conditions are given in Fig. 3.6. Small deformation is assumed. The entire beam is discretized by 25x4 elements. The following material constants are used: density $\rho = 1$; Young's modulus $E = 10^4$; plastic tangent modulus $E_T = 0.01E$; Poisson's ratio $\nu = 0.25$; uniaxial yield stress $\tau_y = 300$. The Krieg-Key plasticity model [Krieg and Key, 1976] is employed and isotropic hardening is assumed.

The explicit predictor-corrector method [Hughes and Liu, 1978] is employed with the following computational parameters: $\beta = 0$; $\gamma = 0.5$; time step size $\Delta t = 0.0075$; and number of time steps = 1000.

The time histories for the tip displacement (point A) and stress τ_{11} at point B are reported in Fig. 3.6. It can be seen that the displacement history for the IPS2 element is identical with that using the SRI element, while several percent differences are observed in the stress history in the plastic range. The system response obtained by the IPS element is also included in Fig. 3.6. The maximum difference for the displacement is approximately 10%. To test the sensitivity of the IPS2 element to irregular element shapes, the displacement and stress histories for a fairly skewed finite element mesh are included in Fig. 3.6. Numerical solutions show that a small amount of stiffness is introduced by skewing the elements.

PLANE STRAIN ELASTIC–PLASTIC BEAM

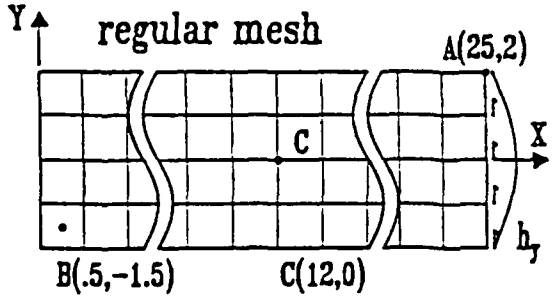

ρ=1 E=10^4 ν=0.25

E/E_T=100 τ_y=300

isotropic hardening

$h_y = 15(1-y^2/4)$

β=.0 γ=.5 Δt=.0075

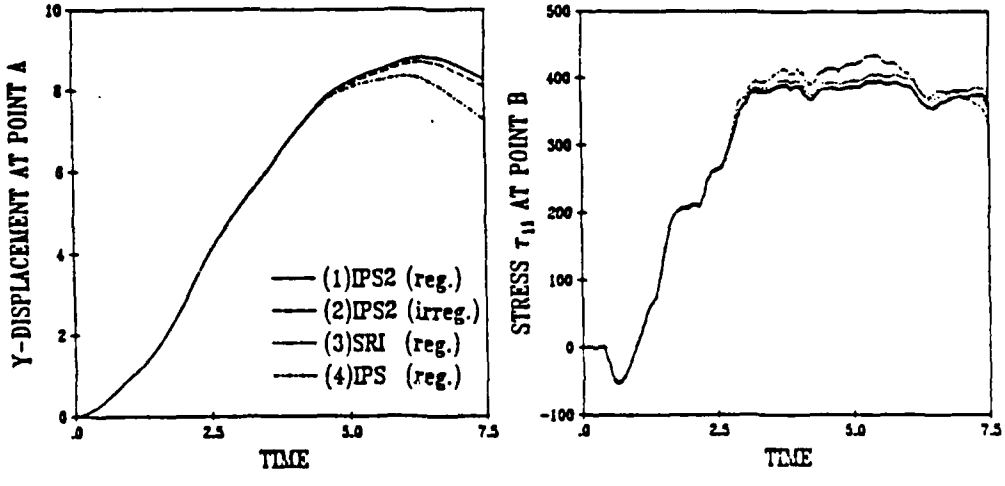

Fig. 6

It is also worthwhile to mention that the computer time consumed by the SRI element is about 3.5 times of the proposed IPS2 elements (using the expression for internal force vector given by Eq. (3.30)).

Also included in this numerical investigation are the convergence studies for the IPS element. Fig. 3.7 shows the convergence properties for E/E_T = 100 and 10, respectively. When the mesh is refined, the responses converge to those of the SRI element.

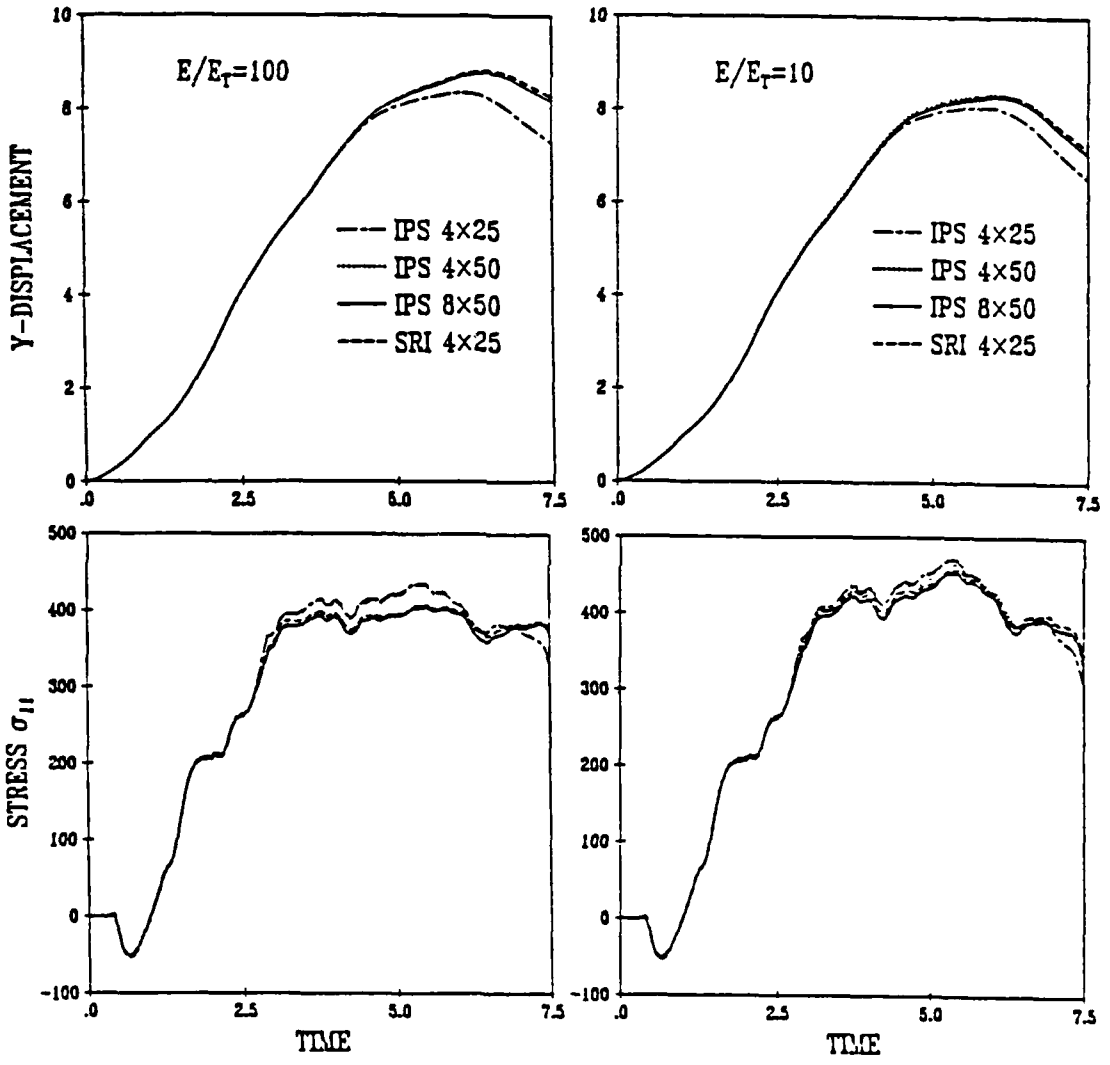
E/E$_T$=100
E/E$_T$=10
IPS 4x25
IPS 4x50
IPS 8x50
SRI 4x25
Y-DISPLACEMENT
STRESS σ_{11}
TIME
TIME

Fig. 7

3.6.4 Two Dimensional Solid with a Circular Hole

A dynamic finite deformation/rotation problem with plastic hardening is considered here. As shown in the problem statement given in Fig. 3.8, a plane strain square body with a circular hole positioned at the center of the solid is subjected to a uniformly distributed load. Due to symmetry, only a quadrant of the solid is modelled by 360 elements. The dimensions, material properties, essential and traction boundary conditions and computational parameters are included in the same figure. The radial return procedure given in Krieg and Key [1976] is employed and isotropic hardening is assumed. This problem is solved by degenerating the ALE code to the Lagrangian description. In other words, the mesh velocities are prescribed to be the same as material velocities. Both the SRI and IPS2 elements have been tested in this problem.

The dynamic responses of this system can be observed from Fig. 3.9 in which the mesh configurations are plotted for various times. The x-displacement for point A and the stress τ_{22} for point B are reported versus time in Fig. 3.10 for both the SRI and IPS2 elements. The time interval from $t = 0$ to $t \approx 0.30$ can be recognized as the elastic-plastic loading period. The displacement and stress histories for the SRI and IPS2 elements agree very well as can be seen in Fig. 3.10. The elastic unloading occurs after $t \approx 0.30$, and a small amount of phase shift appears between these elements. However, both elements exhibit the same shapes in the displacement and stress time history

2-D ELASTIC-PLASTIC SOLID WITH A HOLE

ρ=1 E=10^4 ν=0.25 E/E_T=100 τ_y=1000 isotropic hardening

β=.0 γ=.6 Δt=.0005 $h_y(t>0)$=-200

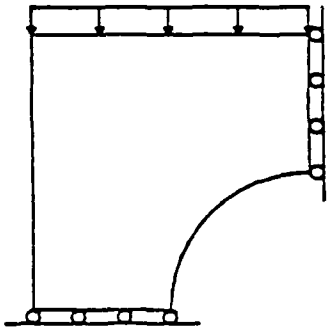

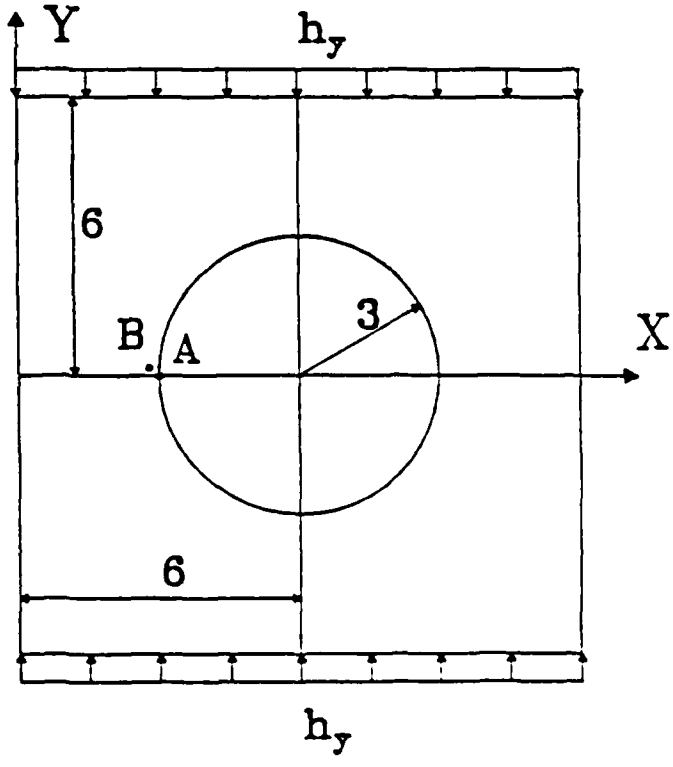

A(3.00,0.00)
B(2.95,0.10)

Fig. 8

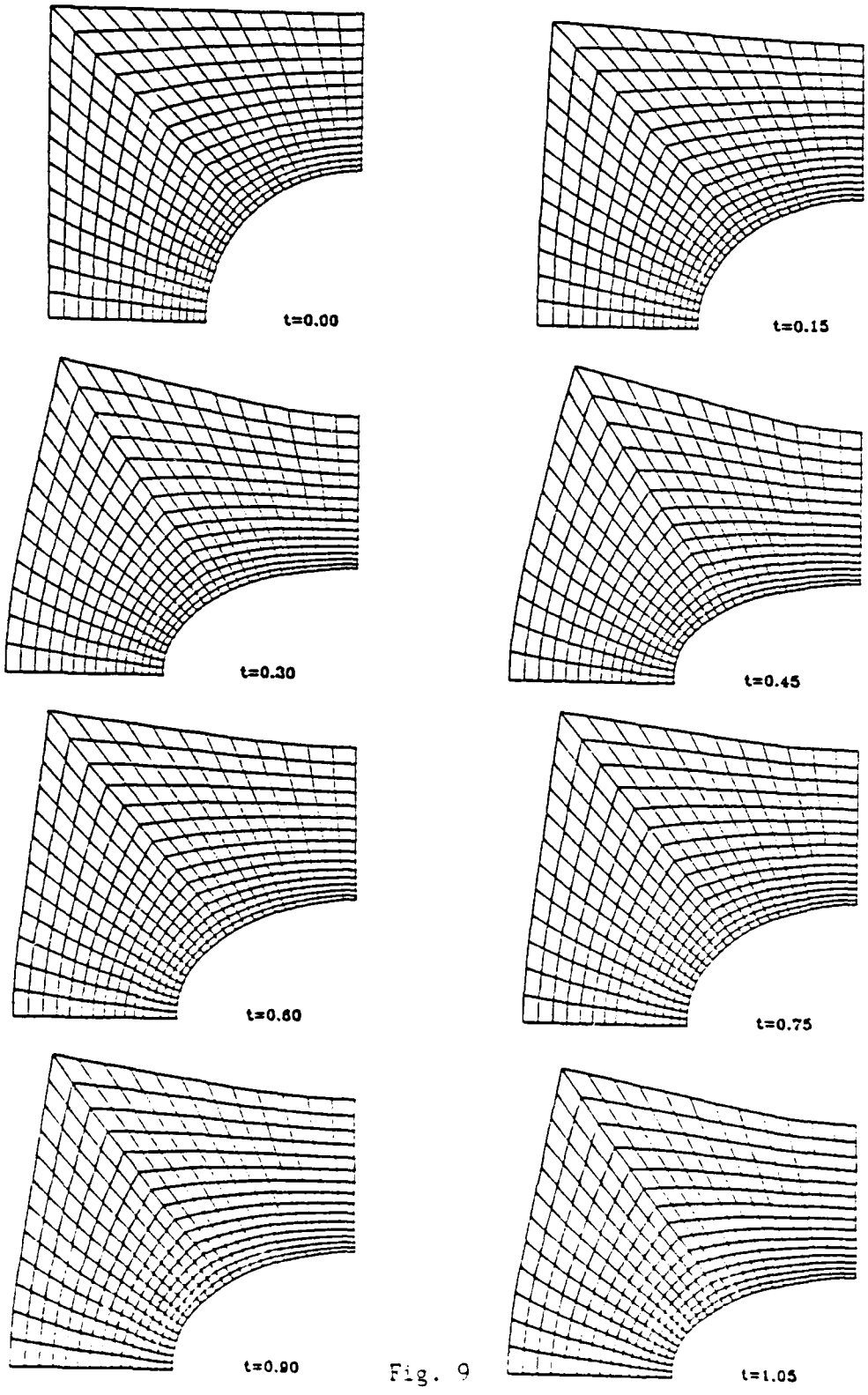

Fig. 9

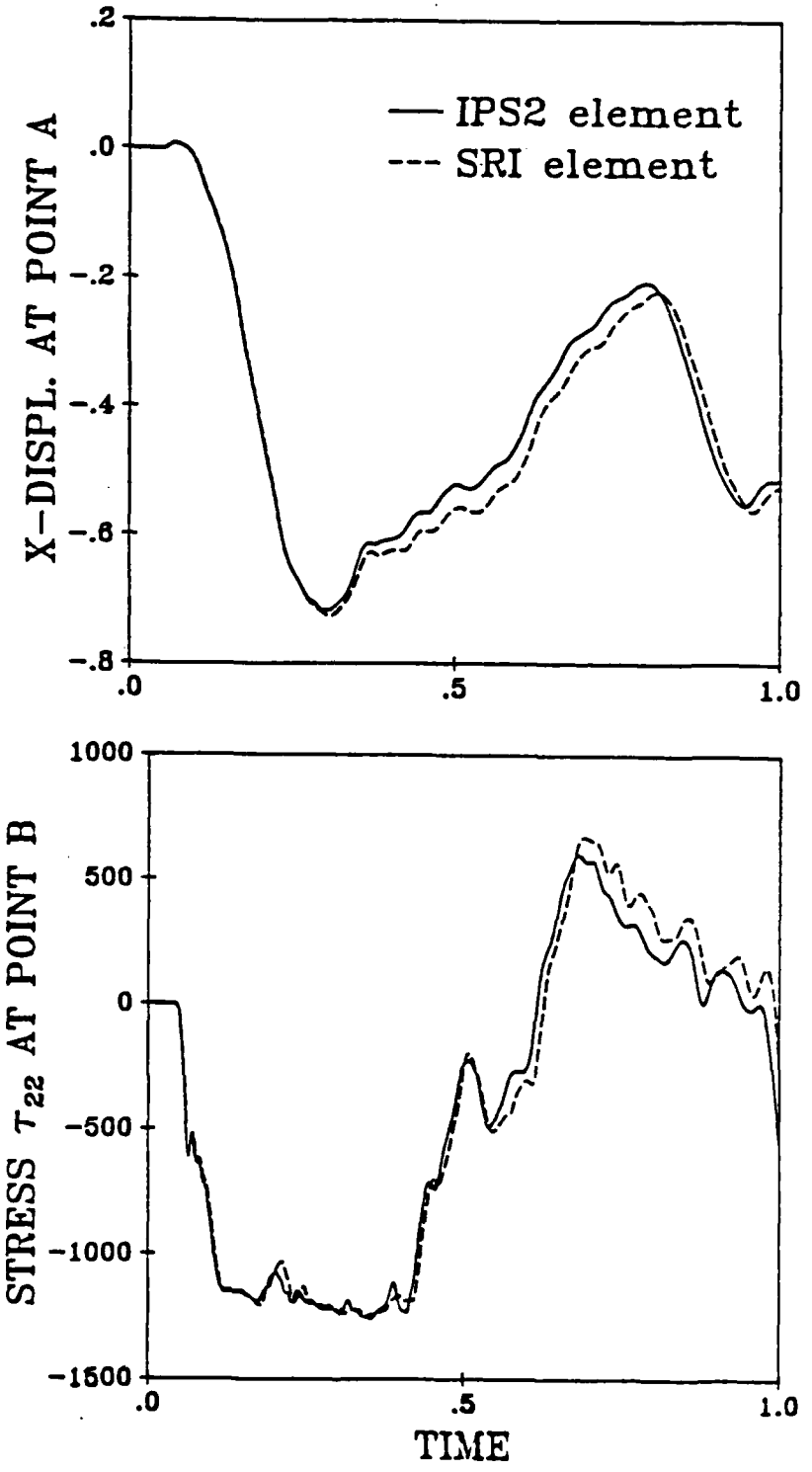
.2
.0
-.2
-.4
-.6
-.8
X-DISPL. AT POINT A
IPS2 element
SRI element
.0
.5
1.0
1000
500
0
-500
-1000
-1500
STRESS τ_{22} AT POINT B
.0
.5
1.0
TIME

Fig. 10

plots. After $t \approx 0.75$, the elastic loading occurs and the error introduced in the unloading period is retained.

It can be seen from Fig. 3.10 that the IPS2 element is stiffer than the SRI element (the same phenomenon as Example 3). The computer time consumed by the SRI element (on Harris 800) is around nine hours while the IPS2 element requires only 2.5 hours (based on the expression for internal force vector given by Eq. (3.30)). The computer time ratio between the SRI and the IPS2 elements for this example is approximately 3.5.

3.6.5 Strain Concentration with ALE Mesh

A plane strain thick beam as shown in Fig. 3.11 is considered as a test problem for the ALE method. The dimensions, material properties, essential and natural boundary conditions, and computational parameters are given in Fig. 3.11. Constant shear loading is applied at one end of the beam as a Heaviside function. Small deformation is assumed and only the upper half of the beam is modelled by the IPS2 elements because of the anti-symmetry conditions in this example.

This example is analyzed by three mesh setups: (1) 20x4 fixed uniform mesh, (2) 10x4 fixed uniform mesh, and (3) 10x4 ALE mesh. The initial layout for the 10x4 ALE mexh is the same as the 10x4 uniform mesh. As the plastic yielding effects are detected, the mesh velocities are programmed to move according to an ad hoc function: $v_1 = 0.15(X-a)^2-1.4\,|\,X-a\,|$, uah= 0 for $0 \leq X \leq 5$, or $a = 10$ for $5 \leq X \sim 10$, such that the finite element mexh is concentrated only in the high strain (or stress) regions. When the mesh size is smaller than 0.5, the mesh motions are terminated because of the restricton of critical time step for explicit time integration. The final configuration of this ALE mesh is shown in Fig. 3.11. The stress distribution of τ_{11} along the line $y = 1.75$ for these mesh setups are reported in Fig. 3.12 at the instant of that maximum deflection occurs ($t = 0.9$). As can be seen from these results, the ALE mesh provides fairly good stress distribution as compared to that of the 20x4 uniform mesh.

STRAIN CONCENTRATION WITH ALE MESH

ρ=1 E=10^4 ν=0.25 E/E_T=100 τ_y=600 isotropic hardening

β=.0 γ=.6 Δt=.004 $h_y(t>0)$=-20

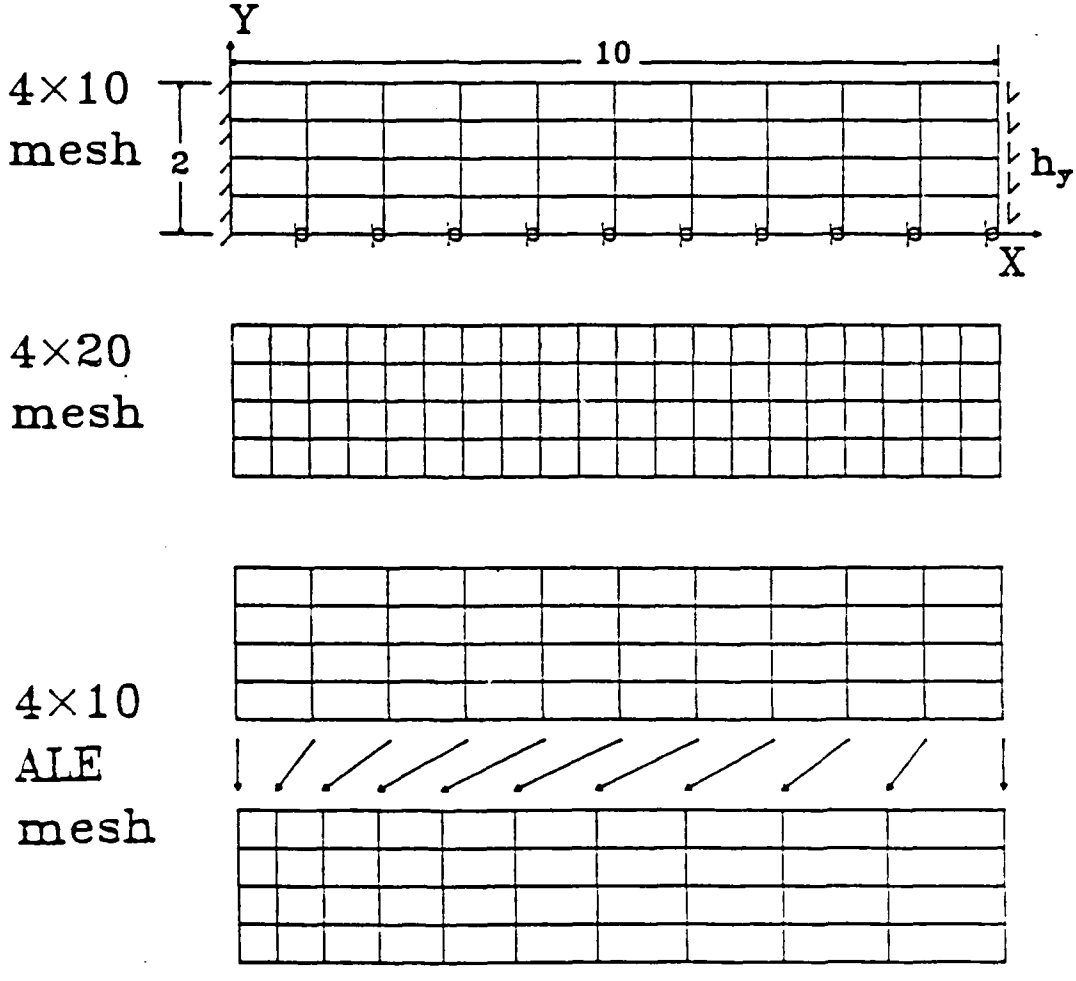

Fig. 11

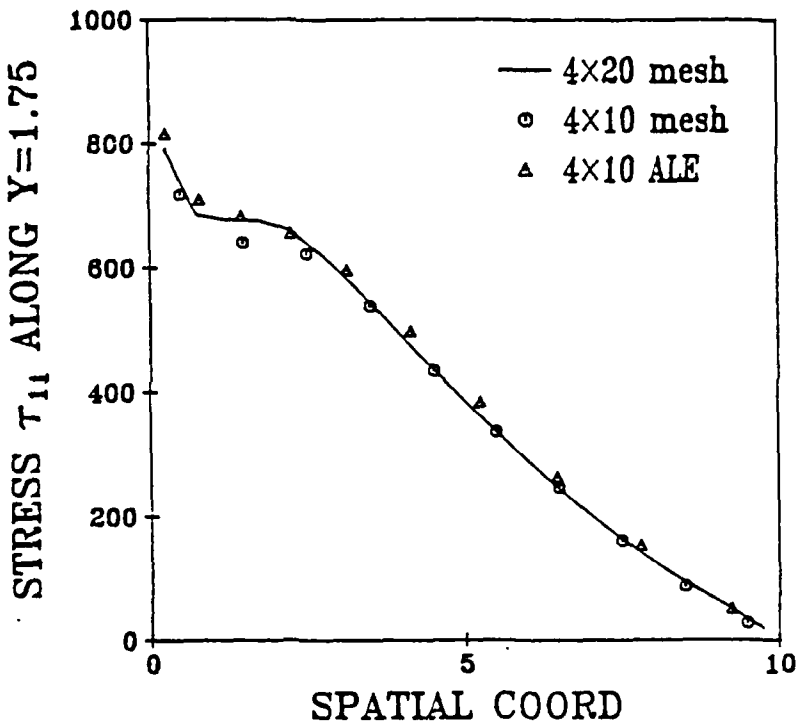
1000
800
600
400
200
0
0
5
10
STRESS τ_{11} ALONG Y=1.75
SPATIAL COORD
4×20 mesh
4×10 mesh
4×10 ALE

Fig. 12

REFERENCES

Belytschko, T., Stolarski, H., Liu, W. K., Carpetner, N. and Ong, S.-J., "Stress Projection for Membrane and Shear Locking in Shell Finite Elements," Computer Methods in Applied Mechanics and Engineering, Vol. 51, pp. 221-258, 1985.

Belytschko, T., Ong, S.-J., Liu, W. K. and Kennedy, J. M., "Hourglass Control in Linear and Nonlinear Problems," Computer Methods in Applied Mechanics and Engineering, Vol. 43, pp. 251-276, 1984.

Belytschko, T., "An Overview of Semidiscretization and Time Integration Procedures", in Computational Methods for Transient Analysis, T. Belytschko and T. J. R. Hughes eds., North-Holland, Amsterdam, pp. 1-63, 1983.

Belytschko, T., Flanagan, D. P. and Kennedy, J. M., "Finite Element Methods with User-Controlled Meshes for Fluid-Structure Interaction", Computer Methods in Applied Mechanics and Engineering, Vol. 33, pp. 669-688, 1982.

Belytschko, T., Kennedy, J. M. and Schoeberle, D. F., "Quasi-Eulerian Finite Element Formulation for Fluid-Structure Interaction", Journal of Pressure Vessel Technology, ASME, Vol. 102, pp. 62-69, 1980.

Belytschko, T. and Kennedy, J. M., "Computer Models for Subassembly Simulation", Nuclear Engineering Design, Vol. 49, pp. 17-38, 1978.

Brooks, A. N. and Hughes, T. J. R., "Streamline Upwind/Petrov-Galerkin Formulations for Convection Dominated Flows with Particular Emphasis on the Incompressible Navier-Stokes Equations", Computer Methods in Applied Mechanics and Engineering, Vol. 32, pp. 199-259, 1982.

Christie, I., Griffiths, D. F., Mitchell, F. R. and Zienkiewicz, O. C., "Finite Element Methods for Second Order Differential Equations with Significant First Derivatives", International Journal for Numerical Methods in Engineering, Vol. 10, pp. 1389-1396, 1976.

Dendy, J. E., "Two Methods of Galerkin Type Achieving Optimum L^2 Rates of Convergence for First Order Hyperbolics," International Journal for Numerical Methods in Engineering, Vol. 11, pp. 637-653, 1974.

Derbalian, K. A., Lee, E. H., Mallett, R. L. and McMeeking, R. M., "Finite Element Metal Forming Analysis with Spacially Fixed Mesh", in Applications of Numerical Methods to Forming Process, H. Armen and R. F. Jones, Jr. eds., AMD-Vol. 28, pp. 39-47. ASME Winter Annual Meeting, San Francisco, California, Dec. 10-15, 1978.

Donea, J., "A Taylor-Galerkin Method for Convective Transport Problems", International Journal for Numerical Methods in Engineering, Vol. 20, pp. 101-119, 1984.

Donea, J., Fasoli-Stella, P. and Giuliani, S., "Lagrangian and Eulerian Finite Element Techniques for Transient Fluid-Structure Interaction Problems", Transactions of the 4th Structural Mechanics in Reactor Technology, paper B1/2, 1977.

Haber, R. B. and Koh, H. M., "Explicit Expressions for Energy Release Rates Using Virtual Crack Extensions", International Journal for Numerical Methods in Engineering, Vol. 21, pp. 301-315, 1985.

Haber, R. B., "A Mixed Eulerian-Lagrangian Displacement Model for Large Deformation Analysis in Solid Mechanics", Computer Methods in Applied Mechanics and Engineering, Vol. 43, pp. 277-292, 1984.

Haber, R. B. and Abel, J. F., "Contact-Slip Analysis Using Mixed Displacements", Journal of Engineering Mechanics, ASCE, Vol. 109, pp. 411-429, 1983.

Heinrich, J. C., Huyakorn, P. S., Zienkiewicz, O. C. and Mitchell, A. R., "An Upwind Finite Element Scheme for Two-Dimensional Convective Transport", International Journal for Numerical Methods in Engineering, Vol. 11, pp. 131-145, 1977.

Hirt, C. W., Amsden, A. A. and Cook, J. L., "An Arbitrary Lagrangian Eulerian Computing Method for All Flow Speeds", Journal of Computational Physics, Vol. 14, pp. 227-253, 1974.

Hughes, T. J. R. and Tezduyar, T. E., "Finite Element Methods for First-Order Hyperbolic Systems with Particular Emphasis on the Compressible Euler Equations", Computer Methods in Applied Mechanics and Engineering, Vol. 45, pp. 217-284, 1984.

Hughes, T. J. R., Liu, W. K. and Zimmerman, T. K., "Lagrangian-Eulerian Finite Element Formulation for Incompressible Viscous Flows", U.S.-Japan Seminar on Interdisciplinary Finite Element Analysis, Cornell University, Ithaca, New York, 1978. Also in Computer Methods in Applied Mechanics and Engineering, Vol. 29, pp. 329-349, 1981.

Hughes, T. J. R. and Winget, J. M., "Finite Rotation Effects in Numerical Integration of Rate Constitutive Equations Arising in Large Deformation Analysis", International Journal of Numerical Methods in Engineering, Vol. 16, pp. 1862-1867, 1980.

Hughes, T. J. R. and Liu, W. K., "Implicit-Explicit Finite Elements in Transient Analysis", Journal of Applied Mechanics, Vol. 45, pp. 371-378, 1978.

Hughes, T. J. R., "A Simple Scheme for Developing Upwind Finite Elements", International Journal of Numerical Methods in Engineering, Vol. 12, pp. 1359-1365, 1978.

Krieg, R. D. and Key, S. W., "Implementation of a Time Independent Plasticity Theory into Structural Computer Programs", Constitutive Equations in Viscoplasticity: Computational and Engineering Aspects, AMD-Vol. 20, pp. 125-137, ASME, New York, 1976.

Liu, W. K., Ong, J. S. and Uras, R. A., "Finite Element Stabilization Matrices - a Unification Approach", Computer Methods in Applied Mechanics and Engineering, Vol. 53, pp. 13-46, 1985.

Liu, W. K., Belytschko, T., Ong, J. S. and Law, E. S., "The Use of Stabilization Matrices in Nonlinear Analysis", in Innovative Methods for Nonlinear Problems, W. K. Liu, T. Belytschko and K. C. Park eds., Pineridge Press, Swansea U.K., pp. 233-258, 1984. Also in Engineering Computations, Vol. 2, pp. 47-55, 1985.

Liu, W. K., "Notes on Advanced Finite Element Methods", Department of Mechanical and Nuclear Engineering, Northwestern University, Evanston, Illinois 1984.

Liu, W. K. and Belytschko, T., "Fluid Structure Interaction with Sloshing", Transactions of the 7th Structural Mechanics in Reactor Technology, Vol. B, pp. 11-18, 1983.

Liu, W. K. and Ma, D., "Computer Implementation Aspects for Fluid Structure Interaction Problems", Computer Methods in Applied Mechanics and Engineering, Vol. 31, pp. 129-148, 1982.

Liu, W. K., "Development of Finite Element Procedures for Fluid Structure Interaction", Ph.D. Dissertation, Califonia Institute of Technology, Pasadena, California, 1980.

Lohner, R., Morgan, K. and Zienkiewicz, O. C., "The Solution of Nonlinear Hyperbolic Equation Systems by the Finite Element Method", International Journal for Numerical Methods in Fluids, Vol. 4, pp. 1043-1063, 1984.

Malvern, L. E., "Introduction to the Mechanics of a Continuous Medium", Prentice-Hall, Englewood Cliffs, New Jersey, 1965.

Morton, K. W. and Parrott, A. K., "Generalized Galerkin Methods for First-Order Hyperbolic Equations", Journal of Computational Physics, Vol. 36, pp. 249-270, 1980.

Noh, W. F., "CEL: A Time-Dependent Two-Space-Dimensional Coupled Eulerian-Lagrangian Code", in Methods in Computational Physics, Vol. 3, B. Alder, S. Fernbach and M. Rotenberg eds., Academic Press, New York, 1964.

Pracht, W. E., "Calculating Three-Dimensional Fluid Flows at All Flow Speeds with an Eulerian-Lagrangian Computing Mesh", Journal of Computational Physics, Vol. 17, pp. 132-159, 1975.

Prager, W., "An Elementary Discussion of Definitions of Stress Rate", Quarterly of Applied Mathematics, Vol. 18, pp. 403-407, 1961.

Graff, K. F., "Wave Motion in Elastic Solids", Ohio State University Press, Columbus, Ohio, 1975.

Richtmyer, R. D. and Morton, K. W., "Difference Methods for Initial-Value Problems", Interscience, New York, 2nd ed., 1967.

Roache, P. J., "Computational Fluid Dynamics", Hermosa Publishers, Albuquerque, New Mexico, 1972.

Spalding, D. B., "A Novel Finite Difference Formulation for Differential Expressions involving Both First and Second Derivatives", International Journal for Numerical Methods in Engineering, Vol. 4, pp. 551-559, 1972.

Stein, L. R., Gentry, R. A. and Hirt, C. W., "Computational Simulation of Transient Blast Loading on Three-Dimensional Structures", Computer Methods in Applied Mechanics and Engineering, Vol. 11, pp. 57-74, 1977.

Trulio, J. G., "Theory and Structure of the AFTON Codes", Air Force Weapons Laboratory, AFWL-TR-66-19, 1966.

Washizu, K., "Variational Methods in Elasticity and Plasticity", 2nd ed., Pergamon Press, Oxford, 1975.

Zienkiewicz, O. C., "The Finite Element Method", McGraw Hill, New York, 1977.

END

DATE

FILMED

DTIC

JULY 88